The Pennsylvania State University
The Graduate School
Eberly College of Science

TRANSPORT IN NONLINEAR CHAINS AND ACROSS SEVERAL CONDENSED MATTER INTERFACES

A Dissertation in
Physics
by
Sanghamitra Neogi

Submitted in Partial Fulfillment
of the Requirements
for the Degree of

Doctor of Philosophy

December 2011

The thesis of Sanghamitra Neogi was reviewed and approved* by the following:

Gerald D. Mahan
Distinguished Professor of Physics
Dissertation Advisor, Chair of Committee

Jorge O. Sofo
Professor of Physics
Professor of Materials Science and Engineering

Jun Zhu
Assistant Professor of Physics

John Badding
Professor of Chemistry

Nitin Samarth
Professor of Physics
Head of the Department of Physics

*Signatures are on file in the Graduate School.

Abstract

In recent years, with the advances in experimental techniques, the characteristic length scales of the materials synthesized, are becoming increasingly small. Many of these microscopic structures found their places in important commercial applications. However, the thermal loads imposed on these devices and structures create a major obstacle toward their applicability. This challenge is driving a renewed interest among researchers from various disciplines, toward the topic of thermal management. The interest in the topic of thermal transport in small scale structures, served as the motivation for the work performed in this dissertation. More specifically, the following topics were investigated:

- **Transport in One-Dimensional Nonlinear Systems:** Thermal transport in materials can be explained in terms of the diffusive motion of the heat carriers at the microscopic level. An important and surprising situation emerges in some low dimensional model systems; the thermal conductivity diverges with system size. It was shown (Toda, 1979) that nonlinearity has an important effect on the heat transport in low dimensional systems. We investigate the transport of energy in a nonlinear one-dimensional chain. We show that solitons are spontaneous generated when we apply forcing functions at the end of the chain. We investigate the different characteristics of these solitons generated in the chain.

- **Transport in Fluids — Study of Pair Distribution Function:** Thermal transport in fluids depends on the distribution of particles in the fluid. It

is well known that the two-particle distribution function can describe most of the thermodynamic properties for classical fluids in thermal equilibrium. We review the approximate integral equation theories (Percus-Yevick, Hypernetted chain approximation) to obtain the pair distribution function of classical fluids. We find that these methods are highly dependent on the choice of the thermodynamic parameters of the fluid. We solve several Lennard-Jones fluid systems with different density and temperature values and prepare a density-temperature compressibility diagram. This diagram shows the region of applicability of these theories and helps us obtain the pair distribution function for a Lennard-Jones fluid with known thermodynamic parameters. We also suggest a modification of the integral-equation theories to obtain the pair distribution functions of quantum fluids.

- **Thermal Transport Across Interfaces:** When thermal energy is transported from one material to another, there is a discontinuity in temperature at the interface between them. This thermal boundary resistance is known as Kapitza resistance. The scattering of phonons at interfaces is one of the main reasons behind the presence of thermal boundary resistance. We explore the scattering of acoustic waves at several solid-solid interfaces using lattice dynamical methods. We derive matrix equations to obtain the reflection and transmission coefficients for an acoustic wave incident on the interface. These coefficients can reproduce the familiar expressions in the continuum limit and are consistent with the conservation relations.

  We discuss a method to obtain the thermal boundary resistance for neutral solid-fluid interfaces. The acoustic mismatch theory works poorly for solid-fluid interfaces. One reason is that this theory only includes the long wavelength acoustic phonons. Our theory includes all the phonon modes in the solid and all the sound modes in the fluid, in the calculation of the thermal boundary resistance. We provide an application of the method to obtain the thermal boundary resistance at the interface between solid Argon and liquid Neon. Our method yields the value for Kapitza conductance for solid Argon-fluid Neon interface to be $0.0374 \mathrm{GW/Km^2}$.

Table of Contents

List of Figures

List of Tables

List of Symbols

$\mathbf{J}_Q$	Heat flux, p. 2, 54, 88
κ	Thermal conductivity, p. 2
∇T	Gradient of local temperature, p. 2
$\mathcal{T}$	Phonon transmission coefficient, p. 5, 89
Z	Acoustic impedance, p. 5
V	Potential energy, p. 8
Q	Displacement of atoms in one-dimensional quartic chain, p. 9
K_4	Quartic spring constant, p. 9
m	Mass of atoms in the quartic chain, p. 9
τ	Dimensionless time variable with unit of inverse distance, p. 9
v_0	Velocity of first atom in the quartic chain, p. 9
q	Spatial part of normal mode solutions of all atoms in quartic lattice, p. 10
s	Sum of all spatial parts of normal mode solutions in quartic lattice, p. 10
a_0	Maximum displacement of the atoms in the quartic chain, p. 15
v	Soliton "wavenumber", p. 15
$\omega(v)$	Soliton "frequency", p. 15

q_j	Relative displacements of atoms in the quartic chain, p. 16
a	Maximum relative displacement of the atoms in the quartic chain, p. 16
A	Amplitude of applied pulse, p. 24
T	Duration of applied pulse, p. 24
H_N	Hamiltonian for a system of N particles, p. 33
T_N	Kinetic energy for a system of N particles, p. 33
V_N	Potential energy for a system of N particles, p. 33
p_i	Momentum of i^{th} particle, p. 33
$\mathbf{r}$	Position of particle in the N-particle system, p. 33
$v(\mathbf{r}_i, \mathbf{r}_j)$	Pairwise interaction potential, p. 33
$\rho^{(n)}(\mathbf{r}_1, \mathbf{r}_2, \ldots \mathbf{r}_n$	n-body probability density, p. 33
$\delta(\mathbf{r} - \mathbf{r}')$	Dirac-delta function, p. 33
Ξ	Grand canonical partition function, p. 34
z	Fugacity, p. 34
k_B	Boltzmann constant, p. 34, 89
$\mathcal{F}_2(\mathbf{r}_1, \mathbf{r}_2)$	Ursell function, p. 34
$g^{(n)}(\mathbf{r}_1, \mathbf{r}_2, \ldots \mathbf{r}_n)$	n-particle distribution function, p. 35
ρ	Number density of the N-particle system, p. 35
$g^{(2)}(\mathbf{r}_1, \mathbf{r}_2)$	Two-particle distribution function, p. 36
$g(r)$	Radial distribution function, p. 36
u	Internal energy, p. 37
P	Pressure, p. 37
$U(\mathbf{r})$	External potential imposed to the system, p. 38

$\mathbf{x}$	Position of fixed particles in the system, p. 38
$\rho^{(n)}(\mathbf{r}_1, \mathbf{r}_2, \ldots \mathbf{r}_n \vert U)$	n-particle distribution function in the presence of an external potential U, p. 38
$\rho_0(\mathbf{r})$	Density of the system without external potential, p. 38
$c(\mathbf{r}, \mathbf{r}')$	Direct correlation function, p. 38
σ,ϵ	Lennard-Jones parameters, p. 41
ρ^*, T^*	Reduced density and temperature for Lennard-Jones system, p. 41
r^*, k^*	Reduced length variables for Lennard-Jones system, p. 41
H	Hamiltonian, p. 45
$\hbar$	Planck's constant, p. 45
V	Central pair potential, p. 45
Ψ	Many-particle wavefunction, p. 45
ψ	Two-body wavefunction, p. 45
a, b, V_0	Parameters for the square-well potential between helium-4 atoms, p. 45
E_0	Ground state energy of helium-4, p. 47
n	Number density of helium-4 system, p. 48
$S(k)$	Structure function of liquid helium-4 as a function of wavevector k, p. 48
c	Velocity of sound, p. 52
ΔT	Temperature discontinuity at the interface, p. 54, 89
R	Thermal boundary resistance or Kapitza resistance, p. 54
σ	Thermal boundary conductance, p. 54, 89
m	Mass of atoms in the one-dimensional chain, p. 56
K	Harmonic spring constants in the chain, p. 56

Q Displacement of masses from their equilibrium position, p. 56

a Equilibrium distance of masses in the chain, p. 57

u Traveling wave solution for one-dimensional chain, p. 57

q Wavevector of traveling waves, p. 57

ω Frequency of traveling waves, p. 57

I Amplitude of the incident wave on the interface between two one-dimensional harmonic chains, p. 57

R Amplitude of reflected wave from the interface, p. 57

T Amplitude of transmitted wave, p. 57

Δ Determinant of the matrix with the coefficients of R and T, p. 58

θ Wavevector $\times$ the equilibrium distance , p. 58

f Ratio of the spring constants, p. 58

v Group velocity of phonon in the one-dimensional harmonic chain, p. 60

J Thermal current, p. 60

$R^{(c)}$, $T^{(c)}$ Reflection and transmission coefficients in the continuum limit, p. 60

ρ_i, v_i Mass density and speed of sound in medium i, p. 60

P_j Momentum of masses in the rhombic lattice, p. 62

V Potential energy of the masses in the rhombic lattice, p. 62

$\hat{\delta}$ Unit vector along the separation between nearest neighbors in the rhombic lattice, p. 62

$\mathbf{Q_{l,m}}$ Displacement of the mass at the $(l,\ m)^{\text{th}}$ lattice site in the rhombic lattice, p. 62

$\hat{e}$ Polarization vector of phonons in the rhombic lattice, p. 62

$\mathbf{q}$	Wavevector of phonons in the rhombic lattice, p. 62
$\mathbf{r_{lm}}$	Position of the $(l,\ m)^{\text{th}}$ lattice site in the rhombic lattice, p. 62
ω_L, ω_T	Frequencies of longitudinal and transverse phonons in the rhombic lattice, respectively, p. 63
$\hat{e}_l$, $\hat{e}_t$	Polarization vectors for longitudinal and transverse phonons in the rhombic lattice, respectively, p. 63
q_i, q_R, q_T	z-component of the wavevectors for the incident, reflected, and transmitted waves, respectively, p. 64
$\mathbf{Q_{l,m}}$	Displacement of the mass at the $(l,\ m)^{\text{th}}$ lattice site in lattice A, p. 64
$\mathbf{W_{l,m}}$	Displacement of the mass at the $(l,\ m)^{\text{th}}$ lattice site in lattice B, p. 64
A_p	Amplitude of phonon near the interface, p. 64
$\hat{\delta}_2$	Unit vector along the separation between next nearest neighbors in the square lattice, p. 67
s	$\exp(iq_z a)$, p. 69
M	Coefficients of the phonon amplitudes in equation of motion for masses near the interface, p. 74
R_{ni}	Coefficient of reflection into the n^{th} mode from the incident i^{th} mode, p. 75
T_{ni}	Coefficient of transmission into the n^{th} mode from the incident i^{th} mode, p. 75
$\underline{\mathrm{D}}$	Dynamical matrix of the FCC lattice, p. 78, 105
λ	Polarization index of phonons, p. 88
$\hbar\omega_\lambda$	Energy of phonon with polarization λ, p. 88
$\mathbf{q}$	Phonon wavevector, p. 88
$\hat{n}\cdot\mathbf{v}_\lambda$	Phonon velocity along the direction of the unit normal $\hat{n}$, p. 88

$n_B\big(\omega_\lambda(\mathbf{q})\big)$ Bose-Einstein occupation factor for phonons at temperature T, p. 88

V_{ss} Potential energy between the solid atoms, p. 90

K Solid spring constant, p. 90

$\delta_{\mathbf{s}}$ Vector distance between neighboring solid atoms, p. 90

$\mathbf{Q}$ Displacement of atoms from their equilibrium positions, p. 90

$\mathbf{R}^{(0)}$ Equilibrium position of solid atoms, p. 90

M_s Mass of solid atom, p. 90

ω Frequency of phonon in the solid, p. 90

$n(\mathbf{r}|U)$ One-particle probability density in the presence of an external potential U, p. 91

$g_{sf}(\mathbf{R}_s^{(0)}, \mathbf{R}_f^{(0)})$ Fluid distribution function near the solid interface, p. 91

$g_{ff}(\mathbf{R}_{fn}^{(0)}, \mathbf{R}_{fm}^{(0)})$ Fluid pair distribution function near the solid interface, p. 92

$\omega_{\mathbf{k}\lambda}$ Sound wave frequency in fluid with wavevector $\mathbf{k}$ and polarization λ, p. 92

M_f Mass of fluid atom, p. 92

$\hat{\epsilon}_{\mathbf{k}\lambda}$ Polarization vector of sound waves in fluid, p. 92

V_{ff} Interaction potential between fluid atoms, p. 92

ω_l, ω_t Longitudinal and transverse sound wave frequencies in fluid, p. 93

ω_0 Long range density fluctuations in fluid, p. 93

$\mathbf{R}_f$ Equilibrium position of fluid atom, p. 93

$\mathbf{q}_f$ Displacement of fluid atom from its equilibrium position, p. 93

$\delta_{\mathbf{f}}$ Vector distance between neighboring fluid atoms, p. 93

$V_{sf}(r)$ Solid-fluid interaction potential, p. 94

$\mathbf{F}_{sf}(r)$ Average force exerted by fluid on solid, p. 94

δ Vector distance between a solid atom and a neighboring fluid atom, p. 94

$\mathbf{k}$ Component of the wavevector of waves parallel to the solid-fluid interface, p. 95

k_i Component of the wavevector of incident wave perpendicular to the solid-fluid interface, p. 95

k_{sn} Component of the wavevector of reflected wave of polarization n perpendicular to the solid-fluid interface, p. 95

$\hat{e}_i$ Polarization vector of incident phonon, p. 95

$\hat{e}_{sn}$ Polarization vector of reflected phonon, p. 95

I_i Amplitude of incident phonon, p. 95

R_{sn} Amplitude of reflected phonon, p. 95

k_{fn} Component of the wavevector of transmitted wave of polarization n perpendicular to the solid-fluid interface, p. 95

$\hat{e}_{fn}$ Polarization vector of transmitted wave, p. 95

T_{sn} Amplitude of transmitted wave, p. 95

$\mathcal{M}$ Solid-fluid coupling matrix, p. 99

ϕ_k Angle between the component of the wavevector parallel to the interface and x-axis, p. 100

$\mathcal{U}, \mathcal{V}$ Fluid-solid coupling matrices, p. 102

C_{pn} Coefficients of the reflection and transmission amplitudes in the solid-fluid interface matrix equation, p. 104

Acknowledgments

It was a long journey and quite difficult at times. However, I consider myself to be very fortunate to be in the company of some great people who kept me motivated during this journey. All through my educational career, I am very fortunate to receive guidance from a number of great teachers. During my high school, Sujit Ghose, Joydev Mandal, Murali Mohan Banerjee, and Subhash Ghosh motivated me towards choosing a career in science over the commonly chosen engineering discipline. After I joined Jadavpur University for my undergraduate studies, the lectures of Narayan Banerjee, Soumitra Sengupta turned out to be sources of great inspiration. I met Kamales Kar, Abhijit Chakraborty of Saha Institute of Nuclear Physics during this time. They allowed me to visit the institute libraries to access the different international journals available there and motivated me greatly towards a career in research. I am grateful to Dr. Sreerup Roychoudhury for all the helpful discussions during my IIT days. I learned a great deal during a brief period of working with Dr. Rajesh Gopakumar. His clarity in the understanding of different topics in physics, was awe-inspiring to me. Learning quantum field theory basics from him was truly a great opportunity. After joining PennState, I enjoyed the lectures by Prof. John Collins and Prof. Jainendra Jain very much. I hope I can continue building upon the foundation my teachers initiated in me.

I consider myself fortunate to work with my advisor Prof. Gerald Mahan. He has always been very encouraging and supportive towards me. His appreciative comments always used to boost my confidence and helped me stay motivated. It was a real pleasure talking to him and hear the background stories about the topic of interest. His vastness of knowledge sets a model for me, which I hope to acquire sometime in my life. I am thankful to Prof. Jainendra Jain for the numerous discussions we had over the years. He was always very approachable and provided some critical insight which would later encourage me to think deeply about the topic of discussion. I feel fortunate to receive his guidance during my study. I would like to thank Prof. Jorge Sofo, for the great many hours he spent with me discussing about the oxide-water system. I have learned many things from him

within a short time.

I am thankful to Dr. Richard Robinett and the Physics department for giving me the teaching support over all the years of my graduate study. I specially grateful to Dr. Stephen Van Hook and Mr. Paul Lucas for providing me with the recommendation when I badly needed it. I would like to thank Mr. John Hopkins for allowing me to have the flexibility in the teaching duty during the last few months of thesis writing.

I feel blessed to have great friends, who helped me go through the worst of the days. I could not have made it without the constant support of Swayamjit Ray, Sreejith Ganesh Jaya, Anusha Gullapalli, Ketia Shoemaker, Carmen and last but not least, Lakshmi Anand, during the last few years. Association with Piali Aditya, Shivakumar Jolad, Christian Cruz, Sumithra Surendralal, Ashley Dasilva, Nitin Kumar, Meenakshi Singh, Nitesh Kumar, Aruna Kesavan, George Paily at Department of Physics, made the graduate school experience quite pleasurable. I would like to thank Kanika Vyas, Bhavana Achary, Rini Ghosh and Tanushree Dutta for supporting me during the tough times. Thank you to Sunando Roy, Somesh Roy, Simanti Banerjee, Josh West, Ross Martin, Katherine Staab for the fun times.

Music has always been a source of support for me and has brought me in touch with some great friends. I would like to thank my teacher Arijit Mahalanabis for sharing the great treasure of hindustani classical music with me. I would also like to thank my music group friends, specially Dr. Murali Haran, Lakshmi Anand, Piyush Thakre, Benedict Samuel, Neela Yennawar, Shankar Shastry, Umamahesh Srinivas, for being there with me and making the meetings such a great source of joy. I specially thank Dr. Latha Bhushan and Dr. Bhushan Jayarao for their continuous support.

Lastly, and most importantly, I would like to thank my parents. My mother is my first teacher and she has been a constant source of inspiration for me. My father provided me with great support, always, whenever I needed. Their unconditional love and trust made it all possible for me.

Dedication

To my Mother,

for being the constant source of inspiration

To my Father,

for the unconditional love and support

Chapter 1

Introduction

Transport phenomena are ubiquitous in nature and facilitate all physical transformations in the universe. A comprehensive understanding of Nature cannot be achieved without a thorough knowledge of the concepts encompassed in transport phenomena. Transport of energy, mass and momentum play an important role in a variety of natural processes. Transport, alongwith other physical and chemical processes leads to formation of fascinating structures, ranging from nanoscale structures to new geographical landscapes. The transport of energy between the sun and the earth drives the seasonal change in the weather. The synthesis of DNA and proteins within cells requires the transport of energy and necessary ingredients to the relevant sites. Transport facilitates supply of nutrients and removal of waste products at the cellular level and also, at a macroscopic level in all organic systems. Ionic transport between the neurons is key to the proper functioning of brains of animals. In short, transport phenomena involve all aspects of physical changes in the universe and are fundamental to the success of life on the earth.

Generally speaking, transport phenomena involve all situations when a physical system undergoes some transformation by transferring information with external systems. This transfer is usually carried out by particles characteristic to the system and the physical parameters involved in the transformation. Examples of such carriers are electrons, photons, phonons, and molecules and the examples of the physical parameters are mass, energy, and momentum.

1.1 Transport in Microscopic Systems

The characteristic length scales of the materials synthesized are becoming increasingly small with the advances in experimental techniques. Many of these microscopic structures found their places in important commercial applications, while research is going on toward finding materials with even smaller length scales. Examples of some of these structures are nanocomposites, semiconductor quantum dots, and superlattices. Examples of applications include microelectromechanical sensors, microelectronic and optoelectronic devices, and integrated circuit chips. The thermal loads imposed on these devices and structures create a major obstacle toward their applicability. This challenge is driving a renewed interest among researchers from various disciplines, toward the topic of thermal management. Investigations are going on to find ways to carry away heat from these small scale structures more effectively. The size of the microstructure poses a greater concern, because many times the size of the microstructure is comparable to the characteristic length scales of the heat carriers in the system. Hence, researchers are not only in the pursuit of devices with more efficient thermal management, but also focused toward better understanding of the underlying physical mechanisms [10].

1.1.1 Low-Dimensional Systems: Effect of Nonlinearity

The investigation of heat transport in solids has a history of more than two hundred years, dating back to the proposition of Fourier's law. This law asserts that close to equilibrium, the thermal flux is proportional to the gradient of temperature,

$$\mathbf{J}_Q = -\kappa \nabla T, \tag{1.1}$$

where the heat flux $\mathbf{J}_Q$ is the amount of heat transported through an unit surface per unit time, ∇T is the local temperature gradient and the proportionality constant κ is the thermal conductivity, an intensive variable, independent of the size of the system. Fourier's law explains the diffusion of thermal energy through the system, which is referred to as the "normal transport" of heat in the literature [11]. The diffusive nature of thermal transport can be understood in terms of the motion of the heat carriers at the microscopic level. Electrons, lattice vibrations

(phonons), atoms and molecules are the main carriers of thermal energy in the solid. These carriers suffer random collisions while moving through the solid and thermal energy diffuses through the system.

Fourier's law is successful in providing an accurate description of heat transport phenomena in three-dimensional systems. However, this is a phenomenological law and there is no rigorous derivation of this law starting from a microscopic Hamiltonian description. This conceptual issue has motivated a large number of investigations on heat transport in model systems ([12], [13], [14]). An important and surprising conclusion that emerges from these studies is that the thermal conductivity in some of these low dimensional model systems, is divergent [15]. Numerous studies have sought to understand the mechanisms of heat transport in classical low dimensional systems [14]. Toda [15] showed that in classical disordered systems, the thermal conductivity is enhanced by the introduction of anharmonicity. A particularly important discovery that highlighted the role of nonlinearity in one-dimensional heat transport was led by Fermi, Pasta and Ulam (FPU). A series of computer experiments revealed that the time evolution of a one-dimensional chain of coupled nonlinear classical oscillators, does not evolve towards equipartition but instead tend to return to the initial state ([16], [17], [18]). The FPU-like systems brought the issue of "anomalous" heat transport into focus and since then, a large number of investigation revealed the complex interplay among nonlinearity, complete integrability, and deterministic chaos in these systems ([19], [20], [21]).

In recent years, the discovery of carbon nanotubes [22] and carbon nanowires [23] has attracted an increasing attention towards one-dimensional and quasi-one-dimensional systems. Studies reported an unusual high thermal conductivity for these systems [24]. This discovery not only renewed the interest in the theoretical investigation of low-dimensional systems but, created great promises for technological applications in microscopic systems as well.

1.1.2 Thermal Transport in Fluids

One of the most important challenges faced by technological developments in the microelectronic industry, is to control the temperature by carrying the heat away from these small scale structures effectively. This requires cooling agents with

high thermal conductivity. The concept of nanofluids is proposed to overcome the shortcomings of some of the conventional heat transfer materials ([25], [26]). The suspended particles alter the correlation between the fluid atoms and influence the transport properties of nanofluids. This in turn improves the heat transfer performance of these systems.

Thermal transport in fluids can also be described by Fourier's law Eq. (1.1), in the linear response regime. The thermal conductivity in a fluid varies with density and temperature. The mechanism behind heat transport is mainly because of the random collisions between moving atoms or molecules. In addition, fluid can also transport through self-diffusion, which does not involve transfer of energy via collisions. The structure of the fluid or the knowledge of the correlation between fluid atoms is crucial in the determination of the various transport properties of a fluid.

1.1.3 Transport Across Boundaries: Surface Physics

Physics at the interfaces is always unpredictable and fascinating. With the decrease in the system size, the interfaces between materials become increasingly important. When thermal energy is transported from one material to another, the temperature is not continuous at the interface between them. This thermal boundary resistance is called Kapitza resistance, named after Kapitza [27], who first discovered the thermal boundary resistance for metal - superfluid helium interfaces. The observations of thermal boundary resistance have been reported for various different materials ([28], [29], [30], [31], [32], [33]) afterwards.

The first theoretical model, known as the acoustic mismatch model (AMT) was proposed by Khalatnikov [34] (1952) to explain the origins of the thermal boundary resistance. The difference in the densities and sound speeds result in a mismatch in the acoustic impedances ($Z = \rho c$, ρ is the mass density and c is the speed of sound) between the two sides of the interface. The AMT model predicts the functional relationship between the phonon transmission and the acoustic impedances. The transmission coefficient t_{AB} for phonons in the side A, incident normal to the

interface with material B, would have the form:

$$\mathcal{T}_{AB} = \frac{4Z_A Z_B}{(Z_A + Z_B)^2}, \tag{1.2}$$

This model assumes that no scattering takes place at the interface. The alternative model, proposed by Schwartz [32] is known as the diffuse mismatch model (DMT). DMT assumes that all the phonons that are incident on the interface gets scattered, and the probability of scattering is directly proportional to the phonon density of states of the two opposite sides of the interface.

Both of these models explain the existence of the thermal boundary resistance but, they fail to give good estimates of thermal boundary resistance for real interfaces. One of the main reasons is that these models do not incorporate the structure of the interface in them. A great many studies have been carried out to investigate the effect of surface defects on the phonon transmission across the interface ([35], [36], [37]). A better theory was proposed by Young and Maris [38] and later modified by Mahan and Pettersson [39], for solid-solid interfaces. However, the theory for solid-fluid interfaces has not progressed as much. Some molecular dynamics calculations are reported ([40], [41], [42], [43], [44]), but work is still going on to formulate an analytical theory.

The dissertation is organized as follows. In Chapter 2, we discuss the transport in one-dimensional monatomic lattices with nonlinear interaction potential between the atoms. The discussion focuses on the spontaneous generation of solitons in the quartic lattice and the investigation of the properties of the solitons generated. Chapter 3 contains a study of the pair correlation in fluids. We review the integral equation techniques for the theoretical determination of pair distribution function of classical fluids and provide applications of these technique for different fluids. In Chapter 4, we discuss the scattering of phonons at several solid-solid model interfaces. In Chapter 5, we investigate the thermal transport at the interface between an ideal gas solid and an ideal gas fluid. A method is described here to evaluate the Kapitza resistance of the interface between a neutral insulating solid and a neutral fluid system. We provide an application of the method to obtain the thermal boundary resistance at the interface between solid Argon and liquid Neon.

Chapter 2

Transport in One-dimensional Nonlinear Systems

2.1 Introduction

A general approach to non-equilibrium phenomena is to define the transport coefficients through phenomenological constitutive equations. Close to equilibrium, energy transport in a solid is expressed through Fourier's law (Eq. (1.1)). It is found that Fourier's law is not obeyed for the case of one-dimensional lattices. The thermal conductivity diverges in the thermodynamic limit, as $N^{1/2}$ where N is the number of particles of the system [45]. In order to explain this behavior, it is speculated that the transport in one-dimensional systems is dominated by nonlinear phenomena. Toda showed that a nonlinear lattice has modes that have an infinite lifetime. This suggests that instead of treating the nonlinear interaction as perturbation to the harmonic system, we need to formulate a theory for transport in one-dimension which deals with the nonlinear interaction on its own.

2.1.1 Solitons

A soliton is a solitary wave, i.e. a spatially localized wave, with exceptional stability properties. The name, soliton, is chosen because of the reason that apart from having wave-like properties, a soliton also exhibits particle-like properties: it represents a local maximum in the energy density and it preserves its shape and

velocity when it moves, just like a particle does. Solitons are widely used to describe various phenomena across many disciplines of science, from hydrodynamic tsunamis and fiber optic communications to solid state physics and the dynamics of biological molecules.

John Scott Russell, a hydrodynamic engineer, in 1834 [46] reported the first observations of solitary waves on a canal near Edinburgh. Several years later, in 1895, Korteweg and de Vries [47] derived an equation to describe hydrodynamic solitons. This phenomenon made a comeback during a numerical experiment carried out by Fermi, Past and Ulam (FPU), in 1953, with one of the first computers at Los Alamos [16]. They observed that when energy is fed into a one-dimensional lattice of particles coupled to each other by an anharmonic potential, the anticipated equipartition of energy among the different modes of the lattice is not achieved. Instead, the supplied energy returns to the initial state. The solution to the FPU paradox was provided by Zabusky and Kruskal in terms of solitons, ten years later [48].

Solitons provide a very useful approach to describe the physics of a nonlinear system. It is efficient to approximately describe the physics of the system by the appropriate soliton solution and then consider the possible perturbations of the exact soliton solution to improve the theory. Moreover, it is now known that solitons can emerge spontaneously in a physical system in which some energy is fed in, even if the excitation does not match exactly the soliton solution [49]. The energy can be supplied as thermal energy or by an excitation with an electromagnetic wave or in the form of mechanical stress. It has been found that many physical system satisfy the criteria to sustain solitons, at least for some range of excitations. This means that if a system possesses the necessary properties to allow the existence of solitons, it is highly likely that any large excitation will indeed lead to their formation and this feature explains the interest of solitons in physics.

2.1.2 Role in Transport

The interest in solitons arises from their role in thermal transport in one-dimensional systems. Toda [15] first proposed that energy is mainly transported by solitons in nonlinear lattices, and showed that in the case of a lattice with exponential inter-

action, the heat flux in the isotopically disordered lattice is enhanced by the introduction of the nonlinearity. In recent years, heat conductivity in low-dimensional systems has attracted an increasing attention [45, 50, 51] due to the discovery of nanotubes and nanowires. In these studies [45], it has been speculated that solitonlike propagation is generically favored in one-dimensional systems. The study of solitons in one-dimensional nonlinear lattices would help better understand the heat transport in one-dimensional systems.

There have been numerous investigations on the lattice dynamics of quartic and other nonlinear lattices using different analytical [48, 52, 53, 54, 55, 56, 57, 58, 59, 60, 61, 62, 63] and numerical approaches [49, 64, 65, 66, 67, 68, 69, 70]. In these studies, the potential contains quadratic terms along with nonlinear cubic or quartic terms (Fermi-Pasta-Ulam or FPU problem). The quadratic term describes phonons on the lattices, which affect the existence and stability of solitons. In this chapter, we investigate the traveling solitons on a purely quartic lattice. Phonons do not exist in a pure quartic lattice and this would help us better understand the nature of solitons in one-dimensional nonlinear lattices. We generate the solitons in the quartic lattice with the application of various forcing functions and determine the properties of the solitons thus obtained.

2.2 One-Dimensional Quartic Lattice

Our discussion is limited to the type of lattice, whose potential energy between adjacent atoms contains a nonlinear quartic term,

$$V\left(Q_{j+1}, Q_j\right) = +\frac{K_4}{4}(Q_{j+1} - Q_j)^4, \tag{2.1}$$

where, $Q_j(t)$ is the displacement of an atom at site j at time t, and K_4 is the quartic spring constant.

2.2.1 Equations of Motion

The interactions between the first neighbors are sufficient for a general description of the classical vibrations on a one-dimensional lattice. Therefore, the general

equation of motion for the j^{th} atom in a quartic lattice consisting of N atoms is

$$m\frac{d^2}{dt^2}Q_j = -K_4\left[(Q_j - Q_{j-1})^3 + (Q_j - Q_{j+1})^3\right], \quad 2 \leq j \leq N. \tag{2.2}$$

The one-dimensional chain is considered to have free boundaries. The equations of motion for the end atoms of the chain are given by

$$m\frac{d^2}{dt^2}Q_1 = -K_4\left[(Q_1 - Q_2)^3\right], \tag{2.3}$$

$$m\frac{d^2}{dt^2}Q_N = -K_4\left[(Q_N - Q_{N-1})^3\right] \tag{2.4}$$

In order to write the above equation in a dimensionless form, a parameter τ is defined, that plays the role of time but has the dimensional unit of inverse distance, $\tau = t\sqrt{\frac{K_4}{m}}$. The equations of motion, Eq.s (2.2 - 2.4) become

$$\frac{d^2}{d\tau^2}Q_1 = -(Q_1 - Q_2)^3, \tag{2.5}$$

$$\frac{d^2}{d\tau^2}Q_N = -(Q_N - Q_{N-1})^3, \tag{2.6}$$

$$\frac{d^2}{d\tau^2}Q_j = -(Q_j - Q_{j-1})^3 - (Q_j - Q_{j+1})^3, \quad 2 \leq j \leq N. \tag{2.7}$$

The above equations are the primary starting point of further calculations. An interesting feature noted from the equations of motion is that if the equations Eq.s (2.5 - 2.7) for all the atoms are added together, some sum rules can be generated:

$$\sum_{j=0}^{\infty}\ddot{Q}_j(\tau) = 0, \tag{2.8}$$

$$\sum_{j=0}^{\infty}\dot{Q}_j(\tau) = v_0, \tag{2.9}$$

$$\sum_{j=0}^{\infty}Q_j(\tau) = v_0\tau. \tag{2.10}$$

2.2.2 Normal Modes of Quartic Lattices

In this part, we discuss the stationary solitons in the quartic lattices. The solution of Eq. (2.5-2.7) can be factored into a time part and a space part following the technique of Kiselev [71],

$$Q_j(t) = q_j a_0 cn(a_0\tau),\ \tau = t\sqrt{\frac{K}{m}} \tag{2.11}$$

The cnoidal function cn(u) is taken at $k^2 = 1/2$, where $d^2cn(u)/du^2 = -cn(u)^3$. The constant a_0 is an amplitude that factors out once the solution is inserted into Eqs. (2.5-2.7). The remaining part is left as the equations for the constants q_j

$$q_j = (q_j - q_{j-1})^3 + (q_j - q_{j+1})^3,\ 2 \leq j \leq N \tag{2.12}$$

Now, for $j = 1$, the first atom in the chain, Eq. (2.5) becomes

$$q_1 = (q_1 - q_2)^3. \tag{2.13}$$

The above equation can be solved for q_2,

$$q_2 = q_1 - (q_1)^{\frac{1}{3}}. \tag{2.14}$$

A similar equation can be written for q_3

$$q_3 = q_2 - (q_1 + q_2)^{\frac{1}{3}}. \tag{2.15}$$

The result can be generalized to any value

$$s_n = \sum_{j=1}^{n} q_j,\quad q_{n+1} = q_n - (s_n)^{\frac{1}{3}}. \tag{2.16}$$

The real root of a negative number is taken: $(-a)^{1/3} = -(a)^{1/3}$ if $a > 0$. Assuming that the center-of-mass of the chain does not move, we get

$$s_N = 0 \tag{2.17}$$

which is the eigenvalue condition. Since the chains have inversion symmetry, a simpler way to solve the normal vibrational modes is presented using the feature that the modes are either symmetric or antisymmetric. The technique depends upon whether the chain has an even or odd number of atoms.

1. if $N = 2M + 1$ is odd, then:

   - Antisymmetric solutions have the center atom with zero amplitude $q_{M+1} = 0$, which gives
   $$q_M^3 = s_M. \tag{2.18}$$
   - Symmetric solutions have $q_{M+1} \neq 0$. The eigenvalue condition can be used to write
   $$-\frac{q_{M+1}}{2} = s_M. \tag{2.19}$$

2. If $N = 2M$ is even, then:

   - Antisymmetric chains have $q_{M+l} = -q_{M+1-l}$, which gives the eigenvalue equation
   $$8q_M^3 = s_M. \tag{2.20}$$
   - Symmetric chains have $q_{M+l} = q_{M+1-l}$, so the eigenvalue equation needs to take only half of the chain into consideration.
   $$s_M = 0. \tag{2.21}$$

A table of solutions found using the above method is shown in Tab. 2.1. For larger values of N, only half of the displacements are shown, since symmetry dictates the others. For all values of N, N modes are found that are either symmetric or antisymmetric in nature. In each case, a positive value for q_1 is taken. The same set of solutions is obtained with a changed sign if a negative starting value is taken.

The stationary soliton solutions for the infinite chain found by Kiselev [71, 72] were localized, and certainly were neither symmetric nor antisymmetric with respect to the center of the chain. They were symmetric or antisymmetric with respect to local displacements. So there is no reason to expect that all solutions are symmetric or antisymmetric with the center of the chain. Therefore, to find

N	A/S	q_1	q_2	q_3	q_4
2	A	$1/\sqrt{8}$	$-1/\sqrt{8}$		
3	A	1	0	-1	
	S	$1/\sqrt{27}$	$-2/\sqrt{27}$	$1/\sqrt{27}$	
4	A	0.053	-0.323	0.323	-0.053
	A	1.936	0.690	-0.690	-1.936
	S	0.353	-0.353	-0.353	0.353
5	A	0.316	-0.365	0	
	A	3.161	1.693	0	
	S	0.0087	-0.197	0.376	
	S	0.687	-0.195	-0.985	
6	A	2×10^{-4}	-0.0583	0.3290	
	A	$1/\sqrt{8}$	$-1/\sqrt{8}$	$-1/\sqrt{8}$	
	A	4.673	3.001	1.028	
	S	1	0	-1	
	S	0.188	-0.385	0.197	
7	A	0.078	-0.349	0.298	0
	A	0.495	-0.296	-0.880	0
	A	6.471	4.608	2.378	0
	S	6.5×10^{-7}	-8.66×10^{-3}	0.1967	-0.3762
	S	0.350	-0.355	-0.187	0.390
	S	1.475	0.337	-0.882	-1.858

Table 2.1. Eigenvalues of Symmetric (S) and Antisymmetric (A) Vibrations of Chains of N Atoms

other solutions the eigenvalue condition Eq. (2.17) is used, which results in soliton solutions in longer chains. From here on, these kind of solutions will be called soliton solutions. For example, the following is a valid solution for $N = 6$:

$$q_1 = 0.05313, q_2 = -0.3228, q_3 = 0.3233, q_4 = -0.0538,$$
$$q_5 = 7.6 \times 10^{-4}, q_6 = -10^{-12} \tag{2.22}$$

The result resembles the first symmetric mode for $N = 4$, with the two atoms at the right end not moving much. The inverse is also a solution, with $q_1 = -10^{-7}$. There appears to be more solutions than the number of atoms. The first symmetric mode for $N = 3$ is also a soliton, since it strongly resembles the mode in $N = 3$, where $1/\sqrt{27} = 0.1925 \approx 0.1967$.

2.2.3 Traveling Solitons

Here, we discuss the traveling solitons in the quartic lattices. Our focus is to show the spontaneous generation of solitons in the lattice and to discuss the properties of the solitons thus generated. A forcing function of zero duration or an impulse is applied to one of the free ends of the chain of atoms to generate traveling solitons on the quartic lattice. The ends remain unclamped (are free to move) at all times, even after the application of the impulse.

The impulse can be mathematically represented by a delta function pulse, $f(\tau) = v_0\delta(\tau)$, here v_0 is the impulse strength and has the dimension of $[L]^3$. The application of the impulse is numerically modeled as follows: at $\tau = 0$, the displacements of the atoms are zero ($Q_j = 0, 1 \leq j \leq N$) and all the atoms, except the one at the end, are at rest, ($\dot{Q}_j = 0,\ 2 \leq j \leq N$). The end atom has an initial velocity, ($\dot{Q}_1 = v_0$), due to the application of the impulse. Mass of an atom, m and quartic spring constant, K_4 are chosen to have unit values throughout this investigation. The method of finite differences is used to solve the equations of motion, Eq.s (2.5-2.7) numerically.

Figure 2.1 shows the displacements of the atoms in time. They all move to the right a distance a_0 and stop. The sum rules mentioned in Eqs. (2.8-2.10) are obeyed in Fig. 2.1.

In order to find out the number of atoms in motion while the soliton propagates through the chain, number of atoms that have relative displacements greater than a chosen minimum value is counted. Reference [49] reports that only 3 atoms are in motion at all times. It is found here that the number of atoms in motion depends on the choice of the cut-off value for the minimum relative displacement. Table 2.2 shows the percentage of times number of atoms in motion for different choice of the minimum relative displacement. As can be seen from the table, for the choice of a lower minimum relative displacement, more number of atoms are in motion and vice versa. For most values of the cut-off, initially only one or two atoms are in motion while the soliton is in formation; once the soliton starts propagating, 3-4 atoms are in motion at all times.

Traveling solitons are found to exist in chains of atoms with free boundaries. If the atom farthest from the point of application of the impulse, is clamped in its position or is bound to a wall, soliton generation is not affected. If the atom at the

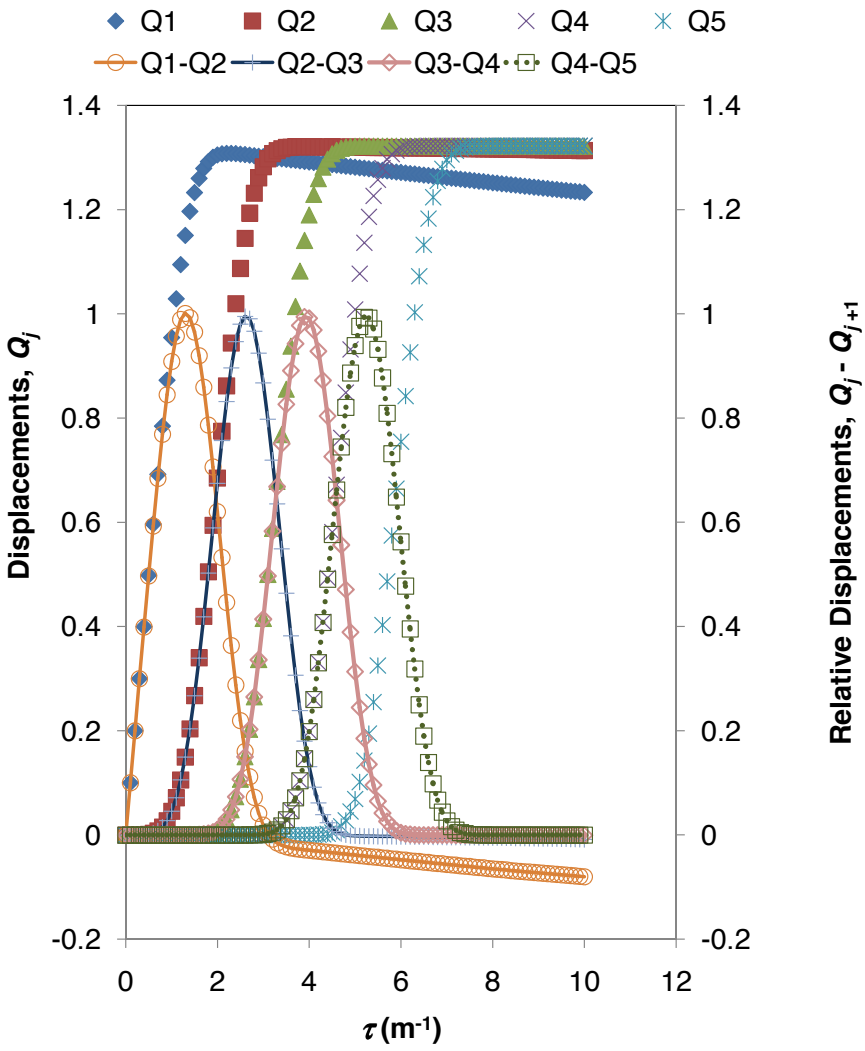

Figure 2.1. Generation of solitons on quartic lattice with delta function pulse; Impulse strength, $v_0 = 1$units; Lattice parameters, $K_4 = 1$, $m = 1$; Number of atoms in the chain, $N = 50$;

Min Rel. Displ. (Order)	Times different number of atoms-in-motion (%) 1	2	3	4	5
10^{-1}	2.12	46.73	51.05	0.00	0.00
10^{-2}	1.37	2.97	80.15	15.50	0.00
10^{-3}	0.87	2.65	39.6	56.88	0.00
10^{-4}	0.55	2.47	7.69	89.30	0.00
10^{-5}	0.35	2.25	4.87	69.41	23.13

Table 2.2. Percentage of times different number of atoms in motion during the propagation of the soliton through the chain

point of application is clamped in its position after the application of the impulse, a soliton is still generated but, its amplitude is comparable to the unclamped one only for a high impulse strength. On the other hand, if the atom at the point of application of the impulse is bound to a wall, the bound atom has an equation of motion,

$$\dot{Q}_1 = v_0, \tag{2.23}$$

$$\ddot{Q}_1 = -(Q_1 - Q_2)^3 - Q_1^3, \tag{2.24}$$

and

$$\ddot{Q}_j = -(Q_j - Q_{j+1})^3 - (Q_j - Q_{j-1})^3, \quad 2 \leq j \leq N. \tag{2.25}$$

A soliton can never be generated in this case, for any value of v_0. Instead, the atoms at the other end of the chain all continue to vibrate, and the effect of impulse is petered after a few atoms. However, a soliton is obtained for every value of v_0 for a chain with free boundaries.

2.2.3.1 Approximate Wave Form

The general solution for a traveling soliton can be written as

$$Q_j = a_0 f[vj - \omega(v)\tau], \tag{2.26}$$

where a_0 is the maximum displacement of the atoms in the chain or the amplitude of the soliton wave. The two parameters v and $\omega(v)$ can be treated as the "wave vector", and the "frequency" of the soliton wave respectively. It is a characteristics of quartic lattices that "frequency" parameter of the soliton wave depends on the amplitude a_0. Hence $\omega(v)$ can be written as $\beta(v)a_0$. Henceforth, the parameters v and β would be referred as the "wave vector" and "frequency" of the soliton solutions. It can be noted from Fig. 2.1 that the atoms displace smoothly to their final value with no ringing (except for the end atom). The wave form shown in Fig. 2.1 is approximately described by the formula

$$Q_j(\tau) = \frac{a_0}{2}[1 - \tanh(\phi_j)] \tag{2.27}$$

with

$$\phi_j = vj - \beta a_0. \tag{2.28}$$

This formula is a good but not perfect description of the soliton motion. Using the above form for the displacements of the atoms, the relative displacements between the atoms can be written as

$$q_j(\tau) = \frac{a}{(\cosh(vj - \beta a_0 \tau))^2}, \tag{2.29}$$

where, a is the maximum relative displacements of the atoms.

Reference [49] has given a formula for the soliton solutions of the FPU problem assuming that only three atoms are in motion at all times during the propagation of the soliton,

$$\begin{cases} q_j = \pm\frac{a}{2}[1 + \cos(\frac{2\pi}{3}j - \omega\tau)] & \text{if} \quad -\pi < \frac{2\pi}{3}j - \omega\tau < \pi, \\ q_j = 0 & \text{otherwise,} \end{cases} \tag{2.30}$$

and the relations for the frequency $\omega(v)$ and the velocity v are given as functions of a:

$$\begin{aligned} &\omega = \sqrt{3 + (45/16)a^2}, \\ &v_S = \omega/(2\pi/3) = 3\sqrt{3 + (45/16)a^2}/(2\pi). \end{aligned} \tag{2.31}$$

Reference [53] has reported an exact solution for the lattice waves in a quartic lattice with period of three lattice sites. The lattice wave has a cosine solution,

$$q_j = a\cos(\theta_j),\ \theta_j \equiv \frac{2\pi}{3}j - \omega_3\tau, \tag{2.32}$$

with

$$\omega_3^2 = \frac{9}{4m}a^2K_4 \tag{2.33}$$

These formula can be rewritten in the same way as mentioned in reference [49] to satisfy the soliton solutions in quartic lattice,

$$q_j = \frac{a}{2}[1+\cos(\frac{2\pi}{3}j - \omega_3\tau)] \quad \text{if} \quad -\pi < \frac{2\pi}{3}j - \omega\tau < \pi, \tag{2.34}$$

with

$$\omega_3^2 = \frac{9}{4m}a^2K_4.$$

A comparison between these analytical solutions Eq.s (2.29,2.30,2.34) and our numerical data is shown in Fig. 2.2. The numerical values of the relative displacements of the 20th atom in the chain are plotted against time along with the analytical values obtained using various formulas, [Eqs. (2.29, 2.30, 2.34)] in Fig. 2.2.

Now, an analytical solution for the displacements of the atoms of the period three lattice wave is given in reference [53],

$$Q_j = a_0\sin(\frac{2\pi}{3}j - \omega_3\tau - \frac{\pi}{3}). \tag{2.35}$$

This formula is modified in a similar fashion as in Eq. (2.34),

$$Q_j = \frac{a_0}{2}[1-\sin(\frac{2\pi}{3}j - \omega_3\tau - \frac{\pi}{3})], \quad -\frac{\pi}{2} < \frac{2\pi}{3}j - \omega_3\tau - \frac{\pi}{3} < \frac{\pi}{2}. \tag{2.36}$$

Analytical values are obtained using the above formula for atomic displacements for both $\omega = \omega_3$ and $\omega = \sqrt{3+(45/16)a^2}$. The analytical values obtained using the above analytical expressions Eqs. (2.27,2.36) are compared with numerical data of the displacements of the 20th atom in the chain and is shown in Fig. 2.3.

As can be noticed from both Fig. 2.2 and Fig. 2.3 that the form of the analytical

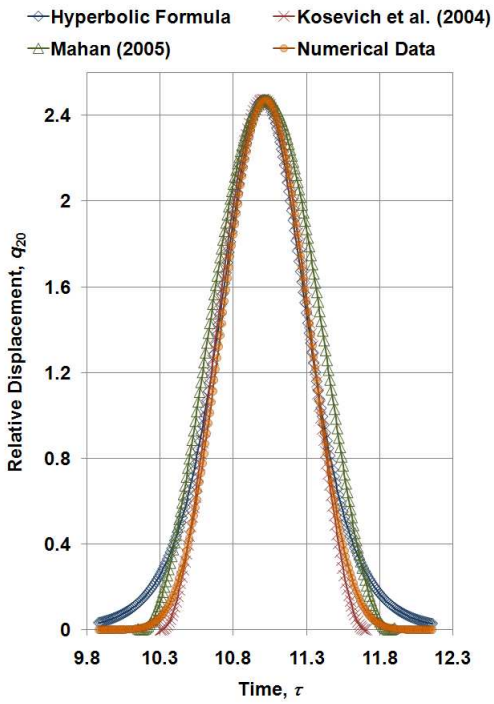

Figure 2.2. Comparison between the numerically and analytically obtained values of the relative displacements of the 20th atom

solutions reported in reference [53, 49] as well as our proposed solution match with that of the numerical data. The values obtained using the tanh solution match closely the data for the atomic displacements but, it doesn't match that well with the tails of the numerical relative displacements data.

2.2.3.2 Parameters of the Soliton

Using the approximate wave form given in Eqs. (2.27, 2.28), the soliton parameters (β, v) can be deduced from the numerical data in the following way. First, τ_j is defined as the value of time when the displacement of the j^{th} atom is half its maximum amplitude and $\phi_j(\tau_j) = 0$, $\tau_j = vj/\beta a_0$. A numerical derivative of $Q_j(\tau)$ is taken at $\tau = \tau_j$,

$$\frac{d}{d\tau}Q_j(\tau) = \frac{a_0^2\beta}{2\cosh(\phi_j)^2}, \tag{2.37}$$

$$(\frac{d}{d\tau}Q_j(\tau))_{\tau_j} = \frac{a_0^2\beta}{2}. \tag{2.38}$$

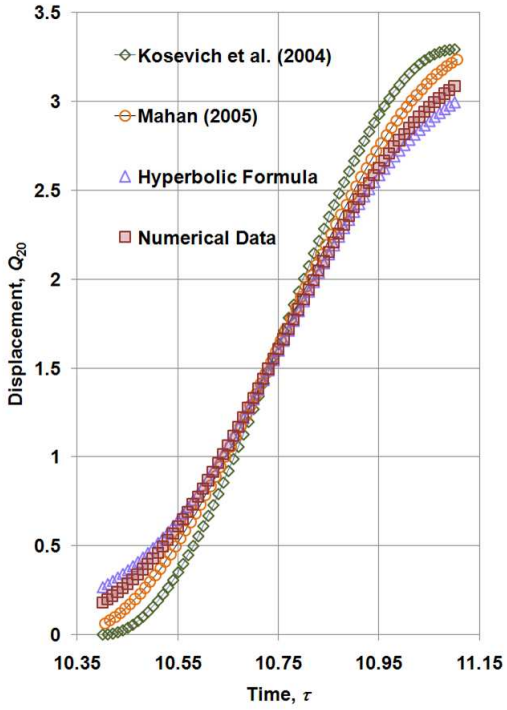

Figure 2.3. Comparison between the numerically and analytically obtained values of the displacements of the 20th atom

The slope is proportional to β. The other parameter v is obtained from the displacement of the $(j+1)^{th}$ atom at $\tau = \tau_j$,

$$Q_{j+1}(\tau_j) = \frac{a_0}{2}[1 - \tanh(v)], \tag{2.39}$$

$$v = \frac{1}{2}\ln[\frac{a_0}{Q_{j+1}(\tau_j)} - 1]. \tag{2.40}$$

The values of these parameters, obtained using the above Eqs. (2.38, 2.40) for some of the solitons, are shown in Tab. 2.3.

The values of the "frequency" parameters, β, obtained for the solitons generated above, are constant and not functions of a_0 or a. This is different from the cases described in reference [53, 49], where ω is a function of a_0. On the other hand, the values of "wave vector" parameters are constant like reference [53, 49], but, they are not equal to the "magic" wavenumber $2\pi/3$.

Now, the strength of a pulse is defined as the area under the curve of $f(\tau)$ vs. τ. In case of an impulse, the strength is simply v_0. The interesting part of the results

v_0	a_0	β	v
0.50	0.93	1.03	2.45
1.00	1.32	1.03	2.45
1.50	1.62	1.03	2.45
2.00	1.87	1.03	2.45

Table 2.3. Parameters of a soliton on the quartic lattice generated by an impulse v_0 on a free end.

shown in Tab. 2.3 is that β and v are independent of v_0, the impulse strength. The only parameter that depends upon v_0 is a_0, soliton amplitude. The relationship between the soliton amplitude and impulse strength can be understood in the following manner: Energy supplied to the lattice by an impulse is $E_{initial} = \frac{1}{2}mv_0^2$. Now, atoms gain energy as a result of the propagation of a soliton, both K.E and P.E. vary as $\approx K_4 a_0^4$. Hence, parameter a_0 is expected to vary as $a_0^4 \propto v_0^2$ or $a_0 \propto v_0^{1/2}$ from dimensional analysis. As can be noted from Tab. 2.3,

$$a_0 = 1.322\sqrt{v_0}, \tag{2.41}$$

which matches the expectation that soliton amplitude should have a square root relationship with the impulse strength.

Now, the maximum relative displacements between adjacent atoms, a, also behave in a similar manner, $a \sim \sqrt{v_0}$ (Fig. 2.4). Henceforth, the peak relative displacement, a would be referred to as soliton amplitude. The maximum relative displacements, a scale linearly with the maximum displacements, a_0; the relationship, as shown in Fig. 2.5, can be approximately described as $a_0 \approx (4/3)a$. As the soliton propagates through the lattice sites, the time it takes for the relative displacements to reach peak value, a, increase linearly. This relationship is utilized to obtain the velocity of soliton, v_S. Soliton velocities, v_S are also observed to have a square root relationship with impulse strength, $v_S \sim \sqrt{v_0}$. And the velocities scale linearly with the soliton amplitudes as shown in the inset of Fig. 2.4.

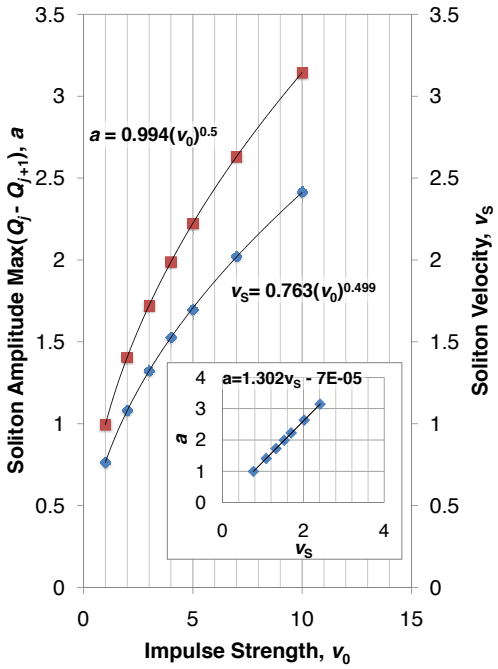

Figure 2.4. Power law relationship of soliton amplitude and soliton velocity with applied impulse strength, v_0; Inset: Soliton amplitude varies linearly with soliton velocity;

2.2.3.3 Stability of the Soliton

Stability of a soliton refers to its ability of maintaining its width and amplitude throughout propagation. The observation that only 3-4 atoms are in motion during soliton propagation, points toward the fact that the soliton is being able to maintain its width. Information about the amplitude can be obtained by comparing the peak values of the relative displacements, a at different lattice sites. Figure 2.6 shows the soliton amplitudes at different lattice sites for various impulse strengths, v_0. The amplitudes are almost constant at all the lattice sites irrespective of impulse strength. The constant value of the amplitudes indicates the formation of stable solitons on the quartic lattice irrespective of impulse strengths.

This result is compared with the solitons generated on a one-dimensional Toda

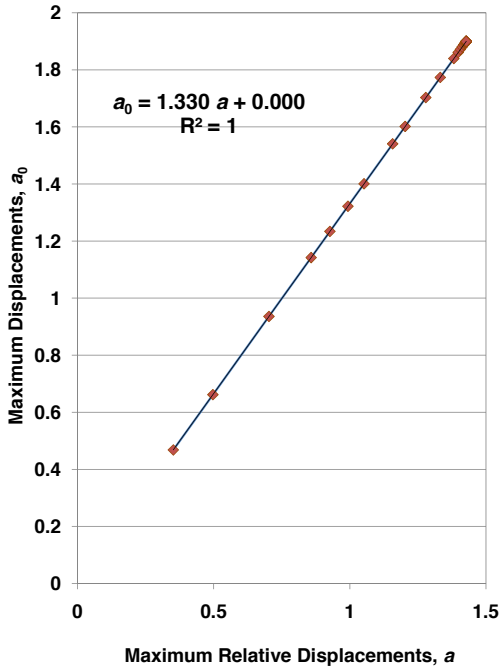

Figure 2.5. Linear relationship between maximum atom displacements and maximum relative displacements, $a_0 \approx (4/3)a$

lattice with interaction potential given by

$$V\left(Q_{j+1}, Q_j\right) = +\frac{a}{b}\exp(-b(Q_{j+1} - Q_j)) + a(Q_{j+1} - Q_j), \tag{2.42}$$

with the application of external impulses, as shown in Fig. 2.7. Soliton amplitudes at different lattice sites are shown in Fig. 2.8 for varied impulse strengths. For weak impulses, the amplitude of soliton decreases as the wave moves along the chain, but the amplitude remains almost constant for impulses beyond a critical strength. A stable soliton is produced on the Toda lattice only when the input impulse is beyond a critical strength. Similar behavior has been reported in literature for a chain of capacitors modeled as Toda lattice [73]. The explanation for this behavior is linked to the presence of phonons in Toda lattice which can be perceived from the oscillatory tail of the displacement-time plot (Fig. 2.7). Some of the energy

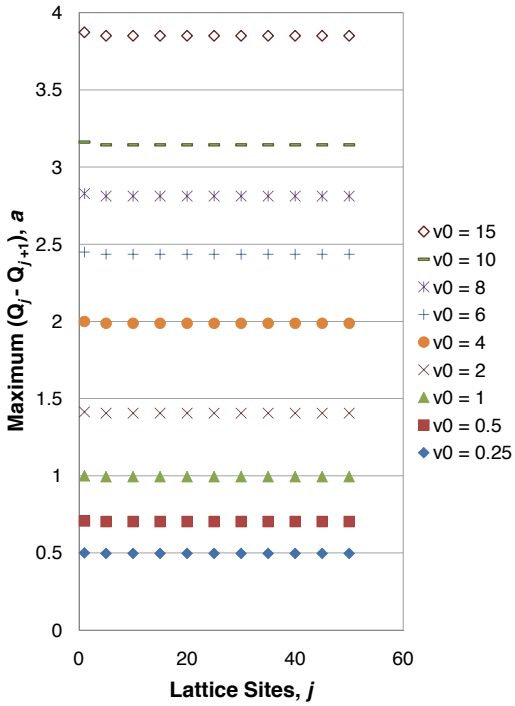

Figure 2.6. Peak relative displacements, a at different lattice sites for various impulse strengths, v_0; Soliton amplitudes are all same for different j showing the existence of stable solitons for all impulse strengths;

supplied to Toda lattice by the impulse is spent in the generation of phonons. Therefore, higher impulse strength is required to produce a stable soliton. In comparison, the energy supplied to the quartic lattice is used entirely for the generation of solitons. Hence, a stable soliton is generated on the quartic lattice for all impulse strengths.

2.2.4 Multiple Solitons

2.2.4.1 Pulse of Constant Height

The parameters (β, v) of solitons generated using an impulse, are found to be constants independent of impulse strengths. This observation motivated the study of generation of solitons using a different forcing function. A pulse of constant

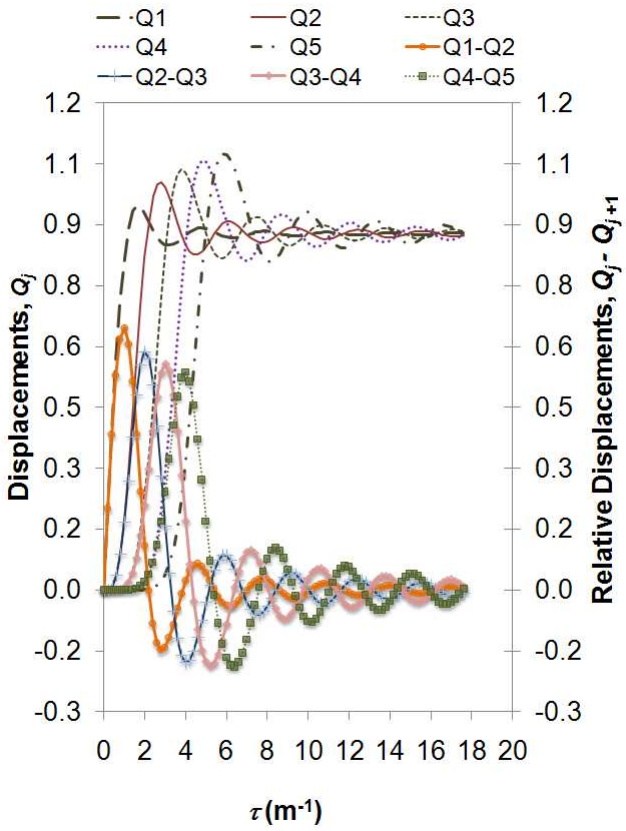

Figure 2.7. Generation of solitons on Toda lattice with constant impulse; Impulse strength, $v_0 = 1$ units; Toda lattice parameters $a = 1,\ b = 1$; Number of atoms in the chain $N = 50$;

height is applied to the free end of the chain for a finite amount of time, $f(\tau) = A\Theta(\tau)\Theta(T-\tau)$. The equations of motion can be written as

$$\dot{Q}_1 = A\tau, \tag{2.43}$$

$$\ddot{Q}_1 = -(Q_1 - Q_2)^3 + A\Theta(\tau)\Theta(T-\tau), \tag{2.44}$$

$$\ddot{Q}_j = -(Q_j - Q_{j+1})^3 - (Q_j - Q_{j-1})^3,\ 2 \le j \le N. \tag{2.45}$$

Here, the dimension of A is $[L]^3$ and that of T is same as τ. Numerical solutions of the above equations for $A = 1.5,\ T = 1$ are shown in Fig. 2.9. The presence of a second soliton can be discerned from the graph. It is interesting to note that when a delta function pulse is applied to the end atom, only one soliton travels

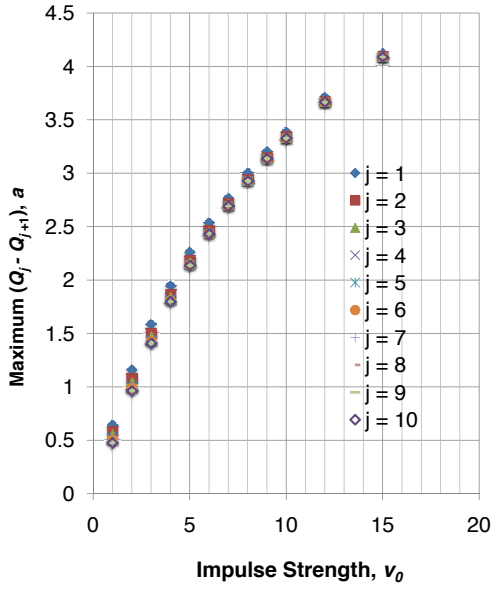

Figure 2.8. Variation of peak relative displacements of the soliton wave form in Toda lattice for different impulse strengths; For $v_0 \leq 10$, amplitude of soliton decreases as j increases, but it becomes constant for stronger impulses; A stable soliton is generated only when $v_0 \geq 10$.

down the chain for all pulse strengths. In contrast, a second soliton is observed to appear whenever strength of the constant-height pulse, $A \times T$ exceeds a threshold value. In an attempt to make sure that this phenomenon does not arise due to the finite size of the lattice, this numerical calculation is repeated for various chain lengths ($N = 50, N = 100, N = 200$). The critical pulse strengths are found to be the same for all chain lengths.

Now, pulse strength can be increased in two ways: (1) increasing pulse height keeping the width constant, (2) increasing pulse width keeping the height constant. Fig. 2.10 shows the minimum pulse height required to produce a second soliton in the chain as the width varied. The minimum pulse height required increases rapidly with decrease in pulse width. In fact, the relationship is observed to be

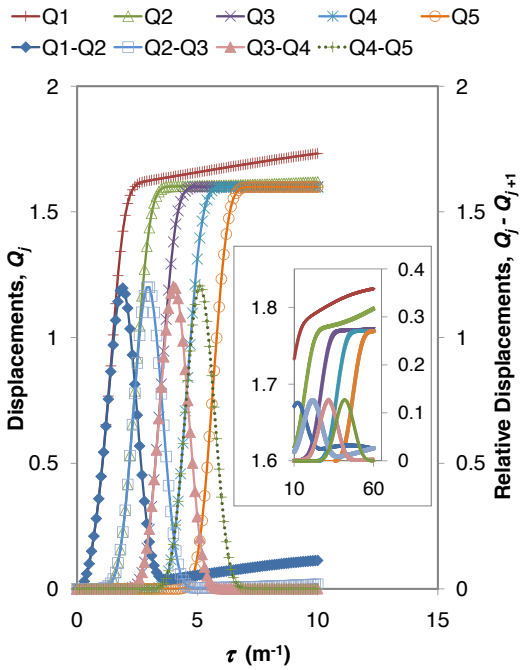

Figure 2.9. Multiple solitons generated on quartic lattice with pulse of constant height; Pulse strength $AT = 1.5$ units; Lattice parameters $K_4 = 1,\ m = 1$; Number of atoms in the chain $N = 50$; Inset: Second soliton in the chain;

$A \approx 1/T^3$. Hence, as $T \to 0,\ A \to \infty$ which explains why multiple solitons are never observed with a delta function pulse. On the other hand, the minimum pulse width required to generate a second soliton increases slowly as the pulse height is reduced as shown in the inset of Fig. 2.10. It can be concluded that it is easier to produce a second soliton by varying the width of forcing function keeping the height constant rather than varying the height keeping the width constant. Once the pulse strength is increased beyond the threshold value, more and more solitons are generated for increments of T keeping a constant pulse height.

Multiple soliton formation has also been observed on the Toda lattice (Fig. 2.11). The critical pulse strength required to produce a second soliton is higher than that of the quartic lattice which can be attributed to the presence of phonons on the Toda lattice. Due to the same reason, more energy is required to generate

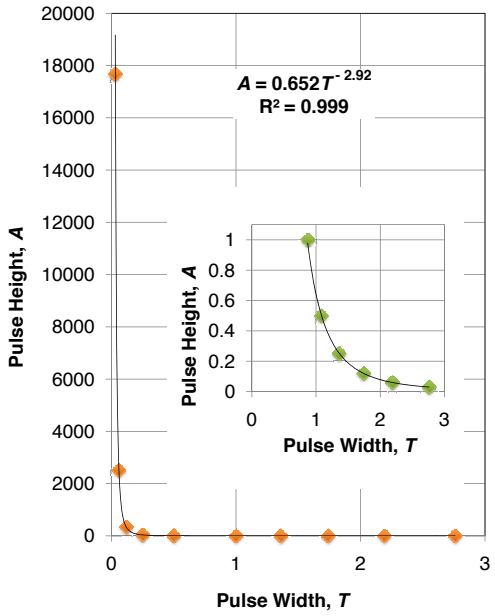

Figure 2.10. Minimum pulse height required to generate a second soliton as a function of pulse width; Inset: Minimum pulse height required for pulse width $T \gtrapprox 1$ units; Minimum pulse width does not increase significantly for small pulse heights;

a third soliton and the increment in energy has to be a fixed amount to generate successive solitons. Similar results were reported in Reference [73] for a chain of capacitors modeled as the Toda lattice.

2.2.4.2 Sinusoidal Pulse

The discovery of multiple solitons with pulse of constant height inspired the investigation of the effect of pulse shape on generation of solitons. A sinusoidal pulse ($f(\tau) = A\Theta(\tau)\Theta(\frac{T}{2} - \tau)\sin(\frac{2\pi\tau}{T})$) is applied to the end atom for half the period $T/2$,

$$\dot{Q}_1 = 0, \tag{2.46}$$

$$\ddot{Q}_1 = -(Q_1 - Q_2)^3 + A\sin(\frac{2\pi\tau}{T})\Theta(\tau)\Theta(\frac{T}{2} - \tau), \tag{2.47}$$

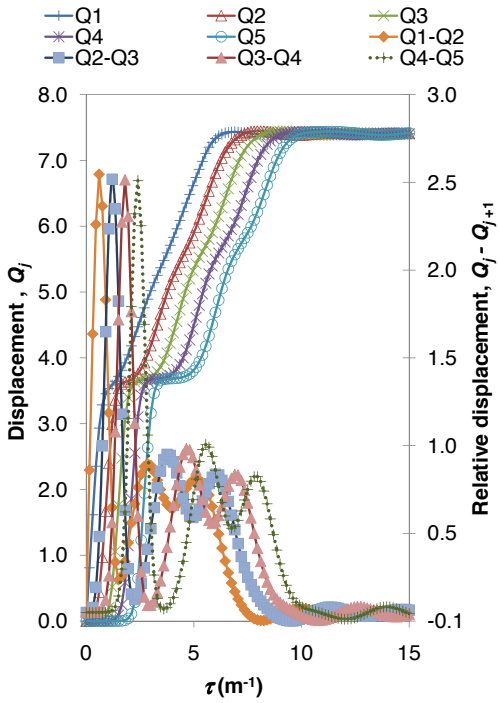

Figure 2.11. Multiple solitons generated in Toda lattice with pulse of constant height; Pulse strength $AT = 5.4$ units; Lattice parameters $a = 1,\ b = 1$; Number of atoms in chain $N = 50$;

$$\ddot{Q}_j = -(Q_j - Q_{j+1})^3 - (Q_j - Q_{j-1})^3,\ 2 \leq j \leq N. \tag{2.48}$$

Here also, A has dimension of $[L]^3$ and T that of τ. Strength of the pulse is given by $\frac{AT}{\pi}$. As the pulse strength is increased, multiple solitons are generated on the quartic lattice similar to the earlier case of pulse of constant height. It is also observed that a weaker pulse is capable of producing multiple solitons if the pulse strength is increased by broadening it rather than increasing the height. Once the second soliton appears in the chain for a critical pulse strength, more number of solitons appear for increments in pulse width as can be noted from Fig. 2.12. Therefore, it can be concluded that the generation of multiple solitons is independent of the pulse shape. Multiple solitons are always generated on the quartic lattice for pulse strength beyond a threshold value, given the pulse is

applied for a finite amount of time.

2.2.4.3 Parameters of Multiple Solitons

The parameters (β, v) are calculated for the multiple solitons, generated using both the sinusoidal pulse and the pulse of constant height. All of these multiple solitons are found to have parameters confined in a very narrow range of values, $\beta \rightarrow (1.02, 1.03)$ and $v \rightarrow (2.45, 2.50)$. Similar result is also obtained using a delta function pulse as shown in Tab. 2.3. Hence, it can be concluded that the parameters (β, v) of solitons generated on one-dimensional monatomic quartic lattice are independent of forcing functions. The other parameter, soliton amplitude, a, increases with the increase in pulse strength. The plot of a against pulse width is shown in Fig. 2.12. The interesting feature to note here is that the amplitudes of all the solitons smoothly increase towards a saturation value. The saturation of the soliton amplitudes with the increase in pulse width, and, the narrow range of (β, v) imply that the traveling solitons generated on the quartic lattice using a forcing function, is very specific in nature. It can be predicted from this findings that the energy of the solitons generated would have a upper bound, although this investigation is not included in this article. The distribution of energy among the multiple solitons is also left for future investigation.

2.3 Summary

A method to generate traveling solitons on a one-dimensional monatomic lattice with quartic interatomic potential is presented here. The method includes application of an external forcing function to one of the ends of a chain of atoms with free boundaries. This method of numerically generating solitons has been referred to as "sharp-pulse method" in literature [49]. As a result, the end atom attains a finite velocity and this movement causes a soliton to move down the chain. The solitons are observed to maintain their amplitudes and widths throughout propagation for all pulse strengths. The effect of varying pulse width and height on the parameters of solitons, (amplitude(a_0 or a), β, v) are investigated. The soliton amplitudes are found to have a square-root relationship with the pulse strength for a delta function pulse. As the pulse width increased keeping the pulse height con-

stant, a new phenomenon is observed when the pulse width is beyond a threshold value. Multiple stable solitons are observed to flow down the chain each maintaining their individual identity as they cross through one another. It is found that the pulse height needs to be excessively large in order to produce multiple solitons for smaller pulse widths. This explains the absence of multiple solitons when a pulse of zero width is used. The appearance of a second soliton in the chain is the onset of generation of more number of solitons. All of these solitons share a very small parameter space in β and v . The multiple solitons have the special property that the amplitudes saturate with the increase in pulse strength. The generation and properties of multiple solitons on the one-dimensional quartic lattice are found to be independent of the forcing function.

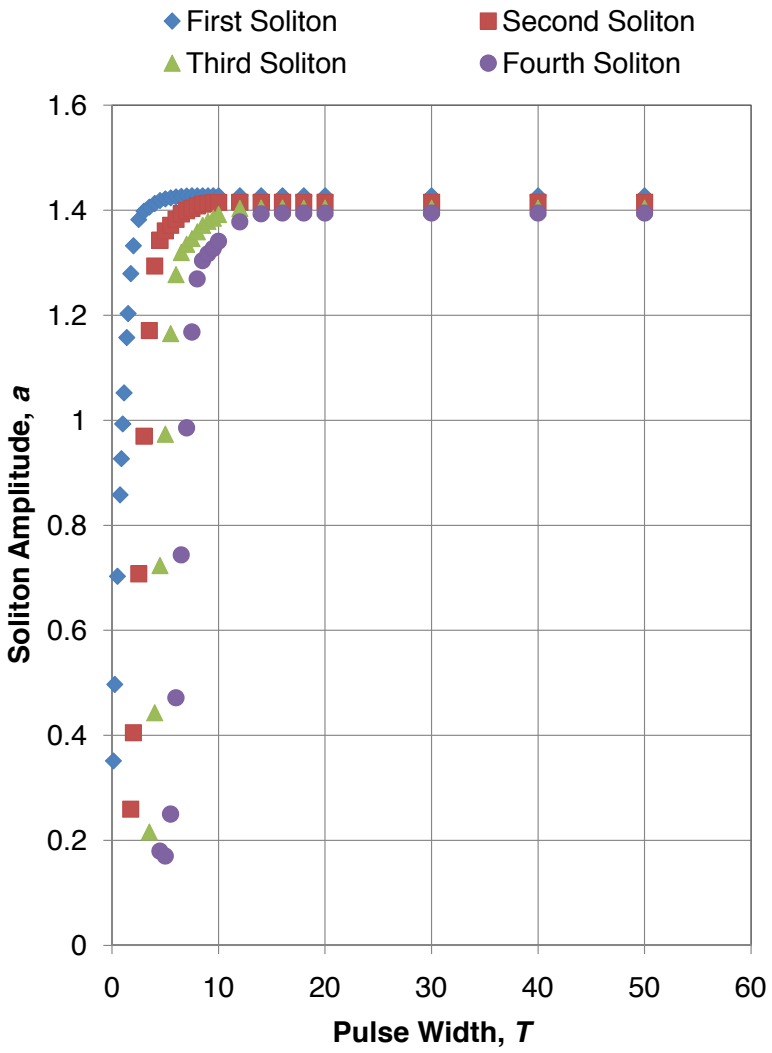

Figure 2.12. Multiple soliton amplitudes as a function of pulse width; Amplitudes tend to saturate with increase in pulse strength;

Chapter 3

Transport in Fluids: Study of Pair Distribution Function

3.1 Introduction

The physical systems of our interest often have great many degrees of freedom. It is difficult to formulate a theory, even an approximate theory, to describe such a system. The ultimate aim of such a theory is to provide quantitative information on the equilibrium properties of the physical system under consideration.

The knowledge of the probability densities and the distribution functions, help us determine the thermodynamic properties of a system under equilibrium conditions. Moreover, these functions provide a complete description of the microscopic structure of the system, and also provide a quantitative measure of the correlations between the positions of different particles. It is well known that the lowest-order distribution functions, the pair distribution function can describe most of the thermodynamic properties for classical fluids in thermal equilibrium.

The distribution functions play a very important role in determining the nature of the bulk excitations in the fluid. The knowledge of these excitations in the fluid is essential to understand transport in fluids. Hence, it is crucial that we investigate the nature of the distribution functions before formulating a transport theory involving fluids.

In this chapter, we review the integral equation techniques, namely the Percus-

Yevick method and the Hypernetted chain method, for determining the pair distribution functions for classical fluids. We apply these methods to obtain the pair distribution function for Lennard-Jones fluids. These methods can generate stable solutions only for fluids with densities and temperatures within a limited region. We provide a guide map of these region and comment on the application of these methods to obtain pair distribution function for a fluid with thermodynamic parameters within this specified region. This discussion would prove very useful when we discuss the thermal transport in fluids in Chapter 5. In the last part of the present chapter, we present a method to modify these theories for a quantum fluid and apply this modified theory to obtain several thermodynamic properties for Helium-4 fluid.

3.2 Relevant Expressions

3.2.1 Equilibrium Probability Densities

We consider a system of N identical particles in a volume Ω in thermal equilibrium at temperature T. The system Hamiltonian is given by

$$H_N = T_N + V_N. \tag{3.1}$$

The Hamiltonian is assumed to be the sum of a coordinate-independent kinetic energy and a momentum-independent potential energy,

$$T_N = \sum_{i=1}^{N} \frac{p_i^2}{2m},\ V_N = \frac{1}{2}\sum_{i\neq j} v(\mathbf{r}_i, \mathbf{r}_j). \tag{3.2}$$

The n-body probability density for the particles in the system, can be defined as,

$$\rho^{(n)}(\mathbf{r}_1, \mathbf{r}_2, \ldots \mathbf{r}_n) = \frac{N!}{(N-n)!}\langle \delta(\mathbf{r}_1 - \mathbf{r}_1') \ldots \delta(\mathbf{r}_n - \mathbf{r}_n')\rangle. \tag{3.3}$$

The average is taken in the grand canonical ensemble. Hence, we can also write the density as

$$\rho^{(n)}(\mathbf{r}_1, \mathbf{r}_2, \ldots \mathbf{r}_n)$$
$$= \frac{1}{\Xi} \sum_{N \geq n}^{\infty} \frac{z^N}{(N-n)!} \int \ldots \int \exp[-\beta V_N(\mathbf{r}_1, \mathbf{r}_2, \ldots \mathbf{r}_N)] d\mathbf{r}_{n+1} d\mathbf{r}_{n+2} \ldots d\mathbf{r}_N, \quad (3.4)$$

where $\beta = \frac{1}{k_B T}$, z is the activity, or fugacity parameter and Ξ is the grand canonical partition function, written as

$$\Xi = \sum_{N=0}^{\infty} \frac{z^N}{N!} \int \ldots \int \exp[-\beta V_N(\mathbf{r}_1, \mathbf{r}_2, \ldots \mathbf{r}_N)] d\mathbf{r}_1 d\mathbf{r}_2 \ldots d\mathbf{r}_N. \quad (3.5)$$

The n-body probability density is the probability of simultaneously finding any one of the n particles in the infinitesimal volume $d\mathbf{r}_1$ around $\mathbf{r}_1$, another particle in $d\mathbf{r}_2$ around $\mathbf{r}_2$, and so on, independent of the positions of the remaining $(N-n)$ particles.

In a noninteracting system of n particles, the two-body probability density attains the form, $\rho^{(2)}(\mathbf{r}_1, \mathbf{r}_2) = \rho^{(1)}(\mathbf{r}_1)\rho^{(1)}(\mathbf{r}_2) = \rho^2$. The deviation of the n-body probability density for the interacting system from that of the noninteracting system is known as Ursell function [74],

$$\mathcal{F}_2(\mathbf{r}_1, \mathbf{r}_2) = \rho^{(2)}(\mathbf{r}_1, \mathbf{r}_2) - \rho^{(1)}(\mathbf{r}_1)\rho^{(1)}(\mathbf{r}_2). \quad (3.6)$$

This function is a measure of the strength of interaction in the system. The normalization relation for the probability density is given by

$$\int \rho^{(n)}(\mathbf{r}_1, \mathbf{r}_2, \ldots \mathbf{r}_n) d\mathbf{r}_1 d\mathbf{r}_2 \ldots d\mathbf{r}_n = \langle \frac{N!}{(N-n)!} \rangle. \quad (3.7)$$

The normalization condition Eq.(3.7), when applied to one-particle and two-particle probability density gives

$$\int \rho^{(1)}(\mathbf{r}) d\mathbf{r} = N, \quad (3.8)$$

and

$$\int \int \rho^{(2)}(\mathbf{r}_1, \mathbf{r}_2) d\mathbf{r}_1 d\mathbf{r}_2 = \langle N^2 \rangle - \langle N \rangle, \quad (3.9)$$

respectively. Hence, the normalization relation for the deviation, Ursell function

is given by:

$$\int\int[\rho^{(2)}(\mathbf{r}_1,\mathbf{r}_2)-\rho^{(1)}(\mathbf{r}_1)\rho^{(1)}(\mathbf{r}_2)]d\mathbf{r}_1d\mathbf{r}_2=\langle N^2\rangle-\langle N\rangle-\langle N\rangle^2. \tag{3.10}$$

The above Eq. (3.10) shows that the relative mean square deviation of particle number in a specific volume is

$$\frac{\langle N^2\rangle-\langle N\rangle^2.}{\langle N\rangle.}=1+\frac{1}{\langle N\rangle}\int\int\mathcal{F}_2(\mathbf{r}_1,\mathbf{r}_2)d\mathbf{r}_1d\mathbf{r}_2. \tag{3.11}$$

3.2.2 Equilibrium Distribution Functions

In order to introduce the concept of the equilibrium distribution functions, let us consider the limiting case when the interparticle separations are large. In this limit, the positions of the particles become independent of each other and the correlation between the positions of the particles decreases. Consequently, the n-particle probability density factorizes into the product of n one-particle probability densities:

$$\rho^{(n)}(\mathbf{r}_1,\mathbf{r}_2,\ldots\mathbf{r}_n)\approx\rho^{(1)}(\mathbf{r}_1)\rho^{(1)}(\mathbf{r}_2)\ldots\rho^{(1)}(\mathbf{r}_n). \tag{3.12}$$

This factorization can be utilized to define a dimensionless n-particle distribution function,

$$g^{(n)}(\mathbf{r}_1,\mathbf{r}_2,\ldots\mathbf{r}_n)=\frac{\rho^{(n)}(\mathbf{r}_1,\mathbf{r}_2,\ldots\mathbf{r}_n)}{\prod_{i=1}^{n}\rho^{(1)}(\mathbf{r}_i)}. \tag{3.13}$$

For a uniform system under equilibrium, the properties of the system are translationally invariant and the one-particle probability density, $\rho^{(1)}(\mathbf{r})$, is a constant ($\frac{N}{V}=\rho$), independent of position. For a homogeneous system, the above equation becomes,

$$g^{(n)}(\mathbf{r}_1,\mathbf{r}_2,\ldots\mathbf{r}_n)=\frac{1}{\rho^n}\rho^{(n)}(\mathbf{r}_1,\mathbf{r}_2,\ldots\mathbf{r}_n). \tag{3.14}$$

Using the definition of n-body probability density Eq. (3.4), and setting $N-n=p$, we can obtain a general expression for the n-particle distribution function:

$$\begin{aligned}&g^{(n)}(\mathbf{r}_1,\mathbf{r}_2,\ldots\mathbf{r}_n)\\&=\frac{z^n}{\rho^n\Xi}\sum_{p\geq0}^{\infty}\frac{z^p}{p!}\int\ldots\int\exp[-\beta V_{n+p}(\mathbf{r}_1,\mathbf{r}_2,\ldots\mathbf{r}_{n+p})]d\mathbf{r}_{n+1}d\mathbf{r}_{n+2}\ldots d\mathbf{r}_{n+p},\end{aligned} \tag{3.15}$$

and specifically, for the the two-particle distribution function:

$$g^{(2)}(\mathbf{r}_1, \mathbf{r}_2) = \frac{z^2}{\rho^2 \Xi} \sum_{p \geq 0}^{\infty} \frac{z^p}{p!} \int \dots \int \exp[-\beta V_{p+2}(\mathbf{r}_1, \mathbf{r}_2, \dots \mathbf{r}_{p+2})] d\mathbf{r}_3 d\mathbf{r}_4 \dots d\mathbf{r}_{p+2}. \quad (3.16)$$

As we mentioned in the introduction of this chapter, the two-particle distribution function is known to describe most of the thermodynamic properties of classical fluids in equilibrium. The rest of this chapter is devoted to the discussion of the techniques to obtain this function for classical fluids. We need to introduce some more expressions before going into that discussion. In terms of the two-particle distribution function, the two-particle probability density becomes,

$$\rho^{(2)}(\mathbf{r}_1, \mathbf{r}_2) = \rho^2 g(\mathbf{r}_1, \mathbf{r}_2) \quad (3.17)$$

and the Ursell function becomes $\mathcal{F}_2(\mathbf{r}_1, \mathbf{r}_2) = \rho^2[g(\mathbf{r}_1, \mathbf{r}_2) - 1]$.

If the system is isotropic, the two-particle distribution function or the pair distribution function is a function of relative coordinates alone,

$$g^{(2)}(\mathbf{r}_1, \mathbf{r}_2) = g(|\mathbf{r}_1 - \mathbf{r}_2|). \quad (3.18)$$

The quantity $g(r)$ is called the radial distribution function. In the limiting case of a dilute gas, $\rho \to 0$, $z \to 0$ with $\rho/z \to 1$ and $\Xi \to 1$; the only term that contribute to the sum in the RHS of Eq. (3.16) is the first term with $p = 0$:

$$g^{(n)}(\mathbf{r}_1, \mathbf{r}_2, \dots \mathbf{r}_n) \underset{\rho \to 0}{\sim} \exp[-\beta V_n(\mathbf{r}_1, \mathbf{r}_2, \dots \mathbf{r}_n)]. \quad (3.19)$$

For a system of particles interacting through pairwise central forces, that is, when the potential energy is of the form,

$$V_N = \frac{1}{2} \sum_{i \neq j}^{N} v(|\mathbf{r}_i - \mathbf{r}_j|), \quad (3.20)$$

the radial distribution function can be approximated as

$$g(r) \underset{\rho \to 0}{\sim} \exp[-\beta v(r)]. \tag{3.21}$$

3.2.3 Relations with thermodynamic quantities

There exist simple expressions for various thermodynamic quantities in terms of the pair distribution function. The expression for internal energy per particle, u is given by

$$\beta u = \frac{3}{2} + \frac{1}{2}\rho \int d\mathbf{r} v(\mathbf{r}) g(\mathbf{r}), \tag{3.22}$$

and the virial pressure relation reads as:

$$\frac{\beta P}{\rho} = 1 + \frac{\rho}{6} \int d\mathbf{r} e^{\beta v(\mathbf{r})} g(\mathbf{r}) \mathbf{r} \cdot \nabla e^{-\beta v(\mathbf{r})}. \tag{3.23}$$

The Ornstein-Zernike compressibility formula is given by

$$\frac{\partial \rho}{\partial \beta P} = 1 + \rho \int d\mathbf{r} [g(\mathbf{r}) - 1]. \tag{3.24}$$

3.3 Integral equation theories for pair distribution functions

The integral equation theories for the pair distribution function of a homogeneous fluid is derived by an elegant method, first proposed by Percus([74],[75]) and later extended by various researchers during 1960's and 70's ([76], [77], [78], [79], [80], [81]). The derivation involves an analysis of systems with inhomogeneity. The inhomogeneity is artificially introduced to the homogeneous system, by fixing some of the particles at the desired positions and subjecting the remaining particles to the force field created by these fixed particles.

Lets consider a system with $(m + n)$ particles, where m of them are fixed and the n remaining particles move in the external potential created by these fixed particles. The positions of the fixed particles are denoted as $\mathbf{x}_i$ with $i = 1, \ldots m$. The form of the inter-particle potential is given in Eq. (3.2) and the imposed

external potential is given by

$$V = \frac{1}{2}\sum_{i\neq j} v(\mathbf{r}_i, \mathbf{r}_j),\ U(\mathbf{r}) = \sum_{i=1}^{m} v(\mathbf{r}, \mathbf{x}_i). \tag{3.25}$$

As we "turn on" the inhomogeneity, the distribution of particles in the system is affected. The starting point of the derivation is to establish a relationship between the n-particle distribution function of the system with this imposed external potential $\rho^{(n)}(\mathbf{r}_1, \mathbf{r}_2, \ldots \mathbf{r}_n|U)$, with that of a regular system without this constraint $\rho^{(m+n)}(\mathbf{x}_1, \mathbf{x}_2, \ldots \mathbf{x}_m; \mathbf{r}_1, \mathbf{r}_2, \ldots \mathbf{r}_n)$. It can be shown that [74]

$$\frac{\rho^{(m+n)}(\mathbf{x}_1, \mathbf{x}_2, \ldots \mathbf{x}_m; \mathbf{r}_1, \mathbf{r}_2, \ldots \mathbf{r}_n)}{\rho^{(m)}(\mathbf{x}_1, \mathbf{x}_2, \ldots \mathbf{x}_m)} = \rho^{(n)}(\mathbf{r}_1, \mathbf{r}_2, \ldots \mathbf{r}_n|U). \tag{3.26}$$

For example, for a system with two particles, one of them fixed, we get $\frac{\rho^{(2)}(\mathbf{x};\mathbf{r})}{\rho^{(1)}(\mathbf{x})} = \rho^{(1)}(\mathbf{r}|U)$. This statement says that the two-particle distribution function is the same as one-particle distribution in the presence of an external potential, which is almost trivially true.

As we are gradually turning on the external field $U(\mathbf{r})$, the density of the system changes from its original value $\rho_0(\mathbf{r})$ to $\rho(\mathbf{r})$. We can treat this imposed external potential as perturbation and expand any function in a series in the difference $(\rho(\mathbf{r}) - \rho_0(\mathbf{r}))$. The expansion of $\rho(\mathbf{r})e^{\beta U(\mathbf{r})}$ yields

$$\begin{aligned}\rho(\mathbf{r})e^{\beta U(\mathbf{r})} = \rho_0(\mathbf{r})e^{\beta U(\mathbf{r})} \times [1 + \int c_2(\mathbf{r}, \mathbf{r}_1)|_0(\rho(\mathbf{r}_1) - \rho_0(\mathbf{r}_1))d\mathbf{r}_1 \\ + \frac{1}{2}\int\int (c_3(\mathbf{r}, \mathbf{r}_1, \mathbf{r}_2) - c_2(\mathbf{r}, \mathbf{r}_1)c_2(\mathbf{r}, \mathbf{r}_2))|_0 \\ \times (\rho(\mathbf{r}_1) - \rho_0(\mathbf{r}_1))(\rho(\mathbf{r}_2) - \rho_0(\mathbf{r}_2))d\mathbf{r}_2 + \ldots].\end{aligned} \tag{3.27}$$

where $c(\mathbf{r}, \mathbf{r}')$ known as the direct correlation function and defined by the relation

$$\frac{\delta(-\beta U(\mathbf{r}))}{\delta\rho(\mathbf{r}')} \equiv \frac{1}{\rho(\mathbf{r}')}\delta(\mathbf{r} - \mathbf{r}') - c(\mathbf{r}, \mathbf{r}'). \tag{3.28}$$

The direct correlation function represents the effect of a density change due to a change in external potential and is related to the pair distribution function by the

following formula

$$g(\mathbf{r},\mathbf{r}'')-1=c(\mathbf{r},\mathbf{r}'')+\int c(\mathbf{r},\mathbf{r}')\rho(\mathbf{r}')(g(\mathbf{r}',\mathbf{r}'')-1)d\mathbf{r}'. \tag{3.29}$$

A detailed derivation of the above relation can be found in standard texts ([82]). We assume $U(\mathbf{r})=0$ and $\mathbf{x}$ is chosen to be at origin. Identifying $\rho(\mathbf{r})$ and $\rho_0(\mathbf{r})$ of the above equation (Eq. (3.27)) as $\rho^{(1)}(\mathbf{r}|U)$ and $\rho^{(1)}(\mathbf{r})$, respectively, and using the relation between them Eq. (3.13), we obtain

$$\rho^{(1)}(\mathbf{r})g(\mathbf{r})e^{\beta v(\mathbf{r})} \quad = \quad \rho^{(1)}(\mathbf{r}) \ + \ (\rho^{(1)}(\mathbf{r}))^2\int c_2(\mathbf{r},\mathbf{r}_1)\,|_0\,(g(\mathbf{r}) \ - \ 1)d\mathbf{r}_1. \tag{3.30}$$

Comparing Eq. (3.29) with Eq. (3.30), we find

$$c(\mathbf{r})=(1-e^{\beta v(\mathbf{r})})g(\mathbf{r}), \tag{3.31}$$

which is the basic expression of the Percus-Yevick (PY) equation. Eliminating $c(\mathbf{r})$ from Eq. (3.30) we can also write PY equation for a uniform system as

$$g(\mathbf{r})e^{\beta v(\mathbf{r})}=1+\rho\int(g(\mathbf{r}-\mathbf{r}')-1)(1-e^{\beta v(\mathbf{r}')})g(\mathbf{r})d\mathbf{r}'. \tag{3.32}$$

A similar procedure can be followed to obtain the integral form of the Hypernetted-chain equation (HNC):

$$\log g(\mathbf{r})+\beta v(\mathbf{r})=\rho\int\left[g(\mathbf{r}-\mathbf{r}')-1\right]\left[g(\mathbf{r}')-1-\log g(\mathbf{r}')-\beta v(\mathbf{r}')\right]d\mathbf{r}'. \tag{3.33}$$

The functional of choice to be expanded is $\log\left[\frac{\rho^{(1)}(1|\phi)}{z^*(1)}\right]$. Comparing with Eq. (3.29) we note that the direct correlation function in HNC theory is given by

$$c(\mathbf{r})=g(\mathbf{r})-1-\beta v(\mathbf{r})-\log[g(\mathbf{r})]. \tag{3.34}$$

Both the equations show correctly that $g(r)\sim\exp[-\beta v(r)]$ in the limit $\rho\to 0$ in accordance with Eq. (3.21).

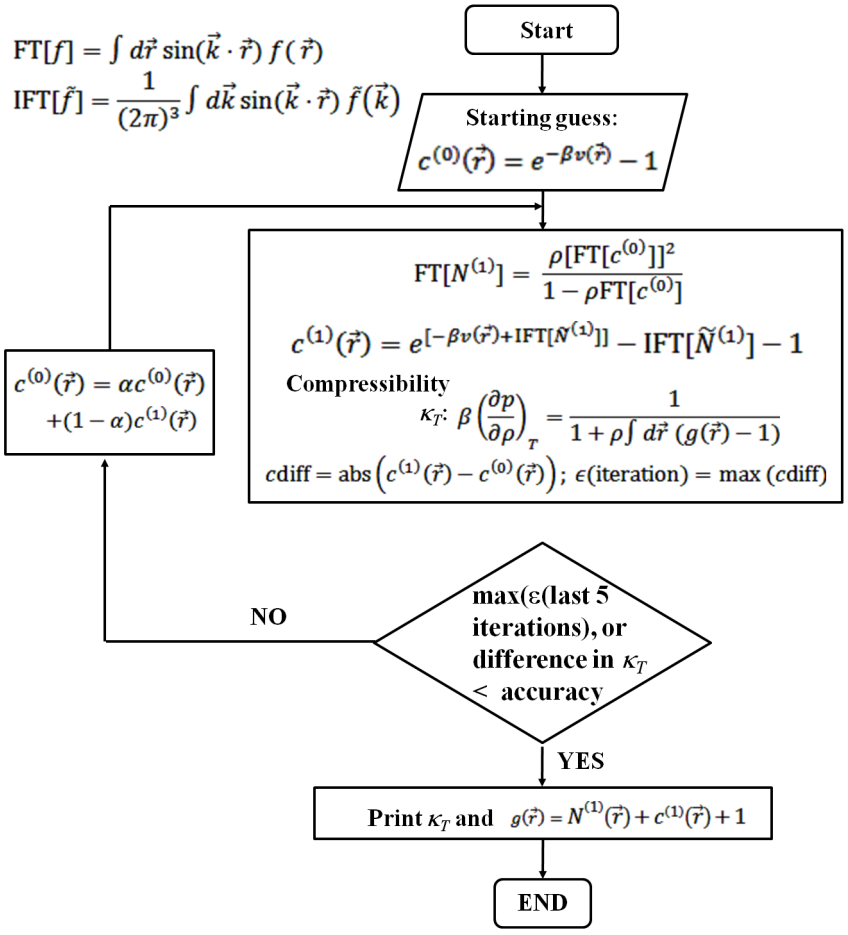

Figure 3.1. Flowchart for computing pair distribution function using HNC integral equation theory

3.4 Method of implementation

The integral equations are numerically solved using iterative methods. We introduce the function $N(\mathbf{r}) \equiv g(\mathbf{r}) - c(\mathbf{r}) - 1$. We start with an initial guess for $c^{(0)}(\mathbf{r})$ and $N^{(0)}(\mathbf{r})$. The Fourier transform $\tilde{c}^{(0)}(\mathbf{k})$ is then used to obtain the Fourier transform $\tilde{N}^{(1)}(\mathbf{k})$. The inverse Fourier transform $N^{(1)}(\mathbf{r})$ is then inserted into the appropriate relation to obtain an improved guess $c^{(1)}(\mathbf{r})$. We use uniform system, so all these functions depend on the magnitude of the length variables only. We have given a flowchart for computing the pair distribution function using the HNC method in Fig. 3.1.

The starting guess of $c^{(0)}(r) = e^{-\beta v(r)} - 1$ is only good for very low densities

only. The method do not converge rapidly enough for higher densities or sometimes do not converge at all. For higher densities, we need to use a different starting guess. After obtaining a good starting point (ρ_0^*, T_0^*) using the method described in the flowchart shown in Fig. 3.1, the final values $\tilde{N}^{(1)}(k)$ from the set (ρ_0^*, T_0^*) is used as the starting guess for the set (ρ_1^*, T_1^*) in the following manner:

$$\left[\tilde{N}^{(0)}(k)\right]_{(\rho_1^*, T_1^*)} = \frac{\rho_1^*}{\rho_0^*} \left[\tilde{N}^{(0)}(k)\right]_{(\rho_0^*, T_0^*)}. \tag{3.35}$$

The iteration procedure described here gives consistent result as long as $\rho\tilde{c}^{(0)}(k) < 1$, or else, either the process diverges or converges to an erroneous result of negative compressibility. Therefore, we need to choose the (ρ, T)-points in the region where this condition is satisfied.

3.5 Results

We use a 12-6 Lennard-Jones interaction as the potential between the particles in the system. The form is given by

$$v(r) = 4\epsilon \left[\left(\frac{\sigma}{r}\right)^{12} - \left(\frac{\sigma}{r}\right)^{6} \right], \tag{3.36}$$

where σ is the "diameter" of the particles when $v(r) = 0$ and ϵ represents the depth of the potential minimum. The parameters σ and ϵ are then used to introduce the dimensionless variables in the following way:

$$\begin{aligned} r^* &= \frac{r}{\sigma}, \qquad k^* = k\sigma \\ \rho^* &= \rho\sigma^3, \qquad T^* = \frac{k_B T}{\epsilon} \end{aligned} \tag{3.37}$$

We have moved around this region by making successive small steps as shown in the table given in Table 3.1. Proceeding this way we found out the region in the fluid-phase diagram, where we can find stable solutions for pair distribution function. The values of the inverse compressibility found in this method are shown in Table 3.1 and also shown in Fig. 3.2.

The boundary of the instability region can be observed clearly. The solutions

$T^*\backslash\rho^*$	0.10	0.11	0.1125	0.15	0.20
1.20	0.3007	0.2226	0.1944		
1.25	0.3007				
1.30	0.4082			0.1782	
1.40	0.5127			0.3272	
1.50				0.4324	0.3302

$T^*\backslash\rho^*$	0.25	0.30	0.35	0.40	0.45	0.60
1.50	0.2828	0.2882	0.3497	0.4814	0.7087	2.4138

$T^*\backslash\rho^*$	0.70	0.75	0.80	0.85	0.90
0.40					3.8842
0.45					6.6542
0.50					8.4523
0.60			1.4308	3.8542	11.2372
0.65			2.2673	4.6286	12.1836
0.68		0.6337			
0.70		0.9249	3.0013	5.6648	13.2002
0.75		1.6070	3.6510	5.9915	12.1486
0.78	0.3820	1.9936	3.9916	6.3733	15.4406
0.79	0.4894				
0.80	0.5946				
0.85	1.0988				
0.95	2.0084				
1.00	2.3953				
1.05	2.7605				
1.10	3.1181				
1.15	3.4408				
1.20	3.6224				
1.30	3.8991				
1.40	4.4522				
1.50	4.7614				

Table 3.1. Points in the $\rho^* - T^*$ diagram where the method gives consistent results.

are unstable beyond this region. The number of iteration steps required to obtain a consistent solution increases rapidly as the chosen (ρ, T) points move closer to the boundary of this region. Hence, it is difficult to obtain stable solutions very close to the boundary. Results for pair distribution functions for three different sets of (ρ, T) are shown in Fig. 3.3. The results show familiar pattern for pair distribution function values: $g(r^*) \approx 0$ for $r^* \lessapprox 1$ and $g(r^*) \to 1$ as $r^* \to \infty$.

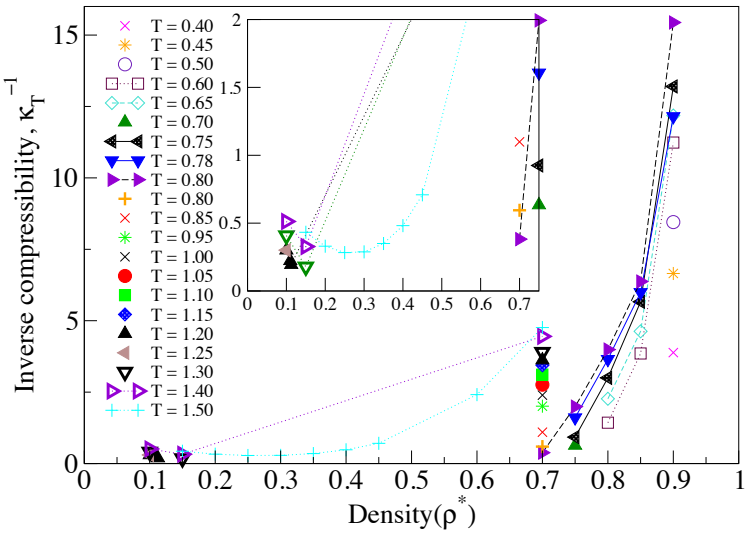

Figure 3.2. Compressibility isotherms for varying density values.

The peaks in the g values are higher and more closely spaced for higher values of densities, as expected.

3.6 Discussion

We determined the values of pair distribution functions for fluids at different densities and temperatures using the integral equation theories. Although we have used a specific form of the potential, namely the 12-6 Lennard-Jones potential, these methods can be used with any other form of potential as well. We found out that these methods can generate stable solutions for pair distribution function for fluids with densities and temperatures only within a specific region. The map of the region is very useful while determining the structure of a unknown fluid with known density and temperature parameters. The region gives a limit for the values of the density and temperature for the fluid of interest, and then we can use any of the methods described above to solve for its pair distribution from the knowledge of the interaction potential.

These methods work equally well for low-dimensional systems which can be used for fluids in confined systems or adsorbed on top of other systems. Also, we can apply these methods to obtain the pair distribution function for fluids in contact with another surface or in the presence of an external potential, as we

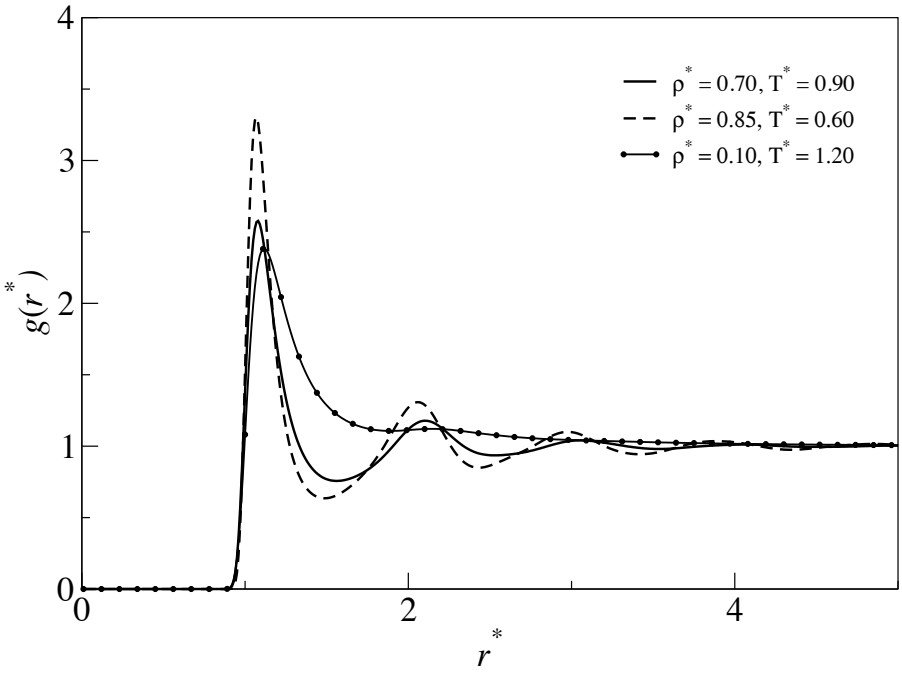

Figure 3.3. Pair distribution function results for three different density and temperature values.

show in chapter 5. We can extend these methods to obtain the pair distribution function of a mixture of binary fluids as well.

3.7 Modification for a quantum fluid

In this section, we modify the integral equation techniques to obtain the pair distribution function for liquid helium-4. The properties of liquid helium can be understood to a great extent in terms of short-range correlations emanating from the strong interactions between particles. The interactions are usually represented by a central pair potential of short range, the most common form being the Lennard-Jones(LJ) potential. An alternate to the LJ potential is the hard-sphere potential. A major success of the hard-sphere potential was that the exact solution of the PY equation can be obtained for this potential ([83], [84]).

For liquid helium, quantum effects are important and has to be incorporated in the theory. Some of the calculations for obtaining the pair distribution function of liquid helium employed Quantum Monte Carlo methods ([85], [86]) but most of the pair distribution function studies used only classical methods ([4] - [6]). There are

several works of the calculation of pair distribution function by either modifying the hard-sphere potential (e.g. considering an extended hard core potential [87]) or adding another form of potential outside the hard-sphere (e.g. an attractive square-well potential). These calculations have been mostly classical ([88], [89]). Here we present a calculation of pair distribution function of liquid helium-4 with square-well potential, incorporating quantum effects.

3.7.1 Theory

3.7.1.1 Ground-State Wavefunction

The Hamiltonian for a system of N ^{4}He atoms of mass m in a volume Ω, interacting through a central pair potential $V(|\mathbf{r}|)$ is given by,

$$H = -\sum_{i=1}^{N} \frac{\hbar^2}{2m} \nabla_i^2 + \sum_{i<j} V(|\mathbf{r}_i - \mathbf{r}_j|). \tag{3.38}$$

The best wavefunction for liquid ^{4}He is the correlated basis function of the Jastrow form. For a many-particle fluid, the wavefunction can be written as

$$\Psi(\mathbf{r_1}, \mathbf{r_2}, \ldots, \mathbf{r_N}) = \prod_{i<j}^{N} \psi(|\mathbf{r}_i - \mathbf{r}_j|) \tag{3.39}$$

$$= \exp \sum_{i<j} \ln[\psi(|\mathbf{r}_i - \mathbf{r}_j|)] \tag{3.40}$$

Now, we must choose a reasonable form for the pair function $\psi(r)$; this function should be small for short distances and should approach a constant for large distances. At small distances, where the two particles interact strongly the pair function is not expected to be very different from the solution of the two-body problem. We choose the potential function between pairs of ^{4}He atoms to be of the form of a hard-sphere with an attractive square well,

$$V(r) = \begin{cases} \infty & r < a \\ -V_0 & a < r < b \\ 0 & b < r \end{cases} \tag{3.41}$$

then the Schr$\acute{}$odinger equation for the two atom wavefunction, in relative coordinates, is

$$E\psi(r) = \big[-\frac{\hbar^2\nabla^2}{m} + V(r)\big]\psi(r). \tag{3.42}$$

The eigenfunctions ($l = 0$) can be written as

$$\psi(r) = \begin{cases} 0 & r < a \\ A\sin[p(r-a)] & a < r < b \\ \sin(kr+\delta) & b < r, \end{cases} \tag{3.43}$$

$$p^2 = k^2 + \frac{mV_0}{\hbar^2}, \tag{3.44}$$

$$E = \frac{\hbar^2 k^2}{m}. \tag{3.45}$$

Now, two ^{4}He atoms form a very weakly bound state, with $E \approx 0$. Hence, we can approximate the eigenfunction as

$$\psi(r) = \begin{cases} 0 & r < a \\ \sin[p_0(r-a)] & a < r < b \\ 1 & b < r, \end{cases} \tag{3.46}$$

$$p_0^2 = \frac{mV_0}{\hbar^2}, \tag{3.47}$$

$$\sin[p_0(b-a)] = 1,\ p_0(b-a) = \frac{\pi}{2} \tag{3.48}$$

3.7.1.2 Integral Equation Methods

One important advantage of using correlated basis functions is that the form of the diagonal density matrix $|\Psi|^2$ is mathematically identical to that of a classical fluid. Accurate computational methods are available which work well for liquids of neutral atoms. The most successful methods are based on the Percus-Yevick(PY) integral equation and the Hypernetted Chain(HNC) approximation. We can reformulate the PY equation Eq. (3.32) for the pair distribution function of a system

of ^{4}He atoms with pair wavefunction described by Eq.3.46 and write it as

$$\frac{g(r)}{\psi^2(r)} = 1 + n\int d\mathbf{y}[g(\mathbf{y}) - 1]g(\mathbf{r}-\mathbf{y})[1 - \frac{1}{\psi^2(\mathbf{r}-\mathbf{y})}]. \tag{3.49}$$

Performing the integration over angular variables and defining $\frac{g(r)}{\psi^2(r)} = g'(r)$, Eq.3.49 can be written as

$$g'(r) = 1 + \frac{2\pi n}{r}\int_0^\infty ydy[\psi^2(y)g'(y) - 1]\int_{|r-y|}^{r+y} zdzg'(z)[\psi^2(z) - 1]. \tag{3.50}$$

On the other hand, the Hypernetted Chain integral equation (HNC) for the pair distribution function of the system of interest is given by

$$\log\frac{g(r)}{\psi^2(r)} = n\int d\mathbf{y}[g(\mathbf{y}) - 1][g(\mathbf{r}-\mathbf{y}) - 1 - \log\frac{g(\mathbf{r}-\mathbf{y})}{\psi^2(\mathbf{r}-\mathbf{y})}]. \tag{3.51}$$

Using a similar definition for $g'(r)$ as in PY equation (Eq.3.49) and after performing the integration over angular variables, we have

$$\log g'(r) = \frac{2\pi n}{r}\int_0^\infty ydy[\psi^2(y)g'(y) - 1]\int_{|r-y|}^{r+y} dzz[\psi^2(z)g'(z) - 1 - \log g'(z)] \tag{3.52}$$

3.7.1.3 Ground State Properties

The ground-state energy E_0 is given by the expectation values of the Hamiltonian in Eq.3.1,

$$E_0 = \langle H\rangle = \int \Psi H\Psi d\mathbf{r}_1 \ldots d\mathbf{r}_N \Big/ \int \Psi^2 d\mathbf{r}_1 \ldots \tag{3.53}$$

If the many-body wavefunction, Ψ has the form shown in Eq.3.39, it is straightforward to show that

$$\int \Psi H\Psi d\mathbf{r}_1 \ldots d\mathbf{r}_N = \int \sum_{i<j}\big[-\frac{\hbar^2}{m}\nabla_i^2 \ln\psi(r_{ij}) + V(r_{ij})\big]\Psi^2 d\mathbf{r}_1 \ldots d\mathbf{r}_N \tag{3.54}$$

In terms of the pair distribution function, the potential energy per particle can be written as

$$\frac{\langle P.E.\rangle}{N} = \frac{n}{2}\int d^3r V(r)g(r), \tag{3.55}$$

and in our case, it is reduced to $V_0 = 15.2598$ K. The kinetic energy per particle can be obtained using

$$\frac{\langle K.E.\rangle}{N} = \frac{n\hbar^2}{4m}\int d^3r \frac{d(\ln[\psi(r)])}{dr}\frac{dg(r)}{dr}, \tag{3.56}$$

and, in our case, Eq.3.56 becomes

$$\frac{\langle K.E.\rangle}{N} = \frac{n\hbar^2\pi}{m}(p_0^2\int_a^b drg'(r)r^2 - 2p_0\int_a^b drg'(r)r\sin[p_0(r-a)]\cos[p_0(r-a)]). \tag{3.57}$$

The liquid structure function $S(k)$ (for $k \neq 0$) is related to the pair distribution function $g(r)$ by the following relation

$$S(\mathbf{k}) = 1 + n\int d\mathbf{r}[g(\mathbf{r}) - 1]\exp(-i\mathbf{k}.\mathbf{r}). \tag{3.58}$$

After carrying out the angular integration, the expression for liquid structure factor becomes

$$S(\mathbf{k}) = 1 + \frac{4\pi n}{|\mathbf{k}|}\int_0^\infty rdr[g(r) - 1]\sin(|\mathbf{k}||\mathbf{r}|). \tag{3.59}$$

3.7.2 Method

The PY integral equation (Eq.3.50) and the HNC approximation integral equation (Eq.3.52) are solved self-consistently for $r \leq R = 100$ Å. The equilibrium density of the system of ^{4}He atoms is chosen to be $n = 0.0218$ Å^{-3} or 2.18×10^{22} atoms/cm^3. The hard-sphere radius for the potential function is taken to be $a = 2.6$ Å,the width and depth are chosen as $b = 4$ Å and $V_0 = -15.26$ K respectively.

In any numerical method it is necessary to truncate the infinite integrals at some stage. These integrals are replaced by a finite sum, assuming that $g(r) \approx 1$ beyond some large but finite radial distance R. We carried out two calculations for the self-consistent PY equation (Eq.3.50), one using $R = 30$ Å and another $R = 100$ Å to investigate the effect of the size of the cutoff. The maximum difference between the two sets of $g(r)$ values for all distances is $3e^{-5}$. For the HNC equations, we performed three calculations using $R = 50$ Å, 60 Å and 70 Å. The three sets of $g(r)$ values differ not more than by 0.005 for all distances.

We used Simpson's three-point approximation to evaluate the integrals at every step of the iteration, using N points evenly distributed over the range $(0, R)$. The step size chosen for the Simpson grid was 0.01, giving the value of N as 10000 for $R = 100$ Å. To investigate the influence of the step size on the accuracy of the results we performed two calculations for $R = 20$ Å, one using 2000 points and one using 4000 points. It is found that the two sets differ nowhere by more than 0.002. The starting value of $g'(r)$ is chosen to be 1 for all values of r. The input values for the next iteration is calculated according to the mixing formula

$$g_{in}^{\prime(i)}(r) = \alpha g_{out}^{\prime(i-1)}(r) + (1-\alpha) g_{in}^{\prime(i-1)}(r). \tag{3.60}$$

where $\alpha = 0.1$ is used to achieve desired convergence. The iterations are assumed to give convergence when value of the residual Res is less than 1, where Res defined by

$$Res = \sum \left[g_{out}^{\prime(i)} - g_{out}^{\prime(i-1)} \right]^2. \tag{3.61}$$

3.7.3 Results

The values of the pair distribution function for ^{4}He obtained using PY (Eq.3.50) and HNC equations (Eq.3.52) are shown in Fig.3.4.

The pair distribution function exhibits familiar features, e.g. $g(r) \to 1$ for large distances. Figure 3.4 shows our results in comparison with earlier classical calculations ([4]-[6]) as also the x-ray [1] and neutron-diffraction data [2, 3]. The different symbols represent the experimental data while the different lines represent theoretical calculations.

We would like to point out here that while the earlier classical calculations yield values which are lower than the experimental data, our values for the pair distribution function lies above the experimental results. We would ascribe this discrepancy to the choice of parameters for the potential function. We used fixed values for the parameters (a, b, V_0) throughout our calculation. Some of the earlier papers (classical calculations) [5, 90] have discussed the effect of varying the parameters to both the pair distribution function and the liquid structure factor. The earlier paper [5] has shown that the peak of the pair distribution function increases with the increase in the hard-sphere radius. And the recent article [90] has

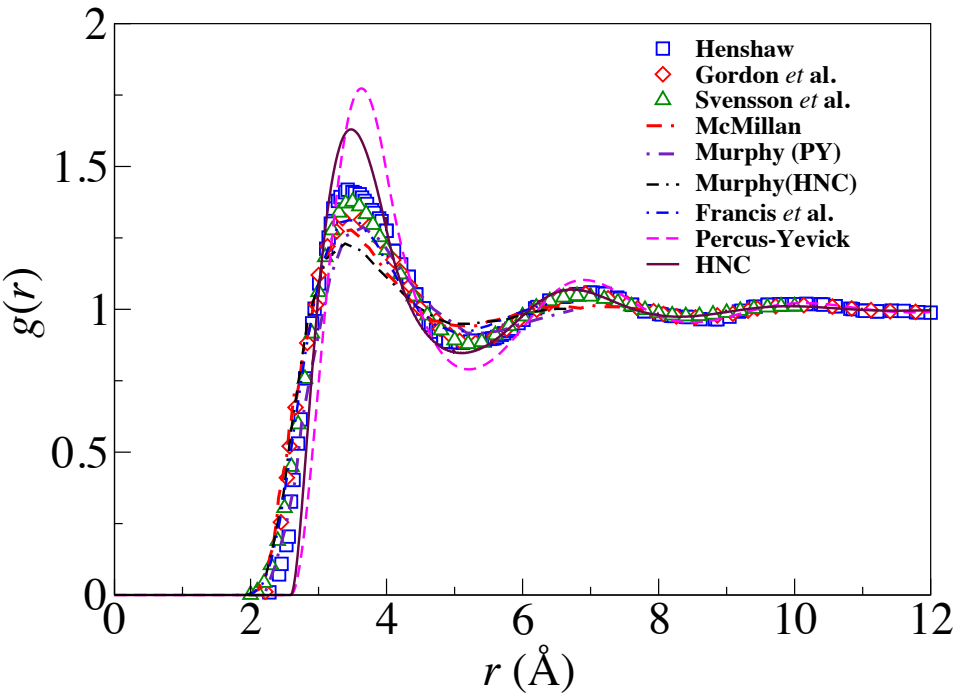

Figure 3.4. Comparison of the computed quantum mechanical pair distribution function with earlier classical calculations and experimental data. The solid line represents the values obtained using Percus-Yevick equation, while the dashed line represents the values obtained using HNC equation. The diamonds are the x-ray data of Gordon *et al.* [1]. The squares and the triangles show the neutron-diffraction data of Henshaw [2] and Svensson *et al.* [3], respectively. The dash-dash-dot (McMillan [4]), dash-dot (Murphy [5] using PY equation), dotted (Murphy [5] using HNC equation) and dash-dot-dot (Francis [6]) lines represent earlier classical calculations.

shown that the peak value of the liquid structure factor increases with the increase of width and depth of the square well part of the potential. Hence, we need to choose the values of the parameter carefully in order to obtain a good quantitative agreement between the theoretically obtained pair distribution function values and the experimental data. The better way would be to obtain the parameters using variational calculation.

The numerically obtained values of the pair distribution function is utilized to obtain the ground state energy for ^{4}He. The average value for the potential energy per particle and the average value of the kinetic energy per particle are -41.67 K and 36.78 K respectively. Hence, the average ground state energy per particle is found to be -4.89 K for the pair distribution function obtained using PY equation. This value differ from the experimentally obtained ground state energy

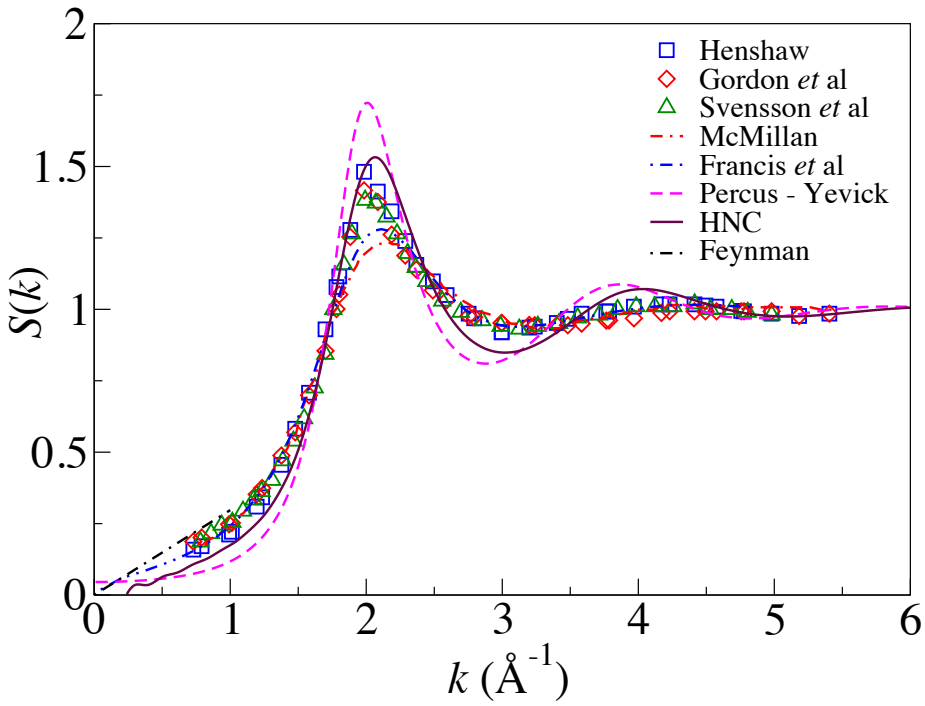

Figure 3.5. Liquid structure factor values of ^{4}He in comparison with experiment and earlier classical calculations. The solid line represents the values obtained using PY equation, while the dashed line represents the values obtained using HNC equation. Our results from HNC approximation match the experiment closely. The diamonds are the x-ray data of Gordon *etal*. [1]. The squares and the triangles show the neutron-diffraction data of Henshaw [2] and Svensson *etal*. [3] respectively. The dash-dash-dot (McMillan [4]) and dash-dot-dot (Francis [6]) lines represent earlier classical calculations. The dash-dot line is computed using Feynman [7] theory with the experimental velocity of sound (267 m/sec).

of ^{4}He atoms by about 31.

Using our results of the pair distribution function and the relation between the pair distribution function and the liquid structure factor (Eq.3.58), we now calculate the liquid structure factor of ^{4}He. The results are shown in Fig.3.5 along with earlier theoretical calculations as well as the x-ray and neutron-diffraction data. We use a similar representation as used in the graph for pair distribution function before: different symbols corresponds to the experimental data and different lines corresponds to theoretical calculations. The theoretical structure factor curves in Fig.3.5 agree well with the experimental data except in the region of diffraction maximum at 2Å^{-1}. Our results using the HNC approximation match the experimental results closely. Here again, we note that our calculation using PY equation

produces a higher peak value while earlier classical calculations produce a lower peak compared to the experimental data. As we discussed in the second paragraph of this section, the choice of the values of the parameters in the potential function is responsible for this discrepancy between results from PY equation and experiment.

The structure factor is expected to approach the Feynman value [7] for small k,

$$S(k) \approx \frac{\hbar k}{2mc}, \quad k \to 0, \tag{3.62}$$

where c is the velocity of sound. This limit is shown by the dash-dot line in Fig.3.5. The structure factors obtained using both the PY and HNC equations approach a constant as k tends to zero. The reason for this discrepancy is that we have restricted ourselves to a pair function that remains a constant for large distances.

3.7.4 Discussion

We proposed a calculation of quantum mechanical pair distribution function using the Percus-Yevick (Eq.3.49) and Hypernetted chain integral equations (Eq.3.51). The interaction potential between the ^{4}He atoms are assumed to be given by a hard-sphere and an attractive square-well. The short-range correlations in liquid helium are commonly treated by writing the many-body wavefunction as a product of pair functions, known as the Jastrow function [91]. We solve exactly the two-body Schrdinger equation for the hard-sphere plus attractive square well potential, and then use the pair wave function to construct the many-body Jastrow wavefunction. The important advantage of such a wavefunction is the formal analogy between its energy expectation values with the configuration-space integrals encountered in classical equilibrium statistical mechanics. We calculate pair distribution function, $g(r)$ of liquid ^{4}He using two approximate integral equation methods, the Percus-Yevick (PY) and Hypernetted Chain (HNC) approximation. We use the values of the pair distribution function to obtain the ground state energy and liquid structure factor, $S(k)$. We compare our theoretically obtained values of $g(r)$ and $S(k)$ to the experimental results ([1] - [3]) and also to earlier classical calculations ([4] - [6]). There is a good qualitative agreement between the theoretically obtained values of the pair distribution function, the liquid structure factor and the experimental

data. However, both of these computed physical quantities have higher peak values compared to the experimental results and the oscillations in the values are more pronounced for large distances. Also, the cutoff in the pair distribution function is shifted by a small amount. The parameters of the interaction potential adjust the position and sharpness of the cutoff and the peak in the pair distribution function. In order to get good quantitative agreement, we need to adjust the parameters of the interaction potential. It would be useful to incorporate a more realistic potential between the atoms, e.g. Aziz potential [92] and compare the pair distribution function, obtained using our proposed method, with experiments.

Chapter 4

Scattering of Phonons at Solid-Solid Interfaces: Several Model Calculations

4.1 Introduction

When heat is conducted from one material to another, there exists a temperature discontinuity, ΔT at the interface between them. For small heat flow across the interface, the temperature discontinuity is proportional to the heat flow J_Q:

$$\Delta T = RJ_Q. \tag{4.1}$$

The proportionality constant R is a measure of the thermal boundary resistance (TBR) of the interface and is called the Kapitza resistance. The thermal boundary resistance is inversely proportional to the area of the interface and has the unit of degrees area per Watt. The inverse of the Kapitza resistance, σ is known as the thermal boundary conductance,

$$J_Q = \sigma\Delta T,\ \sigma = \frac{1}{R}. \tag{4.2}$$

The interest in the problem began with the discovery of the temperature discontinuity at the interface between superfluid Helium and various metals, by Kapitza

[27] in 1941. It was thought of as a superfluid phenomenon, but similar observations have been reported between various different materials ([28]-[33]) afterwards. Kapitza resistance is still not understood in spite of the detailed knowledge of the energy transport in wide variety of solids and in helium II. Observed values of the thermal boundary resistance are always less than expected from theory, i.e., there is more energy exchange across the interface than can be presently accounted for. The heart of the difficulty in the understanding of Kapitza resistance lies in the physics of the interface. Kapitza resistance has been found to vary with the roughness, gas adsorption, and surface oxidation of the interface. The study of Kapitza resistance has an important practical application in reaching low temperatures.

The first theoretical formulation to explain the thermal boundary resistance was presented by Khalatnikov [34] (1952). The model is known as the acoustic mismatch model (AMT). In the acoustic mismatch model, the simplifying assumption is made that the phonon dispersion is governed by continuum acoustics. The model only considers the scattering of phonons of long wavelength at the interface. AMT gives fairly accurate predictions for real interfaces at low temperatures, but the predictions of the model fail at higher temperatures. Moreover, the theory completely neglects the structure of the interface on an atomic scale, because of its continuum character. However, the structure of the interface is crucial in determining the scattering of phonons, specially in the case when the wavelength of the phonon is comparable to the thickness of the interface.

In this chapter, we explore the scattering of acoustic waves at several solid-solid interfaces. First, we consider the interface between two one-dimensional harmonic chains. We derive analytical expressions for the reflection and transmission coefficients for an acoustic wave incident on the interface. These coefficients can reproduce the familiar expressions in the continuum limit and are consistent with the conservation relations. We next consider the scattering of phonons at the interface between two two-dimensional rhombic lattices. The acoustic waves can be of either polarization, longitudinal or transverse. We show that waves of either polarization are completely reflected from the interface. We discuss the interface between two two-dimensional square lattices as well, to show how the arrangement of masses can influence the nature of scattering of phonons at the interface. Finally, we discuss the interface between two three-dimensional FCC lattices to

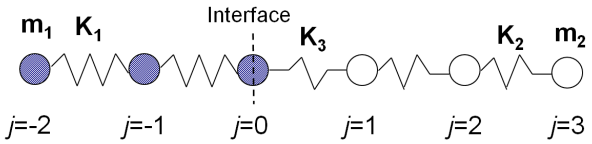

Figure 4.1. One-dimensional lattice model of solid-solid interface

complete the discussion.

4.2 One-Dimensional Lattice Model

Our model system consists of two one-dimensional harmonic chains of different masses and spring constants, connected by a third spring. The system is shown in Fig. 4.1, with the interface marked by the dashed line. The equilibrium distance between two adjacent masses is assumed to be equal to a for the left-chain in Fig. 4.1 and equal to a' for the right-chain, respectively. Let Q_j be the longitudinal displacement of mass at the j^{th} lattice site from its equilibrium position. The equations of motions for the masses in our model system are given by

$$\begin{aligned} m_1\ddot{Q}_j &= K_1(Q_{j+1} + Q_{j-1} - 2Q_j), \quad j \leq -1, \\ m_1\ddot{Q}_0 &= K_3(Q_1 - Q_0) + K_1(Q_{-1} - Q_0), \\ m_2\ddot{Q}_1 &= K_2(Q_2 - Q_1) + K_3(Q_0 - Q_1), \\ m_2\ddot{Q}_j &= K_2(Q_{j+1} + Q_{j-1} - 2Q_j), \quad j \geq 2. \end{aligned} \tag{4.3}$$

The first and the fourth equation represent the equations of motion for the masses in the bulk of the left and the right harmonic chains, respectively. While, the second and the third equation represent the equations of motion for the masses at the interface. We consider an incoming wave with amplitude I, in medium 1 represented by the left-chain. The wave would be partially reflected back to medium 1 with reflection amplitude, R and partially transmitted to medium 2 with transmission amplitude, T. The traveling wave solutions to Eq.s (4.3) can be

written as

$$u_j = \begin{cases} I\exp i(jq_1a - \omega_1 t) + R\exp i(-jq_1a - \omega_1 t) & j \leq 0, \\ T\exp i(jq_2a' - \omega_2 t) & j \geq 1. \end{cases} \quad (4.4)$$

The above equations Eq. (4.4) are solutions to the equations of motion Eq. (4.3), if $\omega_1 = \omega_2 = \omega$. Inserting the solutions to the first and fourth equation in Eq. (4.3), we get

$$\omega^2 = \frac{2K_1}{m_1}(1 - \cos(q_1a)) = \frac{2K_2}{m_2}(1 - \cos(q_2a')), \quad (4.5)$$

$$\sqrt{\frac{K_1}{m_1}}\sin(\frac{q_1a}{2}) = \sqrt{\frac{K_2}{m_2}}\sin(\frac{q_2a'}{2}) \quad (4.6)$$

This relation determines q_2 as a function of q_1.

Now, we describe the procedure to obtain the reflection and transmission coefficients, by simultaneously solving the equations of motion given in Eq. (4.3). Inserting the solution Eq. (4.4) into the second equation in Eq. (4.3) and canceling the factor of $e^{-i\omega t}$ from both sides of the equation, we obtain

$$m_1\omega^2(I + R) = K_3(I + R - Te^{iq_2a'}) + K_1(I + R - (Ie^{-iq_1a} + Re^{iq_1a})). \quad (4.7)$$

In the absence of the interface, the equation of motion for the 0^{th} mass can be written as

$$m_1\ddot{Q}_0 = K_1(Q_1 + Q_{-1} - 2Q_0), \quad (4.8)$$

and inserting the solution Eq. (4.4), we obtain

$$m_1\omega^2(I + R) = K_1(2(I + R) - (Ie^{iq_1a} + Re^{-iq_1a}) - (Ie^{-iq_1a} + Re^{iq_1a})). \quad (4.9)$$

Hence,

$$\begin{aligned} &K_1(2(I + R) - (Ie^{iq_1a} + Re^{-iq_1a}) - (Ie^{-iq_1a} + Re^{iq_1a})) \\ &= K_3(I + R - Te^{iq_2a'}) + K_1(I + R - (Ie^{-iq_1a} + Re^{iq_1a})), \end{aligned}$$

subtracting we get

$$\begin{aligned} K_1((I+R)-(Ie^{iq_1a}+Re^{-iq_1a})) &= K_3(I+R-Te^{iq_2a'}), \\ R[K_1(1-e^{-iq_1a})-K_3]+TK_3e^{iq_2a'} &= I[K_3-K_1(1-e^{iq_1a})]. \end{aligned} \tag{4.10}$$

In a similar way, the equation of motion for the 1st mass yields,

$$\begin{aligned} K_2(T-Te^{iq_2a'}) &= K_3(I+R-Te^{iq_2a'}), \\ RK_3-T[K_2(1-e^{iq_2a'})+K_3e^{iq_2a'}] &= -IK_3. \end{aligned} \tag{4.11}$$

We can combine the two equations for the two masses near the interface, in a matrix form as below:

$$\begin{aligned} &\begin{pmatrix} K_1(1-e^{-iq_1a})-K_3 & K_3e^{iq_2a'} \\ K_3 & -\left(K_2(1-e^{iq_2a'})+K_3e^{iq_2a'}\right) \end{pmatrix}\begin{pmatrix} R \\ T \end{pmatrix} \\ &\qquad = I\begin{pmatrix} K_3-K_1(1-e^{iq_1a}) \\ -K_3 \end{pmatrix}. \end{aligned} \tag{4.12}$$

The reflection and transmission amplitudes are

$$\frac{R}{I} = \frac{1}{\Delta}(1-f_{31}-e^{i\theta_1}+e^{i\theta_2}(f_{31}+f_{32}-1)+e^{i(\theta_1+\theta_2)}(f_{32}-1)), \tag{4.13}$$

$$\frac{T}{I} = -\frac{1}{\Delta}2if_{32}\sin(\theta_1), \tag{4.14}$$

with

$$\Delta = -1+f_{31}+e^{-i\theta_1}-e^{i\theta_2}(f_{31}+f_{32}-1)+e^{i(-\theta_1+\theta_2)}(f_{32}-1), \tag{4.15}$$

$$\text{and} \quad \theta_1 = q_1a\ , \theta_2 = q_2a',\ f_{31} \equiv \frac{K_3}{K_1} \text{ and } \ f_{32} \equiv \frac{K_3}{K_2}. \tag{4.16}$$

The reflection and transmission coefficients are then given by $|\frac{R}{I}|^2 = \frac{R_n}{d}$ and $|\frac{T}{I}|^2 = \frac{T_n}{d}$, respectively, with

$$\begin{aligned} R_n = &(f_{31}+f_{32}-1)^2+1+(f_{31}-1)^2+(f_{32}-1)^2 \\ &+2\cos\theta_1\,(f_{31}-1-(f_{32}-1)\,(f_{31}+f_{32}-1)) \end{aligned}$$

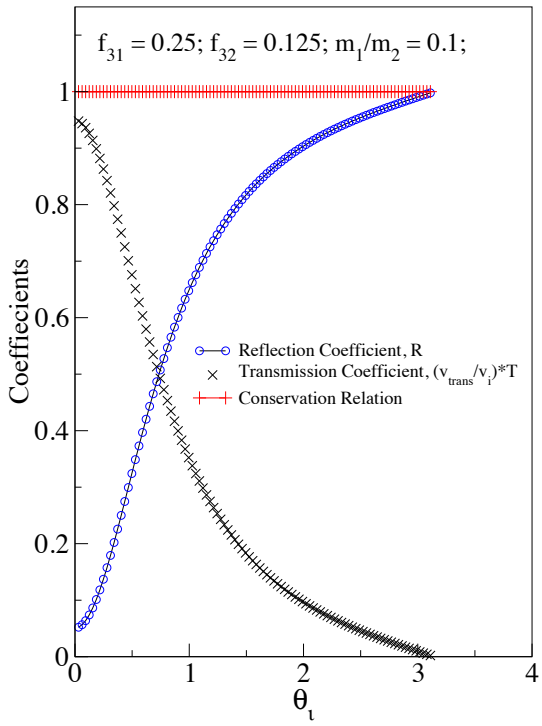

Figure 4.2. Amplitude of reflection and transmission coefficients for a phonon going from medium 1 to medium 2 as a function of incident phonon wave vector; the coefficients obey conservation relation.

$$
\begin{aligned}
&+2\cos\theta_2\left(f_{32}-1-\left(f_{31}-1\right)\left(f_{31}+f_{32}-1\right)\right)\\
&+2\cos(\theta_1+\theta_2)\left(f_{31}-1\right)\left(f_{32}-1\right)-2\cos(\theta_1-\theta_2)\left(f_{31}+f_{32}-1\right),\\
&T_n=4f_{32}^2\sin\theta_1^2,\\
\text{and}\quad &d=\left(f_{31}+f_{32}-1\right)^2+1+\left(f_{31}-1\right)^2+\left(f_{32}-1\right)^2\\
&+2\cos\theta_1\left(f_{31}-1-\left(f_{32}-1\right)\left(f_{31}+f_{32}-1\right)\right)\\
&+2\cos\theta_2\left(f_{32}-1-\left(f_{31}-1\right)\left(f_{31}+f_{32}-1\right)\right)\\
&-2\cos(\theta_1+\theta_2)\left(f_{31}+f_{32}-1\right)+2\cos(\theta_1-\theta_2)\left(f_{31}-1\right)\left(f_{32}-1\right). \qquad (4.17)
\end{aligned}
$$

Figure 4.2 shows an example of the values of the reflection and transmission coefficients as a function of the incident wave vector. The consistency of these expressions can be verified by momentum conservation, which can be shown as follows:

$$
1-|\frac{R}{I}|^2 \;=\; \frac{d-R_n}{d}=\frac{2}{d}\left(-\cos(\theta_1+\theta_2)+\cos(\theta_1-\theta_2)\right)f_{31}f_{32}
$$

$$
\begin{aligned}
&= \frac{4}{d}\sin\theta_1\sin\theta_2 f_{31}f_{32} = \frac{1}{d}\left(\frac{f_{31}\sin\theta_2}{f_{32}\sin\theta_1}\right)4f_{32}^2\sin\theta_1^2 \\
&= \left(\frac{m_2 v_2}{m_1 v_1}\right)|\frac{T}{I}|^2, \qquad (4.18)
\end{aligned}
$$

where, v's are the phonon group velocities,

$$
\begin{aligned}
v_1 &= \frac{d\omega}{dq_1} = \sqrt{\frac{K_1}{m_1}}a\cos\frac{\theta_1}{2}, \\
\text{and} \quad v_2 &= \sqrt{\frac{K_2}{m_2}}a'\cos\frac{\theta_2}{2}. \qquad (4.19)
\end{aligned}
$$

The thermal energy carried by the incoming phonon is the product of the phonon energy $\hbar\omega$, the phonon group velocity $v(=\frac{d\omega}{dq})$, the phonon amplitude, $|I|^2$. The thermal energy carried by the reflected and the transmitted waves can be obtained in a similar fashion. Now,

$$
\begin{aligned}
&\hbar\left(\frac{1}{2}\frac{d\omega^2}{dq_1}\right)\left(1-|\frac{R}{I}|^2\right) \\
&= \frac{\hbar}{d}\left(\frac{K_1 a}{m_1}\sin\theta_1\right)(4\sin\theta_1\sin\theta_2 f_{31}f_{32}) \\
&= \frac{\hbar}{d}\left(\frac{K_1 a}{m_1}\sin\theta_2\frac{f_{31}}{f_{32}}\right)\left(4f_{32}^2\sin\theta_1^2\right) = \hbar\left(\frac{K_1 a}{m_1}\frac{K_2}{K_1}\sin\theta_2\right)|\frac{T}{I}|^2 \\
&= \hbar\left(\frac{a m_2}{m_1 a'}\frac{K_2 a'}{m_2}\sin\theta_2\right)|\frac{T}{I}|^2 \\
&= \frac{m_2/a'}{m_1/a}\hbar\left(\frac{1}{2}\frac{d\omega^2}{dq_2}\right)|\frac{T}{I}|^2, \qquad (4.20)
\end{aligned}
$$

which shows that the three thermal currents are related by the following expression

$$
J_I = J_R + \frac{m_2/a'}{m_1/a}J_T. \qquad (4.21)
$$

It is well known [93] in the continuum theory of acoustics that the reflection and transmission coefficients for a normally incident wave between two media which do not sustain shear stress are given by

$$
\frac{R}{I}^{(c)} = \frac{\rho_2 v_2 - \rho_1 v_1}{\rho_2 v_2 + \rho_1 v_1}, \quad \frac{T}{I}^{(c)} = \frac{2\rho_1 v_1}{\rho_2 v_2 + \rho_1 v_1}, \qquad (4.22)
$$

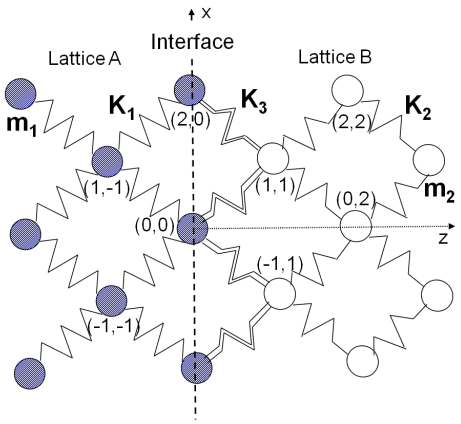

Figure 4.3. Two-dimensional solid-solid interface between two rhombic lattices;

where ρ_i and v_i stand for the mass density and speed of sound in medium i. Expanding the reflection and transmission coefficients shown in Eq. (4.17) to the order (θ_2^2) and using the relation Eq. (4.6) between θ_1 and θ_2, we get

$$\begin{aligned} \lim_{q_2 \to 0} |\frac{R}{I}| &= \frac{\sqrt{K_2 m_2} - \sqrt{K_1 m_1}}{\sqrt{K_2 m_2} + \sqrt{K_1 m_1}}, \\ \lim_{q_2 \to 0} |\frac{T}{I}| &= \frac{2\sqrt{K_1 m_1}}{\sqrt{K_2 m_2} + \sqrt{K_1 m_1}}. \end{aligned} \tag{4.23}$$

In the continuum limit, $v \approx \sqrt{\frac{K}{m}} a \Rightarrow \left(\frac{m}{a}\right) v \approx \sqrt{Km}$. Hence, the reflection and transmission coefficients obtained for the one-dimensional model system, match the expressions for continuum acoustics correctly if we make the obvious connection $\rho v \longleftrightarrow \sqrt{Km}$.

4.3 Two-Dimensional Rhombic Lattice

In the present section, we consider an interface between two two-dimensional rhombic lattices and explore the scattering of phonons at the interface in a fashion similar to the one-dimensional case. Our model system is shown in Fig. 4.3. In lattice A, the masses m_1 are connected to the four nearest neighbors by springs of spring constant K_1. The masses m_2 in lattice B are connected to their four nearest neighbors by springs of spring constant K_2. The masses on opposite sides of the interface are connected by springs of spring constant K_3. The spacing between

the nearest neighbor masses in each of the lattices is $a\sqrt{2}$. The combined lattice preserves the rhombic lattice structure. The boundary layer is at $z = 0$.

4.3.1 Phonon Modes

First, we calculate the sound modes in the bulk of a two-dimensional rhombic lattice, of lattice constant a. The Hamiltonian of the system is written as

$$H = \sum_j \frac{P_j^2}{2m} + V,$$
$$V = \frac{K}{2} \sum_\delta [\hat{\delta} \cdot (\mathbf{Q}_j - \mathbf{Q}_{j+\delta})]^2 \tag{4.24}$$

with $\hat{\delta} = a(\pm 1, \pm 1)$, the vector distance to the nearest neighbors.

In the component form, the potential energy can be written as

$$\begin{aligned} V &= \frac{K}{2} \sum_{l,m} \left[\left(\frac{Q^x_{l,m} + Q^z_{l,m}}{\sqrt{2}} - \frac{Q^x_{l+1,m+1} + Q^z_{l+1,m+1}}{\sqrt{2}} \right)^2 \right. \\ &+ \left(\frac{-Q^x_{l,m} - Q^z_{l,m}}{\sqrt{2}} - \frac{-Q^x_{l-1,m-1} - Q^z_{l-1,m-1}}{\sqrt{2}} \right)^2 \\ &+ \left(\frac{Q^x_{l,m} - Q^z_{l,m}}{\sqrt{2}} - \frac{Q^x_{l+1,m-1} - Q^z_{l+1,m-1}}{\sqrt{2}} \right)^2 \\ &+ \left. \left(\frac{-Q^x_{l,m} + Q^z_{l,m}}{\sqrt{2}} - \frac{-Q^x_{l-1,m+1} + Q^z_{l-1,m+1}}{\sqrt{2}} \right)^2 \right]. \end{aligned} \tag{4.25}$$

The x component of the equations of motion is given by

$$\begin{aligned} -m\ddot{Q}^x_{l,m} &= \frac{K}{2} \left[4Q^x_{l,m} - Q^x_{l+1,m+1} - Q^x_{l-1,m-1} - Q^x_{l+1,m-1} - Q^x_{l-1,m+1} \right. \\ &- \left. Q^z_{l+1,m+1} - Q^z_{l-1,m-1} + Q^z_{l+1,m-1} + Q^z_{l-1,m+1} \right]. \end{aligned} \tag{4.26}$$

The z-component of the equation of motion can be written in a similar fashion by replacing $x \leftrightarrow z$. The solutions to these equations are assumed to be of the form

$$\mathbf{Q}_{l,m} = \hat{e} \exp i(\mathbf{q} \cdot \mathbf{r}_{lm} - \omega t), \tag{4.27}$$

where $\hat{e}$ is the polarization vector and $\mathbf{q}$ is the wave vector. Inserting Eq. (4.27) into the equations of motion, we obtain

$$\begin{aligned} \frac{m}{2K}\omega^2 e_x &= (1-\cos q_x a \cos q_z a)e_x + e_z \sin q_x a \sin q_z a \\ \text{and } \frac{m}{2K}\omega^2 e_z &= (1-\cos q_x a \cos q_z a)e_z + e_x \sin q_x a \sin q_z a, \end{aligned} \tag{4.28}$$

which has the following solutions

- Longitudinal phonons:

$$\omega_L^2 = \frac{2K}{M}(1-\cos(q_x+q_z)a) \tag{4.29}$$

$$\hat{e}_l = \frac{1}{\sqrt{2}}\begin{pmatrix} 1 \\ 1 \end{pmatrix} \tag{4.30}$$

- Transverse phonons:

$$\omega_T^2 = \frac{2K}{M}(1-\cos(q_x-q_z)a) \tag{4.31}$$

$$\hat{e}_t = \frac{1}{\sqrt{2}}\begin{pmatrix} 1 \\ -1 \end{pmatrix} \tag{4.32}$$

4.3.2 Boundary Conditions

We consider an incident wave with amplitude I_i and polarization $\hat{e}_i$, that approaches the interface from the side of lattice A shown in Fig. 4.3. The incident wave can be of either polarization, $i = (l, t)$. This lattice has the feature that the polarization vectors are independent of the direction of the wave vector ans point along the bond directions. This implies that for an incident wave with a particular polarization, there can be only one wave reflected with the opposite polarization, i.e for an incident longitudinal wave the reflected wave would have polarization vector $\hat{e} = -\hat{e}_t$ and for an incident transverse wave, the reflected wave would have polarization vector $\hat{e} = -\hat{e}_l$. The incident, reflected and transmitted waves have the same wave vector parallel to the interface, $q_x \equiv q$. They also have the same value for the frequency, ω. The wave vectors along z-direction for the longitudinal

and transverse waves are different, such that

$$\omega(q, q_i) = \omega_L(q, \pm q_l) = \omega_T(q, \pm q_t),$$

$$\text{which gives, } \cos(q \pm q_i)a = \cos(q \mp q_R)a, \tag{4.33}$$

$$\frac{K_1}{m_1}(1 - \cos(q \pm q_i)a) = \frac{K_2}{m_2}(1 - \cos(q \pm q_T)a), \tag{4.34}$$

where q_R and q_T are the z-component of the wave vectors for the reflected and transmitted wave, respectively. The $\pm$ represents the two different cases for the two polarizations.

4.3.3 Reflection and Transmission Amplitudes

The reflection and transmission coefficients for the scattering of phonons at the interface, are obtained by solving the equations of motion for the masses next to the interface. The displacements of the masses near the interface can be written as a linear combination of the three different waves,

$$\begin{aligned} \mathbf{Q}_{l,m} &= \sum_{p=0}^{1} A_p \hat{e}^{(p)} \exp i(\mathbf{q}^{(p)} \cdot \mathbf{r}_{lm} - \omega t), \quad \text{for masses} \in \text{lattice A} \\ \mathbf{W}_{l,m} &= A_2 \hat{e}^{(2)} \exp i(\mathbf{q}^{(2)} \cdot \mathbf{r}_{lm} - \omega t), \quad \text{for masses} \in \text{lattice B.} \end{aligned} \tag{4.35}$$

Here, the incident phonon with amplitude A_0 has wavevector $\mathbf{q}^{(0)}$ and polarization $\hat{e}^{(0)}$, the reflected phonon with amplitude A_1 has wavevector $\mathbf{q}^{(1)}$ and polarization $\hat{e}^{(1)}$ and the transmitted phonon with amplitude A_2 has wavevector $\mathbf{q}^{(2)}$ and polarization $\hat{e}^{(2)}$. We choose the origin of coordinates to be at the position of a mass in lattice A, for convenience. The x-component of the equation of motion for the $(0,0)^{\text{th}}$ mass is given by

$$\begin{aligned} -m_1 \ddot{Q}^x_{0,0} &= \frac{K_1}{2}\left[2Q^x_{0,0} - Q^x_{-1,-1} - Q^x_{1,-1} + Q^z_{1,-1} - Q^z_{-1,-1}\right] \\ &+ \frac{K_3}{2}\left[2Q^x_{0,0} - W^x_{1,1} - W^x_{-1,1} + W^z_{-1,1} - W^z_{1,1}\right]. \end{aligned} \tag{4.36}$$

In the absence of interface, the equation of motion for the $(0,0)^{\text{th}}$ has the following form

$$\begin{aligned} -m_1\ddot{Q}^x_{0,0} &= \frac{K_1}{2}\left[4Q^x_{0,0} - Q^x_{-1,-1} - Q^x_{1,-1} - Q^x_{1,1} - Q^x_{-1,1}\right. \\ &\quad \left. +Q^z_{1,-1} - Q^z_{-1,-1} + Q^z_{-1,1} - Q^z_{1,1}\right]. \end{aligned} \tag{4.37}$$

Subtracting we obtain

$$\begin{aligned} &\frac{K_1}{2}\left[2Q^x_{0,0} - Q^x_{1,1} - Q^x_{-1,1} + Q^z_{-1,1} - Q^z_{1,1}\right] \\ &= \frac{K_3}{2}\left[2Q^x_{0,0} - W^x_{1,1} - W^x_{-1,1} + W^z_{-1,1} - W^z_{1,1}\right]. \end{aligned} \tag{4.38}$$

Inserting the solutions given in Eq. (4.27), we obtain

$$\begin{aligned} &A_1[\Big(K_1(1-\cos(q_xa)e^{-iq^{(1)}a}) - K_3\Big)\, e^{(1)}_x - K_1\left(i\sin(q_xa)e^{-iq^{(1)}a}\right) e^{(1)}_z] \\ &\qquad +A_2K_3[\cos(q_xa)e^{iq^{(2)}a}e^{(2)}_x + i\sin(q_xa)e^{iq^{(2)}a}e^{(2)}_z] \\ &= A_0[\Big(K_3 - K_1(1-\cos(q_xa)e^{iq^{(0)}a})\Big)\, e^{(0)}_x + K_1\left(i\sin(q_xa)e^{iq^{(0)}a}\right) e^{(0)}_z]. \end{aligned} \tag{4.39}$$

We obtain a similar equation for the z-component of the displacement of the $(0,0)^{\text{th}}$ mass with the replacement of $e_x \leftrightarrow e_z$.

Following the same method, we obtain for the mass in lattice B, next to interface

$$\begin{aligned} &A_1K_3[\cos(q_xa)e^{(1)}_x - i\sin(q_xa)e^{(1)}_z] \\ &+A_2[\Big(K_2(1-\cos(q_xa)e^{-iq^{(2)}a}) - K_3\Big)\, e^{iq^{(2)}a}e^{(2)}_x + K_1 i\sin(q_xa)e^{(1)}_z] \\ &= -A_0K_3[\cos(q_xa)e^{(0)}_x - i\sin(q_xa)e^{(0)}_z]. \end{aligned} \tag{4.40}$$

The equation for the z-component yields a similar expression by replacing $e_x \leftrightarrow e_z$. Eq. (4.39) and Eq. (4.40) are simultaneously solved for the reflection and transmission amplitudes. The transmission coefficients for either polarization is given by $|\frac{T}{I}|^2 = \frac{T_n}{d}$, respectively, where

$$T_n = f^2_{32}\left[\sin\left(\frac{\theta_l + \theta_t}{2}\right)\right]^2, \tag{4.41}$$

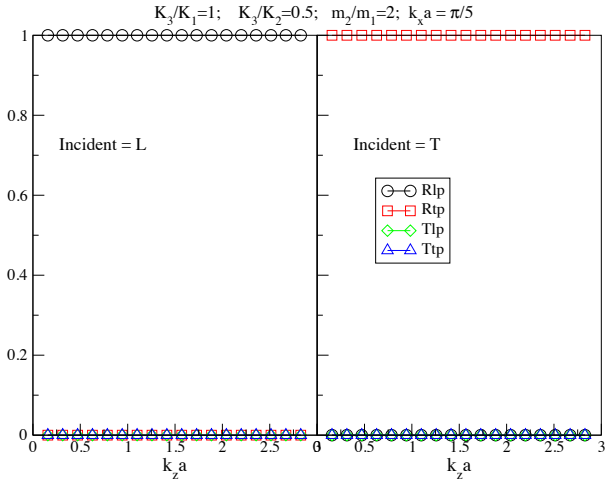

Figure 4.4. Phonon reflection and transmission coefficients at the interface between two rhombic lattices.

$$\text{and} \quad d = \frac{1}{4}((f_{31}+f_{32}-1)^2+1+(f_{31}-1)^2+(f_{32}-1)^2$$
$$-2(f_{31}+f_{32}-1)\cos(\theta^{(2)}+\theta^{(1)})-2(2+(f_{31}+f_{32})(f_{32}-2))\cos(\theta_x-\theta^{(1)})$$
$$-2((f_{31}-1)(f_{31}+f_{32}-1)+1-f_{32})\cos(\theta_x-\theta^{(2)})$$
$$+2(f_{31}-1)(f_{32}-1)\cos(\theta^{(2)}-\theta^{(1)}+2\theta_x)). \tag{4.42}$$

Since, θ_l and θ_t can only be separated by integer multiples of 2π, we can see from Eq. (4.33) that $T_n = 0$ for incident wave of either polarization. This result implies that, incident wave of either polarization is completely reflected from the interface between two two-dimensional rhombic lattices. Figure 4.4 shows the values of the phonon reflection and transmission coefficients at the interface between two rhombic lattices for a particular choice of lattice parameters.

4.4 Two-Dimensional Square Lattice

The somewhat interesting result of the last section inspired us to study one another model interface for a two-dimensional system. Here, we consider an interface between two two-dimensional square lattices. The system is shown in Fig. 4.5. We discuss the scattering of phonons at the interface in a way similar to the rhombic lattice example before. In lattice A, the masses m_1 are connected to the four nearest neighbors by springs of spring constant K and to the four next nearest

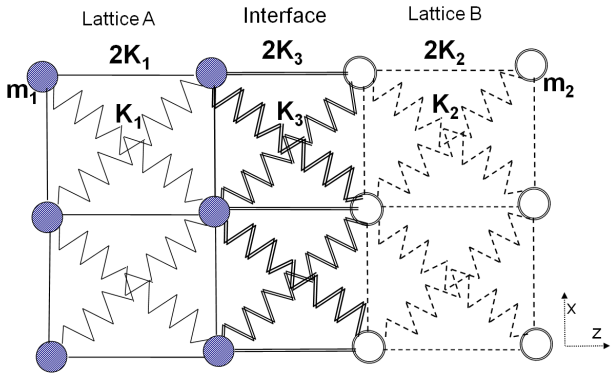

Figure 4.5. Two-dimensional solid-solid interface between two square lattices;

neighbors by springs of stiffness K'. The second neighbor springs stabilize the structure, and give reasonable dispersion for transverse modes. We solve for the case when $K = 2K_1$, $K' = K_1$, which is the isotropic case at long wavelength. The masses m_2 in lattice B are connected to their four nearest neighbors by springs of stiffness $2K_2$ and to their next nearest neighbors by springs of stiffness K_2. The mass at the interface is connected to the nearest mass on opposite side of the interface, by spring of spring constant $2K_3$ and to the next nearest neighbor masses, by springs of stiffness K_3. The boundary layer is at $z = 0$.

4.4.1 Phonon Modes

First, we discuss the bulk modes of phonons on a two-dimensional square lattice, of lattice constant a. The Hamiltonian of the system is written as

$$H = \sum_j \frac{P_j^2}{2m} + V,$$

$$V = \frac{K}{2} \sum_{\delta_1} [\hat{\delta}_1 \cdot (\mathbf{Q}_j - \mathbf{Q}_{j+\delta_1})]^2 + \frac{K'}{2} \sum_{\delta} [\hat{\delta}_2 \cdot (\mathbf{Q}_j - \mathbf{Q}_{j+\delta_2})]^2 \tag{4.43}$$

where the four first neighbors are at $\hat{\delta}_1 = a(\pm 1, 0),\ a(0, \pm 1)$, and the four second neighbors are at $\hat{\delta}_2 = a(\pm 1, \pm 1)$. In the component form, the potential energy can be written as

$$V = K_1 \sum_{l,m} \Big[\left(Q^x_{l,m} - Q^x_{l+1,m}\right)^2 + \left(Q^x_{l,m} - Q^x_{l-1,m}\right)^2$$

$$
\begin{aligned}
&+\left(Q^z_{l,m}-Q^z_{l,m+1}\right)^2+\left(Q^z_{l,m}-Q^z_{l,m-1}\right)^2\Big] \\
&+\frac{K_1}{2}\sum_{l,m}\Bigg[\left(\frac{Q^x_{l,m}+Q^z_{l,m}}{\sqrt{2}}-\frac{Q^x_{l+1,m+1}+Q^z_{l+1,m+1}}{\sqrt{2}}\right)^2 \\
&+\left(\frac{-Q^x_{l,m}-Q^z_{l,m}}{\sqrt{2}}-\frac{-Q^x_{l-1,m-1}-Q^z_{l-1,m-1}}{\sqrt{2}}\right)^2 \\
&+\left(\frac{Q^x_{l,m}-Q^z_{l,m}}{\sqrt{2}}-\frac{Q^x_{l+1,m-1}-Q^z_{l+1,m-1}}{\sqrt{2}}\right)^2 \\
&+\left(\frac{-Q^x_{l,m}+Q^z_{l,m}}{\sqrt{2}}-\frac{-Q^x_{l-1,m+1}+Q^z_{l-1,m+1}}{\sqrt{2}}\right)^2\Bigg]. \qquad (4.44)
\end{aligned}
$$

The x component of the equations of motion is given by

$$
\begin{aligned}
-m_1\ddot{Q}^x_{l,m} &= 2K_1\left[2Q^x_{l,m}-Q^x_{l,m+1}-Q^x_{l,m-1}\right]+\frac{K_1}{2}\left[4Q^x_{l,m}-Q^x_{l+1,m+1}-Q^x_{l-1,m-1}\right. \\
&\left.-Q^x_{l+1,m-1}-Q^x_{l-1,m+1}+Q^z_{l+1,m+1}-Q^z_{l-1,m-1}+Q^z_{l+1,m-1}+Q^z_{l-1,m+1}\right]. \qquad (4.45)
\end{aligned}
$$

The z-component of the equation of motion can be written in a similar fashion by replacing $x \leftrightarrow z$. The solutions to these equations are assumed to be of the form

$$
\mathbf{Q}_{l,m} = \hat{e}\exp i(\mathbf{q}\cdot\mathbf{r}_{lm}-\omega t), \qquad (4.46)
$$

where $\hat{e}$ is the polarization vector and $\mathbf{q}$ is the wave vector. Inserting Eq. (4.46) into the equations of motion, we obtain

$$
\begin{aligned}
\frac{m_1}{2K_1}\omega^2 e_x &= \left[3-2\cos(\theta_x)-\cos(\theta_x)\cos(\theta_z)\right]e_x \\
&+ \left[\sin(\theta_x)\sin(\theta_z)\right]e_z \\
\text{and } \frac{m_1}{2K_1}\omega^2 e_z &= \left[3-(1+2\cos(\theta_x))\cos(\theta_z)\right]e_z \qquad (4.47) \\
&+ \left[\sin(\theta_x)\sin(\theta_z)\right]e_x,
\end{aligned}
$$

where $\theta_i = k_i a$. The above equations Eq. (4.47) have the following solutions

- Longitudinal phonons:

$$
\omega_L^2 = \frac{2K_1}{m_1}\left[4-\cos(\theta_x)-(1+2\cos(\theta_x)\cos(\theta_z)\right] \qquad (4.48)
$$

$$\hat{e}_l = N \begin{pmatrix} \sin(\theta_z/2)\cos(\theta_x/2) \\ \cos(\theta_z/2)\sin(\theta_x/2) \end{pmatrix} \tag{4.49}$$

- Transverse phonons:

$$\omega_T^2 = \frac{2K_1}{m_1}\left[2 - \cos(\theta_x) - \cos(\theta_z)\right] \tag{4.50}$$

$$\hat{e}_t = N \begin{pmatrix} \cos(\theta_z/2)\sin(\theta_x/2) \\ -\sin(\theta_z/2)\cos(\theta_x/2) \end{pmatrix} \tag{4.51}$$

$$N^2 = \frac{1}{\sqrt{1 - \cos(\theta_z)\cos(\theta_x)}} \tag{4.52}$$

4.4.2 Boundary Conditions

We consider an incident wave with amplitude I_i and polarization $\hat{e}_i$, that approaches the interface from the side of lattice A shown in Fig. 4.5. The incident wave can be of either polarization, $i = (l, t)$. In general, there can be two reflected waves, with amplitudes $R_l,\ R_t$ and polarizations $\hat{e}_{Rl},\ \hat{e}_{Rt}$ and two transmitted waves, with amplitudes $T_l,\ T_t$ and polarizations $\hat{e}_{Tl},\ \hat{e}_{Tt}$. The incident, reflected and transmitted waves have the same wave vector parallel to the interface, $q_x \equiv q$. They also have the same value for the frequency, ω. The wave vectors along z-direction for the incident (q_i), reflected (q_R) and transmitted (q_T) waves are all different.

In order to obtain simple algebraic equations for the wavevectors for reflected and transmitted waves, we define $s_{(p)} = \exp(iq_{z^{(p)}}a)$, with $p = i,\, l,\, t$. When a longitudinal phonon with wavevector ($q,\ q_i$) is incident on the surface, the z-component of the wavevectors for the reflected and transmitted waves are obtained the following way:

- Reflected waves:
  - Longitudinal phonons

$$\begin{aligned} & q_{Rl} = -q_i \\ \Rightarrow\ & s_{Rl} = \exp(-iq_i a) = s_i^{-1} \end{aligned} \tag{4.53}$$

– Transverse phonons

$$\frac{2K_1}{m_1}\left[2-\cos(\theta_x)-\left(\frac{s_{Rt}+s_{Rt}^{-1}}{2}\right)\right]$$
$$=\frac{2K_1}{m_1}\left[4-\cos(\theta_x)-(1+2\cos(\theta_x)\cos(q_i a)\right] \tag{4.54}$$

$$\Rightarrow \frac{s_{Rt}+s_{Rt}^{-1}}{2}=(1+2\cos(\theta_x)\cos(q_i a)-2\equiv A. \tag{4.55}$$

The wavevector s_{Rt} is the solution of the quadratic equation:

$$s_{Rt}^2-2As_{Rt}+1=0. \tag{4.56}$$

If $A^2<1$, the solutions are complex with $|s_{Rt}|=1$, and we obtain a propagating wave. We choose the solution with negative imaginary part:

$$s_{Rt}=A-i\sqrt{1-A^2}. \tag{4.57}$$

On the other hand, if $A^2\geq 1$, the solution are real. We choose the solution with $|s_{Rt}|\leq 1$:

$$s_{Rt}=A-sign(A)\sqrt{A^2-1}. \tag{4.58}$$

The wave does not propagate. We still include this solution in our calculation to satisfy zero stress boundary condition.

- Transmitted waves:

  – Longitudinal phonons require to have

$$\frac{2K_2}{m_2}\left[4-\cos(\theta_x)-(1+2\cos(\theta_x)\left(\frac{s_{Tl}+s_{Tl}^{-1}}{2}\right)\right]$$
$$=\frac{2K_1}{m_1}\left[4-\cos(\theta_x)-(1+2\cos(\theta_x)\cos(q_i a)\right]$$
$$\Rightarrow \frac{s_{Tl}+s_{Tl}^{-1}}{2}$$

$$= \frac{4 - \cos(\theta_x) - \frac{m_2}{m_1}\frac{K_1}{K_2}\left[4 - \cos(\theta_x) - (1 + 2\cos(\theta_x)\cos(q_i a)\right]}{1 + 2\cos(\theta_x)}. \quad (4.59)$$

The solutions of the quadratic equation are chosen using the method similar to the case for reflected transverse phonons.

– Similarly, for transverse phonons we have

$$\frac{2K_2}{m_2}\left[2 - \cos(\theta_x) - \left(\frac{s_{Tt} + s_{Tt}^{-1}}{2}\right)\right]$$
$$= \frac{2K_1}{m_1}\left[4 - \cos(\theta_x) - (1 + 2\cos(\theta_x)\cos(q_i a)\right]$$
$$\Rightarrow \frac{s_{Tt} + s_{Tt}^{-1}}{2}$$
$$= 2 - \cos(\theta_x) - \frac{m_2}{m_1}\frac{K_1}{K_2}\left[4 - \cos(\theta_x) - (1 + 2\cos(\theta_x)\cos(q_i a)\right]. \quad (4.60)$$

The same procedure can be repeated for the case when a transverse phonon approaches the interface.

In all cases the reflected waves have polarization:

$$\hat{e}_l = N\begin{pmatrix} -\sin(\theta_{Rl}/2)\cos(\theta_x/2) \\ \cos(\theta_{Rl}/2)\sin(\theta_x/2) \end{pmatrix},$$
$$\hat{e}_t = N\begin{pmatrix} \cos(\theta_{Rt}/2)\sin(\theta_x/2) \\ \sin(\theta_{Rt}/2)\cos(\theta_x/2) \end{pmatrix}, \quad (4.61)$$

and the transmitted waves have polarization:

$$\hat{e}_l = N\begin{pmatrix} \sin(\theta_{Rl}/2)\cos(\theta_x/2) \\ \cos(\theta_{Rl}/2)\sin(\theta_x/2) \end{pmatrix},$$
$$\hat{e}_t = N\begin{pmatrix} \cos(\theta_{Tt}/2)\sin(\theta_x/2) \\ -\sin(\theta_{Tt}/2)\cos(\theta_x/2) \end{pmatrix}. \quad (4.62)$$

4.4.3 Reflection and Transmission Amplitudes

We follow a similar procedure as taken in the case of two dimensional rhombic lattice, to obtain the reflection and transmission amplitudes. The displacements

of the masses near the interface are written as

$$\begin{aligned}\mathbf{Q}_{l,m} &= \sum_{p=0}^{2} A_p \hat{e}^{(p)} \exp i(\mathbf{q}^{(p)} \cdot \mathbf{r}_{lm} - \omega t), \quad \text{for masses} \in \text{lattice A} \\ \mathbf{W}_{l,m} &= \sum_{p=3}^{4} A_p \hat{e}^{(p)} \exp i(\mathbf{q}^{(p)} \cdot \mathbf{r}_{lm} - \omega t), \quad \text{for masses} \in \text{lattice B.} \quad (4.63)\end{aligned}$$

The incident phonon with amplitude A_0 has wavevector $\mathbf{q}^{(0)}$ and polarization $\hat{e}^{(0)}$. The reflected phonon with amplitude $A_p(p = 1, 2)$ has wavevector $\mathbf{q}^{(p)}$ and polarization $\hat{e}^{(p)}$ and the transmitted phonon with amplitude $A_p(p = 3, 4)$ has wavevector $\mathbf{q}^{(p)}$ and polarization $\hat{e}^{(p)}$. As before, we choose the origin of coordinates to be at the position of a mass in lattice A near the interface, for convenience. We then write the equations of motion of the masses in lattices A and B next to the interface. The x-component for the equation of motion for the $(0, 0)^{\text{th}}$ mass is given by

$$\begin{aligned}-m_1 \ddot{Q}^x_{0,0} &= 2K_1 \left[2Q^x_{0,0} - Q^x_{0,1} - Q^x_{0,-1}\right] \\ &+ \frac{K_1}{2} \left[2Q^x_{0,0} - Q^x_{-1,-1} - Q^x_{1,-1} + Q^z_{1,-1} - Q^z_{-1,-1}\right] \\ &+ \frac{K_3}{2} \left[2Q^x_{0,0} - W^x_{1,1} - W^x_{-1,1} + W^z_{-1,1} - W^z_{1,1}\right]. \quad (4.64)\end{aligned}$$

In the absence of interface, the equation of motion for the $(0, 0)^{\text{th}}$ has the following form

$$\begin{aligned}-m_1 \ddot{Q}^x_{0,0} &= 2K_1 \left[2Q^x_{0,0} - Q^x_{0,1} - Q^x_{0,-1}\right] \\ &+ \frac{K_1}{2} \left[4Q^x_{0,0} - Q^x_{-1,-1} - Q^x_{1,-1} - Q^x_{1,1} - Q^x_{-1,1}\right. \\ &\quad \left. + Q^z_{1,-1} - Q^z_{-1,-1} + Q^z_{-1,1} - Q^z_{1,1}\right]. \quad (4.65)\end{aligned}$$

Subtracting we obtain

$$\begin{aligned}&\frac{K_1}{2} \left[2Q^x_{0,0} - Q^x_{1,1} - Q^x_{-1,1} + Q^z_{-1,1} - Q^z_{1,1}\right] \\ &= \frac{K_3}{2} \left[2Q^x_{0,0} - W^x_{1,1} - W^x_{-1,1} + W^z_{-1,1} - W^z_{1,1}\right]. \quad (4.66)\end{aligned}$$

Similarly, for the z-component we obtain

$$2K_1\left[Q^z_{0,0}-Q^z_{0,1}\right]+\frac{K_1}{2}\left[2Q^z_{0,0}-Q^z_{1,1}-Q^z_{-1,1}+Q^x_{-1,1}-Q^x_{1,1}\right]$$
$$=2K_3\left[Q^z_{0,0}-Q^z_{0,1}\right]+\frac{K_3}{2}\left[2Q^z_{0,0}-W^z_{1,1}-W^z_{-1,1}+W^x_{-1,1}-W^x_{1,1}\right]. \tag{4.67}$$

Inserting the solutions given in Eq.(4.63) into Eq.s(4.66) and (4.67), we obtain

$$\sum_{p=1}^{2}A_p[\left(K_1(1-\cos(q_xa)e^{-iq_z^{(p)}a})-K_3\right)e_x^{(p)}-K_1\left(i\sin(q_xa)e^{-iq_z^{(p)}a}\right)e_z^{(p)}]$$
$$+K_3\sum_{p=3}^{4}A_p[\cos(q_xa)e^{iq_z^{(p)}a}e_x^{(p)}+i\sin(q_xa)e^{iq_z^{(p)}a}e_z^{(p)}]$$
$$=A_0[\left(K_3-K_1(1-\cos(q_xa)e^{iq_z^{(0)}a})\right)e_x^{(0)}+K_1\left(i\sin(q_xa)e^{iq_z^{(0)}a}\right)e_z^{(0)}], \tag{4.68}$$

$$\sum_{p=1}^{2}A_p[\left(3(K_1-K_3)-K_1(2+\cos(q_xa)e^{-iq_z^{(p)}a})\right)e_z^{(p)}-K_1\left(i\sin(q_xa)e^{-iq_z^{(p)}a}\right)e_x^{(p)}]$$
$$+K_3\sum_{p=3}^{4}A_p[(2+\cos(q_xa))e^{iq_z^{(p)}a}e_z^{(p)}+i\sin(q_xa)e^{iq_z^{(p)}a}e_x^{(p)}]$$
$$=A_0[\left(3(K_3-K_1)+K_1(2+\cos(q_xa)e^{iq_z^{(0)}a})\right)e_z^{(0)}+K_1\left(i\sin(q_xa)e^{iq_z^{(0)}a}\right)e_x^{(0)}]. \tag{4.69}$$

Following the same method, we obtain for the mass in lattice B, next to interface

$$K_3\sum_{p=1}^{2}A_p[\cos(q_xa)e_x^{(p)}-i\sin(q_xa)e_z^{(p)}]$$
$$+\sum_{p=3}^{4}A_p[\left(K_2(e^{iq_z^{(p)}a}-\cos(q_xa))-K_3e^{iq_z^{(p)}a}\right)e_x^{(p)}+K_2\left(i\sin(q_xa)e^{iq_z^{(p)}a}\right)e_z^{(p)}]$$
$$=K_3A_0[-\cos(q_xa)e_x^{(0)}+i\sin(q_xa)e_z^{(0)}], \tag{4.70}$$

$$K_3\sum_{p=1}^{2}A_p[(2+\cos(q_xa))e_z^{(p)}-i\sin(q_xa)e_x^{(p)}]$$
$$+\sum_{p=3}^{4}A_p[\left(3(K_2-K_3)e^{iq_z^{(p)}a}-K_2(2+\cos(q_xa))\right)e_z^{(p)}+K_2\left(i\sin(q_xa)\right)e_x^{(p)}]$$
$$=K_3A_0[-\left(2+\cos(q_xa)\right)e_z^{(0)}+i\sin(q_xa)e_x^{(0)}]. \tag{4.71}$$

The reflection and transmission amplitudes are obtained be simultaneously solving the equation

$$\sum_{p=0}^{4} M_{np} A_p = 0, \quad n = 1, \ldots 4, \tag{4.72}$$

where

$$\begin{aligned}
M_{1p} \quad (p=0) \quad &= -\left((K_1 - K_3) - K_1 \cos(q_x a) e^{iq_z^{(p)} a}\right) e_x^{(p)} \\
&\quad + iK_1 \sin(q_x a) e^{iq_z^{(p)} a} e_z^{(p)}, \\
M_{1p} \quad (p=1,2) \quad &= \left((K_1 - K_3) - K_1 \cos(q_x a) e^{-iq_z^{(p)} a}\right) e_x^{(p)} \\
&\quad - iK_1 \sin(q_x a) e^{-iq_z^{(p)} a} e_z^{(p)}, \\
M_{1p} \quad (p=3,4) \quad &= K_3 \cos(q_x a) e^{iq_z^{(p)} a} e_x^{(p)} + iK_3 \sin(q_x a) e^{iq_z^{(p)} a} e_z^{(p)}, \\
M_{2p} \quad (p=0) \quad &= -\left(3(K_1 - K_3) - K_1(2 + \cos(q_x a)) e^{iq_z^{(p)} a}\right) e_z^{(p)} \\
&\quad + iK_1 \sin(q_x a) e^{iq_z^{(p)} a} e_x^{(p)}, \\
M_{2p} \quad (p=1,2) \quad &= \left(3(K_1 - K_3) - K_1(2 + \cos(q_x a)) e^{-iq_z^{(p)} a}\right) e_z^{(p)} \\
&\quad - iK_1 \sin(q_x a) e^{-iq_z^{(p)} a} e_x^{(p)}, \\
M_{2p} \quad (p=3,4) \quad &= K_3 (2 + \cos(q_x a)) e^{iq_z^{(p)} a} e_z^{(p)} + iK_3 \sin(q_x a) e^{iq_z^{(p)} a} e_x^{(p)}, \\
M_{3p} \quad (p=0,1,2) \quad &= K_3 \cos(q_x a) e_x^{(p)} - iK_3 \sin(q_x a) e_z^{(p)}, \\
M_{3p} \quad (p=3,4) \quad &= \left((K_2 - K_3) e^{iq_z^{(p)} a} - K_2 \cos(q_x a)\right) e_x^{(p)} + iK_2 \sin(q_x a) e_z^{(p)}, \\
M_{4p} \quad (p=0,1,2) \quad &= K_3 (2 + \cos(q_x a)) e_z^{(p)} - iK_3 \sin(q_x a) e_x^{(p)}, \\
M_{4p} \quad (p=3,4) \quad &= \left(3(K_2 - K_3) e^{iq_z^{(p)} a} - K_2(2 + \cos(q_x a))\right) e_z^{(p)} \\
&\quad + iK_2 \sin(q_x a) e_x^{(p)}.
\end{aligned} \tag{4.73}$$

The reflection and transmission coefficients are defined as $R_{ti} = |A_1|^2$, $R_{li} = |A_2|^2$, $T_{ti} = |A_3|^2$, $T_{li} = |A_4|^2$, where $R_{ni}(n = t,\, l)$ is the coefficient of reflection into n^{th} mode and $T_{ni}(n = t,\, l)$ is the coefficient of transmission into the n^{th} mode. The coefficients satisfy the following conservation rule

$$J_I = J_R + \frac{m_2}{m_1} J_T, \tag{4.74}$$

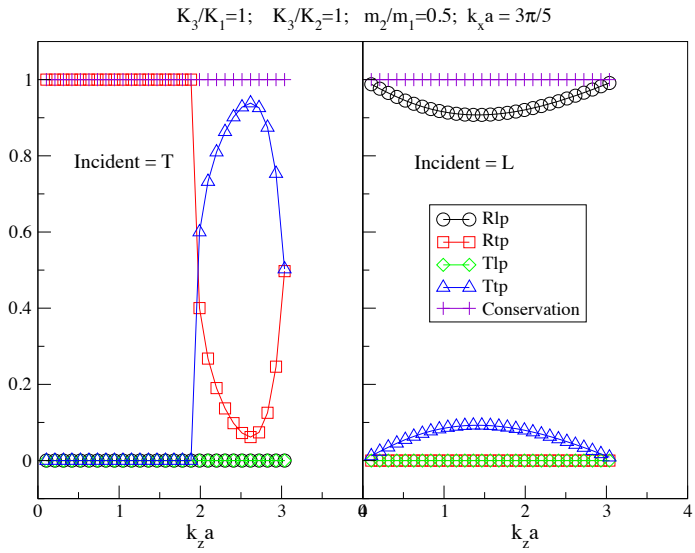

Figure 4.6. Phonon reflection and transmission coefficients at the interface between two square lattices.

with

$$\begin{aligned} \mathbf{J}_I &= \hbar\left(\frac{1}{2}\nabla_k\omega_i^2\right)|A_0|^2, \\ \mathbf{J}_R &= \hbar\left(\frac{1}{2}\nabla_k\omega_{Rn}^2\right)|R_{ni}|^2, \\ \mathbf{J}_T &= \hbar\left(\frac{1}{2}\nabla_k\omega_{Tn}^2\right)|T_{ni}|^2. \end{aligned} \tag{4.75}$$

Figure 4.6 shows the values of the phonon reflection and transmission coefficients at the interface between two square lattices for a particular choice of lattice parameters.

4.5 Three-Dimensional FCC Lattice

In the present section, we consider the interface between two three-dimensional lattices. Although the three-dimensional system has an added degree of complexity over the one and two-dimensional systems we considered in the previous sections, we can follow the exact same procedure to discuss the scattering problem. The two FCC lattices are divided by an interface between two (001) planes of masses as shown in Fig. 4.7. The origin is assumed to be at the site of the (0,0,0) mass,

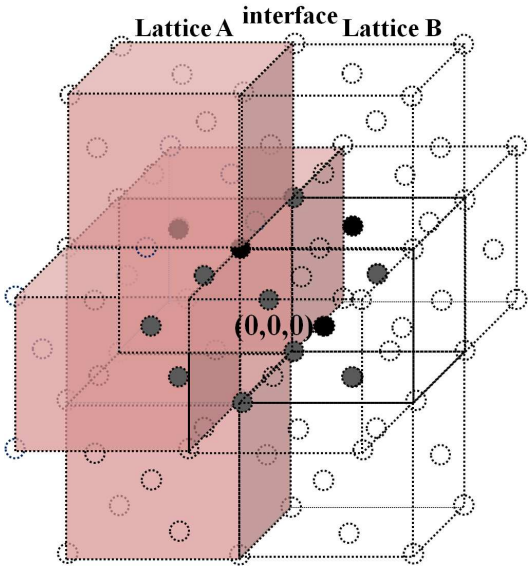

Figure 4.7. Solid-solid interface between two FCC lattices.

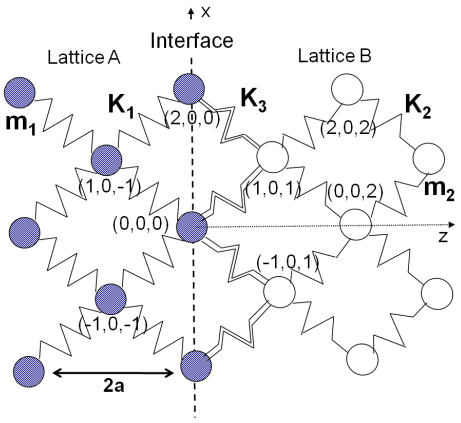

Figure 4.8. Top view of the solid-solid interface between two FCC lattices.

shown in Fig.4.7. The nearest neighbors of the (0,0,0) mass is marked by filled circles. The boundary layer is marked by the $z = 0$ plane. Figure 4.8 shows the top view of the interface. In lattice A, the masses m_1 are connected to their 12 nearest neighbors by springs of spring constant K_1. The masses m_2 in lattice B are connected to their 12 nearest neighbors by springs of stiffness K_2. The mass at the interface is connected to the nearest mass on opposite side of the interface, by spring of spring constant K_3. The spacing between the nearest neighbor masses in each of the lattices is $a\sqrt{2}$.

4.5.1 Phonon Modes

The Hamiltonian of the system can be similarly written as

$$H = \sum_j \frac{P_j^2}{2m} + V,$$
$$V = \frac{K}{2} \sum_\delta [\hat{\delta} \cdot (\mathbf{Q}_j - \mathbf{Q}_{j+\delta})]^2. \tag{4.76}$$

The twelve nearest neighbors are at $\hat{\delta}_1 = a(\pm 1, \pm 1, 0)$, $a(\pm 1, 0, \pm 1)$, $a(0, \pm 1, \pm 1)$. We consider only the nearest neighbor interaction to discuss the phonon modes of the lattice. For insulating solids with short range interaction between the atoms, we can obtain the correct dispersion relation with just the nearest neighbor interaction (We show this in detail in the next chapter for solid Argon). The equation of motion for a mass in the bulk is given by

$$-m_1 \ddot{\mathbf{Q}} = K \sum_\delta [\hat{\delta}\hat{\delta} \cdot (\mathbf{Q}_j - \mathbf{Q}_{j+\delta})]. \tag{4.77}$$

In component form the equation of motion can be written as

$$\begin{aligned} -m_1 \ddot{Q}^x_{l,m,n} = \frac{K}{2} \big[& Q^x_{l+1,m+1,n} + Q^x_{l+1,m,n+1} + Q^x_{l+1,m-1,n} + Q^x_{l+1,m,n-1} \\ & + Q^x_{l-1,m+1,n} + Q^x_{l-1,m,n+1} + Q^x_{l-1,m-1,n} + Q^x_{l-1,m,n-1} - 8Q^x_{l,m,n} \\ & + Q^y_{l+1,m+1,n} + Q^y_{l-1,m-1,n} - Q^y_{l+1,m-1,n} - Q^y_{l-1,m+1,n} \\ & + Q^z_{l+1,m,n+1} + Q^z_{l-1,m,n-1} - Q^z_{l+1,m,n-1} - Q^z_{l-1,m,n+1} \big]. \end{aligned} \tag{4.78}$$

The equations for $\ddot{Q}^y_{l,m,n}$ and $\ddot{Q}^z_{l,m,n}$ are obtained by cyclic permutation of the subscripts and the superscripts in the above equation. The solutions to these equations are assumed to be of the form

$$\mathbf{Q}_{l,m,n} = \hat{e} \exp i(\mathbf{q} \cdot \mathbf{r}_{lmn} - \omega t), \tag{4.79}$$

where $\hat{e}$ is the polarization vector and $\mathbf{q}$ is the wave vector and ω is the frequency of the phonon. Substitution of the solution Eq.(4.79) into the equation of motion

Eq.(4.78) yields,

$$\underline{\mathrm{D}}\hat{e} = \omega^2 \hat{e}. \tag{4.80}$$

The dynamical matrix $\underline{\mathrm{D}}$ is given by

$$\underline{\mathrm{D}} = \frac{K_1}{2m_1} \times \begin{pmatrix} 8 - 4\cos(\theta_x)\cos(\theta_y) & 4\sin(\theta_x)\sin(\theta_y) & 4\sin(\theta_x)\sin(\theta_z) \\ -4\cos(\theta_x)\cos(\theta_z) & & \\ 4\sin(\theta_x)\sin(\theta_y) & 8 - 4\cos(\theta_x)\cos(\theta_y) & 4\sin(\theta_y)\sin(\theta_z) \\ & -4\cos(\theta_y)\cos(\theta_z) & \\ 4\sin(\theta_x)\sin(\theta_z) & 4\sin(\theta_y)\sin(\theta_z) & 8 - 4\cos(\theta_x)\cos(\theta_z) \\ & & -4\cos(\theta_y)\cos(\theta_z) \end{pmatrix}, \tag{4.81}$$

where $\theta_i \equiv q_i a$. The eigenvalue equation Eq.(4.80) has a solution if the secular determinant of the dynamical matrix vanishes,

$$\left|\underline{\mathrm{D}} - \omega^2 \underline{\mathrm{I}}\right| = 0. \tag{4.82}$$

For given values of the wave vector $\mathbf{q}$, the above equation Eq.(4.82) can be solved for the roots of ω^2. On the other hand, given values of the frequency ω and any two components of the wavevectors, we can obtain the the third component of the wavevector by solving Eq.(4.82). However, in a significant fraction of cases, numerical solution of Eq.(4.82) is difficult and usually requires large amount of computation time. We transform Eq.(4.82) into an algebraic equation that can be solved easily. To carry out the transformation we define

$$X = 2\cos(\theta_x),\ Y = 2\cos(\theta_y),\ Z = 2\cos(\theta_z), \tag{4.83}$$

$$\text{and } \Omega = \frac{2M_s\omega^2}{K} - 8. \tag{4.84}$$

After some algebra, Eq.(4.82) can be written in the form

$$\Omega^3 + C_2\Omega^2 + C_1\Omega + C_0 = 0, \tag{4.85}$$

where,

$$
\begin{aligned}
C_2 &= 2(XY + YZ + ZX), \\
C_1 &= 3(X + Y + Z)XYZ + 8(X^2 + Y^2 + Z^2) - 48, \\
C_0 &= 4(XYZ)^2 + 4(X^2 + Y^2)(XY - Z^2) \\
&\quad + 4(Y^2 + Z^2)(YZ - X^2) \\
&\quad + 4(Z^2 + X^2)(ZX - Y^2) + 32(X^2 + Y^2 + Z^2) \\
&\quad - 32(XY + YZ + ZX) + 8(X + Y + Z)XYZ - 128.
\end{aligned}
$$

The roots of the algebraic equation Eq.(4.85) can be used to obtain the phonon frequencies of the FCC lattice. The simplified form of the equation can be used to evaluate the phonon group velocities. The z-component of the group velocity is given by

$$
\begin{aligned}
v_z &= \frac{\partial\omega}{\partial Z}\frac{\partial Z}{\partial q_z} = -\frac{Ka}{2M\omega}\frac{\partial\Omega}{\partial Z}\sin(\theta_z) \\
&= \frac{Ka}{2M\omega}\sin(\theta_z)\left[\left[\Omega^2\frac{\partial C_2}{\partial Z} + \Omega\frac{\partial C_1}{\partial Z} + \frac{\partial C_0}{\partial Z}\right]/(3\Omega^2 + 2C_2\Omega + C_1)\right]. \quad (4.86)
\end{aligned}
$$

Similar expressions can be obtained for the x and y-components of the group velocities by permutation of the variables. In order to obtain the z-component of the wave vector, we define $eZ = \exp(i\theta_z)$ and write Eq.(4.82) as a polynomial in eZ,

$$
CZ_3 eZ^6 + CZ_2 eZ^5 + CZ_1 eZ^4 + CZ_0 eZ^3 + CZ_1 eZ^2 + CZ_2 eZ + CZ_3 = 0, \quad (4.87)
$$

where,

$$
\begin{aligned}
CZ_3 &= 4(X + Y), \\
CZ_2 &= (8 + 3XY)\Omega + 8XY + 32 - 8(X^2 + Y^2) + 4X^2Y^2, \\
CZ_1 &= 2(X + Y)\Omega^2 + 3XY(X + Y)\Omega + 8XY(X + Y) \\
&\quad - 20(X + Y) + 4(X^3 + Y^3), \\
CZ_0 &= \Omega^3 + 2XY\Omega^2 + 8(X^2 + Y^2 - 4)\Omega + 6XY\Omega \\
&\quad + 4(X^2 + Y^2)XY - 16XY + 16(X^2 + Y^2) - 64.
\end{aligned}
$$

For each root $eZ_l\,(l = 1, \ldots 6)$, there is a corresponding root $1/eZ_l$. We found that most of the roots are real, but some of them have a non-zero imaginary part. We choose the roots with positive imaginary part. Using the values of the wave vectors, we can solve Eq.(4.80), for the polarization vectors of the phonons.

4.5.2 Reflection and Transmission Amplitudes

The displacements of masses in the two FCC lattices near the interface can be written as a linear contribution from the incident, reflected and transmitted waves,

$$\mathbf{Q}_{l,m,n} = \sum_{p=0}^{3} A_p \hat{e}^{(p)} \exp i(\mathbf{q}^{(p)} \cdot \mathbf{r}_{lm} - \omega t), \qquad \text{for masses} \in \text{lattice A} \quad (4.88)$$

$$\mathbf{W}_{l,m,n} = \sum_{p=4}^{6} A_p \hat{e}^{(p)} \exp i(\mathbf{q}^{(p)} \cdot \mathbf{r}_{lm} - \omega t), \qquad \text{for masses} \in \text{lattice B.} \quad (4.89)$$

The incident phonon with amplitude A_0 has wavevector $\mathbf{q}^{(0)}$ and polarization $\hat{e}^{(0)}$. The reflected phonon with amplitude $A_p(p = 1, 2, 3)$ has wavevector $\mathbf{q}^{(p)}$ and polarization $\hat{e}^{(p)}$ and the transmitted phonon with amplitude $A_p(p = 4, 5, 6)$ has wavevector $\mathbf{q}^{(p)}$ and polarization $\hat{e}^{(p)}$. As before, we choose the origin of coordinates to be at the position of a mass in lattice A at the interface, as shown in Fig.4.7. The nearest neighbors of the $(0, 0, 0)^{\text{th}}$ mass, in lattice A and lattice B are marked by filled circles. We solve the equations of motion of the masses in lattices A and B next to the interface to obtain the reflection and transmission amplitudes. The x-component for the equation of motion for the $(0, 0, 0)^{\text{th}}$ mass is given by

$$\begin{aligned} -m_1 \ddot{Q}^x_{0,0,0} = \frac{K_1}{2} \big[& Q^x_{1,1,0} + Q^x_{1,-1,0} + Q^x_{-1,1,0} + Q^x_{-1,-1,0} + Q^x_{-1,0,-1} + Q^x_{1,0,-1} \\ & -6Q^x_{0,0,0} + Q^y_{1,1,0} - Q^y_{1,-1,0} - Q^y_{-1,1,0} + Q^y_{-1,-1,0} + Q^z_{-1,0,-1} - Q^z_{1,0,-1} \big] \\ & + \frac{K_3}{2} \left[W^x_{1,0,1} + W^x_{-1,0,1} - 2Q^x_{0,0,0} + W^z_{1,0,1} - W^z_{-1,0,1} \right]. \end{aligned} \quad (4.90)$$

In the absence of interface, the equation of motion for the $(0, 0, 0)^{\text{th}}$ has the following form

$$-m_1 \ddot{Q}^x_{0,0,0} = \frac{K_1}{2} \big[Q^x_{1,1,0} + Q^x_{1,-1,0} + Q^x_{-1,1,0} + Q^x_{-1,-1,0} + Q^x_{-1,0,-1} + Q^x_{1,0,-1}$$

$$Q^x_{1,0,1} + Q^x_{-1,0,1} - 8Q^x_{0,0,0} + Q^y_{1,1,0} - Q^y_{1,-1,0} - Q^y_{-1,1,0} + Q^y_{-1,-1,0} + Q^z_{-1,0,-1} - Q^z_{1,0,-1} + Q^z_{1,0,1} - Q^z_{-1,0,1}\big] . \quad (4.91)$$

Subtracting we obtain

$$\frac{K_1}{2}\left[Q^x_{1,0,1} + Q^x_{-1,0,1} - 2Q^x_{0,0,0} + Q^z_{1,0,1} - Q^z_{-1,0,1}\right] = \frac{K_3}{2}\left[W^x_{1,0,1} + W^x_{-1,0,1} - 2Q^x_{0,0,0} + W^z_{1,0,1} - W^z_{-1,0,1}\right] . \quad (4.92)$$

Similarly, for the y and z-component we obtain

$$\frac{K_1}{2}\left[Q^y_{0,1,1} + Q^y_{0,-1,1} - 2Q^y_{0,0,0} + Q^z_{0,1,1} - Q^z_{0,-1,1}\right] = \frac{K_3}{2}\left[W^y_{0,1,1} + W^y_{0,-1,1} - 2Q^y_{0,0,0} + W^z_{0,1,1} - W^z_{0,-1,1}\right] , \quad (4.93)$$

$$\frac{K_1}{2}\left[Q^z_{1,0,1} + Q^z_{-1,0,1} + Q^z_{0,1,1} + Q^z_{0,-1,1} - 4Q^z_{0,0,0} + Q^x_{1,0,1} - Q^x_{-1,0,1} + Q^y_{0,1,1} - Q^y_{0,-1,1}\right] \quad (4.94)$$

$$= \frac{K_1}{2}\left[W^z_{1,0,1} + W^z_{-1,0,1} + W^z_{0,1,1} + W^z_{0,-1,1} - 4Q^z_{0,0,0} , + W^x_{1,0,1} - W^x_{-1,0,1} + W^y_{0,1,1} - W^y_{0,-1,1}\right] , \quad (4.95)$$

respectively. Inserting the solutions given in Eq.(4.88) into Eq.s(4.92-4.95), we obtain

$$K_1 \sum_{p=1}^{3} A_p[\left(1 - \frac{K_3}{K_1} - \cos(q_x a)e^{-iq_z^{(p)}a}\right) e_x^{(p)} - \left(i\sin(q_x a)e^{-iq_z^{(p)}a}\right) e_z^{(p)}] + K_3 \sum_{p=4}^{6} A_p[\cos(q_x a)e^{iq_z^{(p)}a}e_x^{(p)} + i\sin(q_x a)e^{iq_z^{(p)}a}e_z^{(p)}]$$
$$= A_0[-\left(1 - \frac{K_3}{K_1} - \cos(q_x a)e^{iq_z^{(0)}a})\right) e_x^{(0)} + \left(i\sin(q_x a)e^{iq_z^{(0)}a}\right) e_z^{(0)}], \quad (4.96)$$
$$K_1 \sum_{p=1}^{3} A_p[\left(1 - \frac{K_3}{K_1} - \cos(q_y a)e^{-iq_z^{(p)}a}\right) e_y^{(p)} - \left(i\sin(q_y a)e^{-iq_z^{(p)}a}\right) e_z^{(p)}]$$

$$+K_3\sum_{p=4}^{6}A_p[\cos(q_ya)e^{iq_z^{(p)}a}e_y^{(p)}+i\sin(q_ya)e^{iq_z^{(p)}a}e_z^{(p)}]$$

$$=A_0[-\left(1-\frac{K_3}{K_1}-\cos(q_ya)e^{iq_z^{(0)}a}\right)e_y^{(0)}+\left(i\sin(q_ya)e^{iq_z^{(0)}a}\right)e_z^{(0)}], \tag{4.97}$$

$$K_1\sum_{p=1}^{3}A_p[\left(2(1-\frac{K_3}{K_1})-(\cos(q_xa)+\cos(q_ya))e^{-iq_z^{(p)}a}\right)e_z^{(p)}$$
$$-\left(i\sin(q_xa)e^{-iq_z^{(p)}a}\right)e_x^{(p)}-\left(i\sin(q_ya)e^{-iq_z^{(p)}a}\right)e_y^{(p)}]$$
$$+K_3\sum_{p=4}^{6}A_p[(\cos(q_xa)+\cos(q_ya)e^{iq_z^{(p)}a}e_z^{(p)}$$
$$+i\sin(q_xa)e^{iq_z^{(p)}a}e_x^{(p)}+i\sin(q_ya)e^{iq_z^{(p)}a}e_y^{(p)}]$$
$$=A_0[-\left(2(1-\frac{K_3}{K_1})-(\cos(q_xa)+\cos(q_ya))e^{iq_z^{(0)}a}\right)e_z^{(0)}$$
$$+\left(i\sin(q_xa)e^{iq_z^{(0)}a}\right)e_x^{(0)}+\left(i\sin(q_ya)e^{iq_z^{(0)}a}\right)e_y^{(0)}]. \tag{4.98}$$

Following the same method, we obtain for the mass in lattice B, next to interface

$$K_3\sum_{p=1}^{3}A_p[\cos(q_xa)e_x^{(p)}-i\sin(q_xa)e_z^{(p)}]$$
$$+K_2\sum_{p=4}^{6}A_p[\left(\left(1-\frac{K_3}{K_2}\right)e^{iq_z^{(p)}a}-\cos(q_xa)\right)e_x^{(p)}+i\sin(q_xa)e_z^{(p)}]$$
$$=K_3A_0[-\cos(q_xa)e_x^{(0)}+i\sin(q_xa)e_z^{(0)}], \tag{4.99}$$
$$K_3\sum_{p=1}^{3}A_p[\cos(q_xa)e_x^{(p)}-i\sin(q_xa)e_z^{(p)}]$$
$$+K_2\sum_{p=4}^{6}A_p[\left(\left(1-\frac{K_3}{K_2}\right)e^{iq_z^{(p)}a}-\cos(q_ya)\right)e_y^{(p)}+i\sin(q_{xy}a)e_z^{(p)}]$$
$$=K_3A_0[-\cos(q_ya)e_y^{(0)}+i\sin(q_ya)e_z^{(0)}], \tag{4.100}$$
$$K_3\sum_{p=1}^{3}A_p[(\cos(q_xa)+\cos(q_ya))e_z^{(p)}-i\sin(q_xa)e_x^{(p)}-i\sin(q_ya)e_y^{(p)}]$$
$$+K_2\sum_{p=4}^{6}A_p[\left(2\left(1-\frac{K_3}{K_2}\right)e^{iq_z^{(p)}a}-(\cos(q_xa)+\cos(q_ya))\right)e_z^{(p)}$$

$$
\begin{aligned}
&+i\sin(q_x a)e_x^{(p)} + i\sin(q_y a)e_y^{(p)}] \\
&= K_3 A_0[(\cos(q_x a)+\cos(q_y a))e_z^{(0)} - i\sin(q_x a)e_x^{(0)} - i\sin(q_y a)e_y^{(0)}]. \qquad (4.101)
\end{aligned}
$$

The reflection and transmission amplitudes are obtained be simultaneously solving the equation

$$
\sum_{p=0}^{6} M_{np}A_p = 0, \quad n = 1,\dots 6, \qquad (4.102)
$$

where

$$
\begin{aligned}
M_{1p}(p=0) &= K_1\left(\left(1-\frac{K_3}{K_1}\right) - \cos(q_x a)e^{iq_z^{(0)}a}\right)e_x^{(0)} \\
&- iK_1\sin(q_x a)e^{iq_z^{(0)}a}e_z^{(p0)}, \\
M_{1p}(p=1,2,3) &= K_1\left(\left(1-\frac{K_3}{K_1}\right) - \cos(q_x a)e^{-iq_z^{(p)}a}\right)e_x^{(p)} \\
&- iK_1\sin(q_x a)e^{-iq_z^{(p)}a}e_z^{(p)}, \\
M_{1p}(p=4,5,6) &= K_3\cos(q_x a)e^{iq_z^{(p)}a}e_x^{(p)} + iK_3\sin(q_x a)e^{iq_z^{(p)}a}e_z^{(p)}, \\
M_{2p}(p=0) &= K_1\left(\left(1-\frac{K_3}{K_1}\right) - \cos(q_y a)e^{iq_z^{(0)}a}\right)e_y^{(0)} \\
&- iK_1\sin(q_y a)e^{iq_z^{(0)}a}e_z^{(0)}, \\
M_{2p}(p=1,2,3) &= K_1\left(\left(1-\frac{K_3}{K_1}\right) - \cos(q_y a)e^{-iq_z^{(p)}a}\right)e_y^{(p)} \\
&- iK_1\sin(q_y a)e^{-iq_z^{(p)}a}e_z^{(p)}, \\
M_{2p}(p=4,5,6) &= K_3\cos(q_y a)e^{iq_z^{(p)}a}e_y^{(p)} + iK_3\sin(q_y a)e^{iq_z^{(p)}a}e_z^{(p)}, \\
M_{3p}(p=0) &= K_1\left(2\left(1-\frac{K_3}{K_1}\right) - (\cos(q_x a)+\cos(q_y a))e^{iq_z^{(0)}a}\right)e_z^{(0)} \\
&- iK_1\sin(q_x a)e^{iq_z^{(0)}a}e_x^{(0)} - iK_1\sin(q_y a)e^{iq_z^{(0)}a}e_y^{(0)}, \\
M_{3p}(p=1,2,3) &= K_1\left(2\left(1-\frac{K_3}{K_1}\right) - (\cos(q_x a)+\cos(q_y a))e^{-iq_z^{(p)}a}\right)e_z^{(p)} \\
&- iK_1\sin(q_x a)e^{-iq_z^{(p)}a}e_x^{(p)} - iK_1\sin(q_y a)e^{-iq_z^{(p)}a}e_y^{(p)}, \\
M_{3p}(p=4,5,6) &= K_3(\cos(q_x a)+\cos(q_y a))e^{iq_z^{(p)}a}e_z^{(p)} \\
&+ iK_3\sin(q_x a)e^{iq_z^{(p)}a}e_x^{(p)} + iK_3\sin(q_y a)e^{iq_z^{(p)}a}e_y^{(p)}, \qquad (4.103) \\
M_{4p}(p=0,1,2,3) &= K_3\cos(q_x a)e_x^{(p)} - iK_3\sin(q_x a)e_z^{(p)},
\end{aligned}
$$

$$
\begin{aligned}
M_{4p}(p=4,5,6) &= K_2\left(\left(1-\frac{K_3}{K_2}\right)e^{iq_z^{(p)}a}-\cos(q_xa)\right)e_x^{(p)} \\
&+ iK_2\sin(q_xa)e_z^{(p)}, \\
M_{5p}(p=0,1,2,3) &= K_3\cos(q_ya)e_y^{(p)}-iK_3\sin(q_ya)e_z^{(p)}, \\
M_{5p}(p=4,5,6) &= K_2\left(\left(1-\frac{K_3}{K_2}\right)e^{iq_z^{(p)}a}-\cos(q_ya)\right)e_y^{(p)} \\
&+ iK_2\sin(q_ya)e_z^{(p)}, \\
M_{6p}(p=0,1,2,3) &= K_3(\cos(q_ya)+\cos(q_xa))e_z^{(p)}-iK_3\sin(q_xa)e_x^{(p)} \\
&- iK_3\sin(q_ya)e_y^{(p)}, \\
M_{6p}(p=4,5,6) &= K_2\left(2\left(1-\frac{K_3}{K_2}\right)e^{iq_z^{(p)}a}-(\cos(q_xa)+\cos(q_ya))\right)e_z^{(p)} \\
&+ iK_2\sin(q_xa)e_x^{(p)}+iK_2\sin(q_ya)e_y^{(p)}.
\end{aligned}
$$

The reflection and transmission coefficients are defined as $R_{li}=|A_1|^2,\ R_{t1i}=|A_2|^2,\ R_{t2i}=|A_3|^2,\ T_{li}=|A_4|^2,\ T_{t1i}=|A_5|^2,\ T_{t2i}=|A_6|^2$, where $R_{ni}(n=l,\,t_1,\,t_2)$ is the coefficient of reflection into n^{th} mode and $T_{ni}(n=l,\,t_1,\,t_2)$ is the coefficient of transmission into the n^{th} mode. The coefficients satisfy the following conservation rule

$$
J_I = J_R + \frac{m_2}{m_1}J_T, \tag{4.104}
$$

with

$$
\begin{aligned}
\mathbf{J}_I &= \hbar\left(\frac{1}{2}\nabla_k\omega_i^2\right)|A_0|^2, \\
\mathbf{J}_R &= \hbar\left(\frac{1}{2}\nabla_k\omega_{Rn}^2\right)|R_{ni}|^2, \\
\mathbf{J}_T &= \hbar\left(\frac{1}{2}\nabla_k\omega_{Tn}^2\right)|T_{ni}|^2.
\end{aligned} \tag{4.105}
$$

Figure 4.9 shows the values of the phonon reflection and transmission coefficients at the interface between two FCC lattices for a particular choice of lattice parameters.

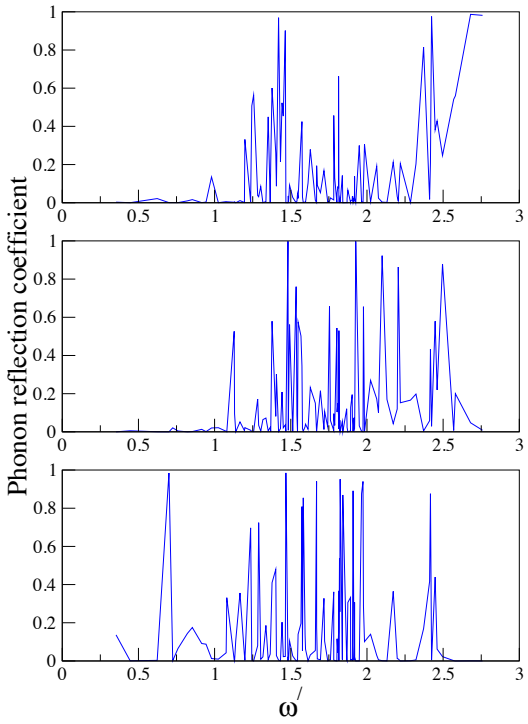

Figure 4.9. Phonon reflection coefficients at the interface between two FCC lattices with $K_3/K_1 = 2$, $K_3/K_2 = 2$ and $m_2/m_1 = 1$. Here $\omega' = \omega/\sqrt{K/m_1}$.

4.6 Discussion

In this chapter, we discuss the scattering of acoustic waves at several solid-solid interfaces. Although there are some articles in the existing literature ([94], [95], [38]) which discuss the topic, we found most of them lacking a detailed description of the method. Here, we provide a thorough prescription for calculation of reflection and transmission of phonons at solid-solid model interfaces. Our discussion includes examples from different dimensions: the interface between two one-dimensional harmonic chains, the interface between two two-dimensional rhombic lattices, the interface between two two-dimensional square lattices and lastly, the interface between two FCC lattices. We include two examples for the two-dimensional case to show how the arrangements of atoms can influence the scattering of phonons at interfaces. We obtain analytical expressions of phonon reflection and transmission coefficients for the first three cases. The three-dimensional case is more complex and involves analysis with transcendental functions. Here we present a method to simplify the equations by converting them into simple algebraic equations. These

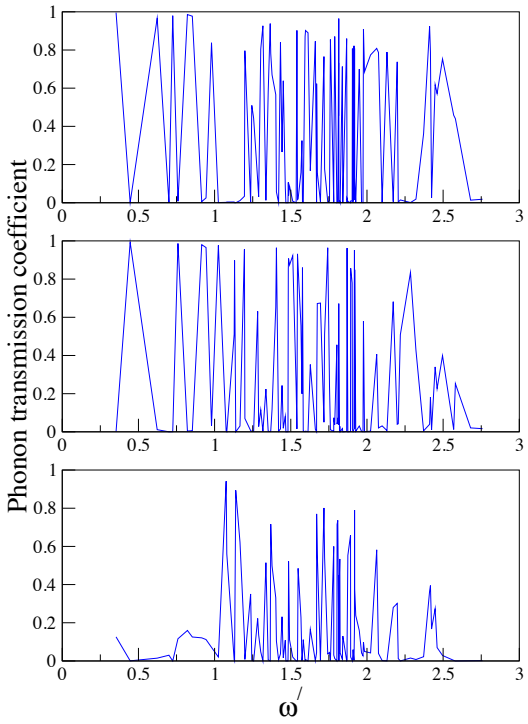

Figure 4.10. Phonon transmission coefficients at the interface between two FCC lattices with $K_3/K_1 = 2$, $K_3/K_2 = 2$ and $m_2/m_1 = 1$. Here $\omega' = \omega/\sqrt{K/m_1}$.

coefficients are consistent with the conservation relations and reproduce the familiar forms in the continuum limit. The method we prescribed is quite general and would be useful for application to other interfaces as well.

Chapter 5

Scattering of Phonon at Solid-Fluid Interface: Kapitza Resistance

5.1 Introduction

The thermal resistance at the interface between two materials is known as Kapitza resistance, named after Kapitza [27] who first observed that there exists a temperature discontinuity at the interface between superfluid liquid helium, and other metals. In this chapter, we continue to explore the scattering of phonons at interfaces. The focus of our discussion is the interface between a solid and a fluid. We confine ourselves to the discussion of insulating solids only, where heat is mainly transported by phonons. Also, our discussion includes only classical fluids. Scattering of phonons at an interface, is the primary reason behind the presence of the thermal boundary resistance. The resistance can be determined from the knowledge of the phonon transmission and reflection coefficients at the interface.

The Young-Maris [38] theory for the thermal boundary resistance works well for the interface between two solids. This theory is based on a microscopic harmonic model of atom vibrations at an interface. Their model included the coupling between all the phonon modes in the two crystals, on each side of the interface. However, this model assumed perfect lattice matching of the two solids at the interface. Pettersson and Mahan [39] extended the Young-Maris theory to apply to all commensurate interfaces. We call this combined theory YMPM, which works

quite well for clean interfaces. Our discussion in the last chapter about phonon scattering at the interface between two FCC lattices, follows the outline described in the Young-Maris theory.

However, the theory for the thermal boundary resistance between solid-fluid interfaces has not progressed as much [96]. The only available theory is the acoustic mismatch theory, which works poorly for solid-fluid interfaces. One reason is that this theory only includes the long wavelength acoustic phonons. AMT theory ignores the transverse excitations in the fluid. Transverse sound waves are shown to exist in fluids at larger values of wave vector ([82], [97], [98]). The transverse sound waves in a fluid are highly damped and totally diffusive at long wavelength. However, these damped waves can diffuse through interfaces ([99], [100]), and they can carry heat away from the interface. Hence the transverse sound waves can still play a role in the thermal boundary resistance. This chapter presents a method of extending the YMPM theory to the solid-liquid interface. We obtain the phonon reflection and transmission coefficients at the solid-fluid interface, by coupling all the phonon modes in the solid with all the sound wave modes in the fluid. We only consider heat flow by sound waves or diffusion and ignore the case of convection. We provide an application of the method to obtain the thermal boundary resistance at the interface between solid Argon and liquid Neon.

5.2 Theory

In a solid, the heat flow along a unit normal vector $\hat{n}$, can be expressed as:

$$J_Q = \sum_{\lambda} \int \frac{d^3q}{(2\pi)^3} \hbar\omega_\lambda(\mathbf{q}) \hat{n} \cdot \mathbf{v}_\lambda n_B[\omega_\lambda(\mathbf{q})], \tag{5.1}$$

where $\mathbf{q}$ is the wave vector of the phonon, λ represents the polarization of the phonon, $\hbar\omega_\lambda(\mathbf{q})$ is the energy of the phonon, $\hat{n} \cdot \mathbf{v}_\lambda$ is the component of the phonon velocity along the direction $\hat{n}$ and $n_B[\omega_\lambda(\mathbf{q})]$ is the Bose-Einstein occupation factor for phonons at a temperature T. At high temperatures, the Bose-Einstein occupation factor can be approximated as $n_B[\omega_\lambda(\mathbf{q})] \approx k_B T/\hbar\omega_\lambda(\mathbf{q})$. The amount of

heat transmitted across the interface, can then be written as,

$$J_{QT} = k_B T_R \sum_{\lambda} \int \frac{d^3q}{(2\pi)^3} \hat{n} \cdot \mathbf{v}_\lambda \mathcal{T}, \tag{5.2}$$

where $\mathcal{T}$ is the phonon transmission coefficient.

In thermal equilibrium, there can be no net heat flow across the interface if the temperatures of the two sides are equal. According to the principle of detailed balance, the number of phonons leaving one side, is the same as the number of phonons returning from the other side with the same wavevector and polarization. This principle enables us to calculate the net heat transfer across the interface from the knowledge of the gross heat transfer from one side of the interface. The net heat transfer would be simply the difference between the gross heat transfers at the two incident phonon temperatures. The difference between the temperatures is ΔT. Hence, the Kapitza conductance can be found from the following expression at high temperatures,

$$\begin{aligned} J_Q &= \sigma \Delta T \\ \sigma &= k_B \sum_{\lambda} \int \frac{d^3q}{(2\pi)^3} \hat{n} \cdot \mathbf{v}_\lambda \mathcal{T} \end{aligned} \tag{5.3}$$

The integral is evaluated only for the phonons with $\hat{n} \cdot \mathbf{v}_\lambda(\mathbf{q}) \geq 0$. In a solid, the number of phonons going toward the interface on an average would be the same as the phonons going away from it. Hence, we can write

$$\sigma = \frac{k_B}{2} \sum_{\lambda} \int \frac{d^3q}{(2\pi)^3} \left| \hat{n} \cdot \mathbf{v}_\lambda \right| \mathcal{T}. \tag{5.4}$$

5.2.1 Phonons in solid

A cartoon of our system is shown in Fig. 5.1. The interface is marked by the plane perpendicular to the z axis. The solid atoms are on the left of the interface and are marked with circles. The fluid atoms are to the right of the interface and are marked with squares. The atoms in the solid are assumed to be arranged in a regular array. The distances to the neighboring atoms in the solid are represented with the vector δ_s and that in the fluid are represented with δ_f. The distance

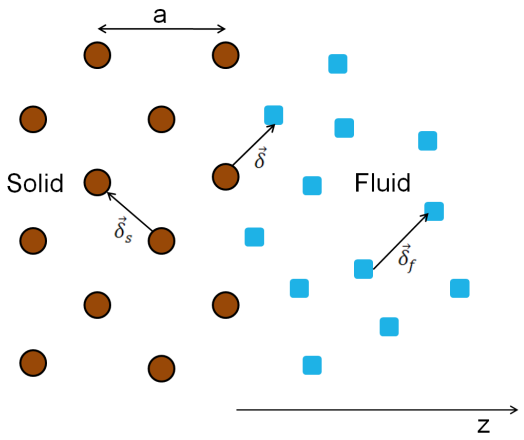

Figure 5.1. Cartoon of solid-fluid interface. Solid atoms are on the left and fluids are to the right. The interface is perpendicular to the z axis. Arrows denote the vectors used in the following equations.

between a solid and a neighboring fluid atom near the interface is represented with δ. We assume that the atoms in the solid undergo small displacements ($\mathbf{Q}_{sj}$) from their equilibrium positions. The potential energy between the atoms in the solid is

$$V_{ss} = \frac{1}{2}\sum_{j,\delta_s} K(\delta_s)[\hat{\delta}_s \cdot (\mathbf{Q}_{sj} - \mathbf{Q}_{s,j+\delta_s})]^2, \tag{5.5}$$

$$\delta_s = \mathbf{R}^{(0)}_{sj} - \mathbf{R}^{(0)}_{s,j+\delta_s} \tag{5.6}$$

where the spring constant K is bond directed. $\mathbf{R}^{(0)}_{sj}$ represents the equilibrium positions of the atoms and δ_s are the distances to the neighboring atoms in various directions. The equation of motion of an atom in the bulk of the solid, far from the interface is given by

$$M_s\omega^2\mathbf{Q}_j = \sum_{\delta_s} K(\delta_s)\hat{\delta}_s\hat{\delta}_s \cdot (\mathbf{Q}_{sj} - \mathbf{Q}_{s,j+\delta_s}), \tag{5.7}$$

where M_s is the mass of the solid atom and ω is the frequency of the phonon in the lattice.

5.2.2 Pair Distribution Function

In order to correctly evaluate solid-fluid and fluid-fluid interaction terms, we need to take account of the fact that the positions of the fluid atoms change as they move around. The information about the short-range correlations between the fluid atoms are contained in the pair distribution function $g(\mathbf{r})$. We consider uniform systems, which implies that the pair distribution function in the bulk of the fluid, is a function of the distance between the atoms only. Throughout the discussion, we assume small displacements for both the solid and fluid atoms, so that $\mathbf{R}_s \approx \mathbf{R}_s^{(0)}$ and $\mathbf{R}_f \approx \mathbf{R}_f^{(0)}$. Within the bulk of the fluid, the probability of finding a fluid atom at $\mathbf{R}_{fm}^{(0)}$ given that there is a fluid atom at $\mathbf{R}_{fn}^{(0)}$, is given by $g(|\mathbf{R}_{fn}^{(0)} - \mathbf{R}_{fm}^{(0)}|)$. The pair distribution function depends on the interaction potential between the atoms and can be evaluated by the method described in Chapter 3.

The one-particle distribution function near the interface can be evaluated in the following way: according to Percus [74], the one particle probability density $n(\mathbf{r}|U)$ in the presence of an external potential U can be written as

$$\begin{aligned} n(\mathbf{r}|U)e^{\beta U(\mathbf{r})} =& n(\mathbf{r}) + \int d^3r_1 \mathcal{F}_2(\mathbf{r}, \mathbf{r}_1) \left(e^{-\beta U(r_1)} - 1\right) \\ &+ \frac{1}{2} \int d^3r_1 \int d^3r_2 \mathcal{F}_3(\mathbf{r}, \mathbf{r}_1, \mathbf{r}_2) \left(e^{-\beta U(r_1)} - 1\right) \left(e^{-\beta U(r_2)} - 1\right) + \ldots \end{aligned} \tag{5.8}$$

where $\mathcal{F}_{2,3}$ are the two and three particle Ursell functions, as defined in Eq. (3.6). If we ignore three particle correlations ($\mathcal{F}_n = 0$ for $n \geq 3$), and use the relationship between Ursell function and pair distribution function (following Eq. (3.17)), we obtain the following expression for one particle distribution function in a uniform system near an interface

$$\begin{aligned} g(\mathbf{r}|V_{sf})e^{\beta V_{sf}(\mathbf{r})} \approx& 1 + n \int d^3r_1 \left[g(|\mathbf{r} - \mathbf{r}_1|) - 1\right] \left(e^{-\beta V_{sf}(r_1)} - 1\right) \\ g_{sf}(\mathbf{R}_{sj}^{(0)}, \mathbf{R}_{fn}^{(0)}) =& g\left(\left(\mathbf{R}_{fn}^{(0)} - \mathbf{R}_{sj}^{(0)}\right) | V_{sf}\left(|\mathbf{R}_{fn}^{(0)} - \mathbf{R}_{sj}^{(0)}|\right)\right). \end{aligned} \tag{5.9}$$

$g_{sf}(\mathbf{R}_{sj}^{(0)}, \mathbf{R}_{fn}^{(0)})$ is the probability that there is a fluid atom at $\mathbf{R}_{fn}^{(0)}$ provided that there is a solid atom at $\mathbf{R}_{sj}^{(0)}$.

As the fluid atom approaches the interface, the fluid pair distribution function

changes because of the presence of the interface potential. We need to define the pair distribution function for the fluid atoms near the interface in a different way compared to the one for the bulk fluid atoms. We define $g_{ff}(\mathbf{R}_{fn}^{(0)}, \mathbf{R}_{fm}^{(0)})$ to be the pair distribution function between the fluid atoms when both the atoms are close to the interface. This function would depend on both the fluid-fluid and the fluid-solid interaction potential. The expression for the two-particle probability density $n_2(\mathbf{r}_1, \mathbf{r}_2|U)$ in the presence of an external potential U can be written as

$$n_2(\mathbf{r}_1, \mathbf{r}_2|U)e^{\beta[U(\mathbf{r}_1)+U(\mathbf{r}_2)]} = n_2(\mathbf{r}_1, \mathbf{r}_2) + \int d^3r_3 \mathcal{F}_3(\mathbf{r}_1, \mathbf{r}_2, \mathbf{r}_3)\left(e^{-\beta U(\mathbf{r}_3)} - 1\right)$$
$$+\frac{1}{2}\int d^3r_3 \int d^3r_4 \mathcal{F}_{24}(\mathbf{r}_1, \mathbf{r}_2, \mathbf{r}_3, \mathbf{r}_4)\left(e^{-\beta U(r_3)} - 1\right)\left(e^{-\beta U(r_4)} - 1\right) + \ldots \quad (5.10)$$

where $n_2(\mathbf{r}_1, \mathbf{r}_2) = g(\mathbf{r}_1 - \mathbf{r}_2)n(\mathbf{r}_1)n(\mathbf{r}_2)$. The form of g_{ff} can be approximated as

$$g_{ff}(\mathbf{R}_{fn}^{(0)}, \mathbf{R}_{fm}^{(0)}) \approx g(|\mathbf{R}_{fn}^{(0)} - \mathbf{R}_{fm}^{(0)}|)e^{-\beta V_{sf}(R_{fn}^{(0)}) - \beta V_{sf}(R_{fm}^{(0)})}. \quad (5.11)$$

5.2.3 Sound Wave Excitations in Fluid

The frequency spectrum for the sound waves in classical fluids in equilibrium, is determined by the general expression ([101], [102]):

$$\omega_{\mathbf{k}\lambda}^2 = \frac{k_B T}{M_f}(1 + 2\hat{\epsilon}_{\mathbf{k}\lambda} \cdot \hat{\epsilon}_{\mathbf{k}1})k^2 + \frac{n}{M_f}\int d\mathbf{r} g(r)(1 - \exp(\mathbf{k} \cdot \mathbf{r}))(\hat{\epsilon}_{\mathbf{k}\lambda} \cdot \nabla)^2 V_{ff}(\mathbf{r}), \quad (5.12)$$

where M_f is the mass of the fluid atom, n is number density of the fluid and T is the temperature of the fluid, respectively. $V_{ff}(\mathbf{r})$ is the interaction potential between the fluid atoms and $g(\mathbf{r})$ is the pair distribution function of the fluid in bulk. $\hat{\epsilon}_{\mathbf{k}\lambda}(\lambda = 1, 2, 3)$ represent the three orthogonal polarization vectors of the sound waves in the fluid. The longitudinal one is given by

$$\hat{\epsilon}_{\mathbf{k}1} = \frac{\mathbf{k}}{|\mathbf{k}|}. \quad (5.13)$$

In general, the wave vectors for the sound wave excitations in fluid are complex. The imaginary part of the wave vector contributes to damping and diffusion of the sound waves. We assume that the fluid atoms are spherically symmetric and

interact with each other via a central potential, $V_{ff}(r)$. For the sound waves traveling in z-direction, the frequencies for the longitudinal and transverse modes are given by:

$$\omega_l^2(k) = 3\omega_0^2 + \frac{n}{M_f}\int d^3r g(r)[1-\exp(ikz)]\frac{\partial^2}{\partial z^2}V_{ff}(r) \tag{5.14}$$

$$\omega_t^2(k) = \omega_0^2 + \frac{n}{M_f}\int d^3r g(r)[1-\exp(ikz)]\frac{\partial^2}{\partial x^2}V_{ff}(r) \tag{5.15}$$

$$\omega_0^2 = k^2\frac{k_BT}{M_f} \tag{5.16}$$

The term ω_0^2 corresponds to the long range density fluctuations in the fluid. Assuming that the fluid atoms undergo small displacements ($\mathbf{q}_f$) from their equilibrium positions ($\mathbf{R}_f$) during the propagation of the sound waves, we can expand the interaction potential in a Taylor series

$$V_{ff}(|\mathbf{R}_{fn}-\mathbf{R}_{fm}|) = V(|\mathbf{R}_{fn}^{(0)}-\mathbf{R}_{fm}^{(0)}|) + (\mathbf{q}_{fn}-\mathbf{q}_{fm})\cdot\mathbf{F}_{ff}(|\mathbf{R}_{fn}^{(0)}-\mathbf{R}_{fm}^{(0)}|) \tag{5.17}$$
$$+\frac{1}{2}\{A_{ff}(R)(\mathbf{q}_{fn}-\mathbf{q}_{fm})^2 + B_{ff}(R)[(\mathbf{q}_{fn}-\mathbf{q}_{fm})\cdot\hat{\delta}_f]^2\},$$

$$\text{where}\quad A_{ff}(R) = \frac{1}{R}\frac{dV_{ff}}{dR},\ \mathbf{F}_{ff}(R) = \hat{\delta}_f A_{ff} \tag{5.18}$$

$$\text{and}\ B_{ff}(R) = \frac{d^2V_{ff}}{dR^2} - A_{ff}(R), \tag{5.19}$$

$$\text{with}\ \delta_f = \mathbf{R}_{fn}^{(0)} - \mathbf{R}_{fm}^{(0)}, \hat{\delta}_f = \frac{\delta_f}{\delta_f}. \tag{5.20}$$

Here, $\mathbf{R}_{fn}$ and $\mathbf{R}_{fm}$ denote the equilibrium positions and $\mathbf{q}_{fn}$ and $\mathbf{q}_{fm}$ denote the displacements of the n^{th} and m^{th} fluid atoms, respectively. The first-order force term vanishes when we take the average over all the fluid atoms. Inserting the approximate potential form (Eq. (5.17)) into the frequency expressions (Eqs. (5.21), (5.15)) and evaluating the integrals in spherical polar coordinates we obtain

$$\omega_l^2(k) = 3\omega_0^2 + \frac{4\pi n}{M_f}\int r^2 dr g(r)\left[A_{ff}(r)\left(1-\frac{\sin(kr)}{kr}\right)\right. \tag{5.21}$$
$$+\ \left. B_{ff}(r)\left(\frac{1}{3}-\frac{\sin(kr)}{kr}-\frac{2\sin(kr)}{(kr)^2}+\frac{\sin(kr)}{(kr)^3}\right)\right],$$

$$\omega_t^2(k) = \omega_0^2 + \frac{4\pi n}{M_f}\int r^2 dr g(r)\left[A_{ff}(r)\left(1-\frac{\sin(kr)}{kr}\right)\right. \tag{5.22}$$

$$+ \quad B_{ff}(r)\left(\frac{1}{6} - \frac{\sin(kr)}{2kr} - \frac{\sin(kr)}{(kr)^2} + \frac{\sin(kr)}{(kr)^3}\right)\Bigg].$$

The equation of motion for an atom in the bulk of the fluid can then be written as

$$M_f\omega^2\mathbf{q}_{fn} = \sum_m [A_{ff}(\delta_f)(\mathbf{q}_{fn} - \mathbf{q}_{fm}) + B_{ff}(\delta_f)\hat{\delta}_f\hat{\delta}_f \cdot (\mathbf{q}_{fn} - \mathbf{q}_{fm})]. \tag{5.23}$$

5.2.4 Solid-Fluid Interaction Potential

The solid and the fluid subsystem is divided by an interface as shown in Fig. 5.1. The solid atoms are assumed to be arranged in locations $\mathbf{R}_{sj} = (\rho_j,\, z_j)$. The vectors ρ_j are parallel to the interface, and $\hat{z}$ is perpendicular to the interface. We consider the interface between a neutral solid and a neutral fluid subsystem. Hence, the potential $V_{sf}(\mathbf{r})$ acting between a solid and a fluid atom can be assumed to be of short-range. The potential is assumed to be a central potential. We make an assumption similar to the fluid system. The phonons in the solid and the sound waves in the fluid, cause only small displacements of the interface solid and fluid atoms. Hence, we can Taylor expand the interface potential around small displacements,

$$V_{sf}(|\mathbf{R}_{sj} - \mathbf{R}_{fm}|) = V(|\mathbf{R}^{(0)}_{sj} - \mathbf{R}^{(0)}_{fm}|) + (\mathbf{Q}_{sj} - \mathbf{q}_{fm}) \cdot \mathbf{F}_{sf}(|\mathbf{Q}^{(0)}_{sj} - \mathbf{R}^{(0)}_{fm}|) \tag{5.24}$$
$$+\frac{1}{2}\{A_{sf}(R)(\mathbf{Q}_{sj} - \mathbf{q}_{fm})^2 + B_{sf}(R)[(\mathbf{Q}_{sj} - \mathbf{q}_{fm}) \cdot \hat{\delta}]^2\},$$
$$\text{where} \quad A_{sf}(R) = \frac{1}{R}\frac{dV_{sf}}{dR},\ \mathbf{F}_{sf}(R) = \hat{\delta}A_{sf} \tag{5.25}$$
$$\text{and} \ \ B_{sf}(R) = \frac{d^2V_{sf}}{dR^2} - A_{sf}(R), \tag{5.26}$$
$$\text{with} \ \ \delta = \mathbf{R}^{(0)}_{sj} - \mathbf{R}^{(0)}_{fm}, \hat{\delta} = \frac{\delta}{\delta}. \tag{5.27}$$

The average force $\mathbf{F}_{sf}$ is not zero, since the fluid exerts some average pressure on the surface of the fluid.

5.2.5 Coupling Between Solid and Fluid

5.2.5.1 Excitations

The solid lattice is assumed to have only one atom in its unit cell. It has three phonon branches: one longitudinal (l) and two transverse ($t1$, $t2$). When one of these phonons is incident on the interface, either it is reflected or transmitted to the fluid with some amplitude. We consider the phonons in the solid to approach the interface from the side of negative z-axis. The incident phonon is labeled with a subscript i. The frequency, polarization and wavevector of the incident phonon is written as ω, $\hat{e}_i$ and ($\mathbf{k}$, k_i), respectively. $\mathbf{k} = (k_x,\, k_y\,, 0)$ represents the component of the wave vector parallel to the interface and k_i is the component perpendicular to the interface. The reflected waves would have same values of frequency ω, and the parallel component of the wave vector $\mathbf{k}$, but different perpendicular component k_{sn} and polarization $\hat{e}_{sn}$. $n\,(= 1, 2, 3)$ denotes one longitudinal and two transverse polarizations. The solid atoms are displaced by both the incident and reflected waves. The displacement of a solid atom can be written as the linear combination:

$$\mathbf{Q}_{sj} = e^{i(\mathbf{k}\cdot\rho_j - \omega t)} \left[\hat{e}_i e^{ik_i z_j} I_i + \sum_{i=1}^{n} R_n \hat{e}_{sn} e^{-ik_{sn} z_j} \right]. \tag{5.28}$$

Here, I_i is the amplitude of the incident wave and R_n is the amplitude of the reflected wave. In general, the polarization vectors for the three reflected waves, $\hat{e}_{sn}$ are not mutually orthogonal.

The transmitted waves in the fluid have the same frequency ω and the same parallel component of the wavevector $\mathbf{k}$ as the incident wave. However, the perpendicular component of the wavevector k_{fn} and the polarization vectors $\hat{e}_{fn}$ are different. Here also, $n = 1, 2, 3$ represents the three polarization directions. The displacement of a fluid atom can be written as

$$\mathbf{q}_{fm} = e^{i(\mathbf{k}\cdot\rho_{fm} - \omega t)} \sum_{i=1}^{n} T_n \hat{e}_{fn} e^{ik_{fn} z_{fm}}. \tag{5.29}$$

Here, T_n is the amplitude of the transmitted wave.

5.2.5.2 Boundary Matching

The boundary is marked by the plane $z = 0$. The solid atoms are assumed to lie at the interface, where $z_j = 0$. The equations of motion of these atoms contain force-terms due to solid-fluid interaction along with the force-terms due to solid-solid interaction:

$$\begin{aligned}\underbrace{M_s\omega^2\mathbf{Q}_{sj}}_{\text{solid atom at } z=0} =& \sum_{\delta_s} \underbrace{K(\delta_s)\hat{\delta}_s\hat{\delta}_s\cdot(\mathbf{Q}_{sj}-\mathbf{Q}_{s,j+\delta_s})}_{\text{solid atoms with } z<0} \\ &+\sum_m \underbrace{[A_{sf}(\delta)(\mathbf{Q}_{sj}-\mathbf{q}_{fm})+B_{sf}(\delta)\hat{\delta}\hat{\delta}\cdot(\mathbf{Q}_{sj}-\mathbf{q}_{fm})]}_{\text{fluid atoms with } z>0} \qquad (5.30)\\ &\text{with } \delta_s = \mathbf{R}^{(0)}_{sj}-\mathbf{R}^{(0)}_{s,j+\delta_s} \text{ and } \delta = \mathbf{R}^{(0)}_{sj}-\mathbf{R}^{(0)}_{fm}.\end{aligned}$$

The summation over δ_s includes the neighboring atoms in the solid near the interface while the summation over δ represents the atoms in the fluid that are near the interface. We would refer to this equation as the solid interface-equation of motion. Similarly, the equation of motion of the fluid atom near the interface has force-terms due to both fluid-fluid and fluid-solid interaction,

$$\begin{aligned}\underbrace{M_f\omega^2\mathbf{q}_{fn}}_{\text{fluid atom with } z\approx 0} =& \sum_j \underbrace{[A_{sf}(\delta)(\mathbf{q}_{fn}-\mathbf{Q}_{sj})+B_{sf}(\delta)\hat{\delta}\hat{\delta}\cdot(\mathbf{q}_{fn}-\mathbf{Q}_{sj})]}_{\text{solid atoms with } z<0} \\ &+\sum_m \underbrace{[A_{ff}(\delta_f)(\mathbf{q}_{fn}-\mathbf{q}_{fm})+B_{ff}(\delta_f)\hat{\delta}_f\hat{\delta}_f\cdot(\mathbf{q}_{fn}-\mathbf{q}_{fm})]}_{\text{fluid atoms with } z>0} \qquad (5.31)\\ &\text{with } \delta = \mathbf{R}^{(0)}_{sj}-\mathbf{R}^{(0)}_{fn} \text{ and } \delta_f = \mathbf{R}^{(0)}_{fm}-\mathbf{R}^{(0)}_{fn}.\end{aligned}$$

The summation over j is due to the atoms of the solid close to the fluid atom, near the interface. The summation over m represents the interaction of the fluid atom with other fluid atoms close by. We would refer to this equation as the fluid interface-equation of motion.

5.2.5.3 Coupling Matrix: $\mathcal{M}$

Due to the short-range of the solid-fluid interaction potential, we need to include only the fluid atoms near the interface in Eq. (5.30). The one particle distribution

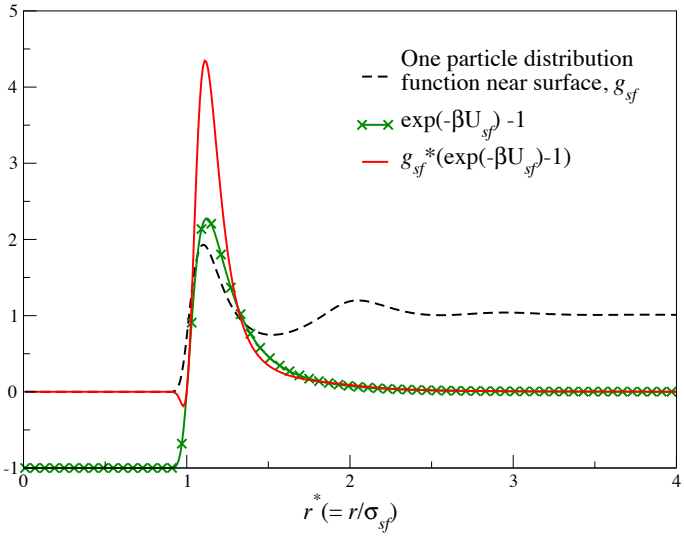

Figure 5.2. Determination of the position of fluid atom near the interface. U_{sf} is the interaction potential between two Lennard-Jones systems, solid Argon and fluid Neon. The density and temperature of the fluid is given by $n = 0.0239\mathring{A}^{-3}$ and $T = 54.345$ K, respectively.

function, $g_{sf}(r)$ provides the information about the position of the fluid atom in the presence of an external potential. The solid-fluid interaction potential provides the range of interaction between the solid and the fluid atoms. Hence, g_{sf} combined with V_{sf} determines the cutoff for the position of the fluid atom near the interface. The solid line in Fig. 5.2 represents the product between the one particle distribution function and the function $(e^{-\beta U_{sf}} - 1)$ for solid Argon-fluid Neon interface and yields the cutoff for the position of the fluid atom near the interface. We include only the fluid atoms with position within the region, where this product function is non-zero, in our analysis.

Using the solid-fluid distribution function and the cutoff function, we replace the force terms in Eqs. (5.30) and integrate over all possible positions of the fluid atoms. We obtain for the solid interface-equation of motion

$$\underbrace{M_s\omega^2\mathbf{Q}_{sj}}_{\text{solid atom at } z=0} = \sum_{\delta_s} \underbrace{K(\delta_s)\hat{\delta}_s\hat{\delta}_s \cdot (\mathbf{Q}_{sj} - \mathbf{Q}_{s,j+\delta_s})}_{\text{solid atoms with } z<0}$$

$$\underbrace{+n\int d^3R g_{sf}(\mathbf{R}_s^{(0)},\mathbf{R})(e^{-\beta U_{sf}(|\mathbf{R}_s^{(0)}-\mathbf{R}|)}-1)[A_{sf}(\delta)\mathcal{I}+B_{sf}(\delta)\hat{\delta}\hat{\delta}]\cdot(\mathbf{Q}_{sj}-\mathbf{q}(\mathbf{R}))}_{\text{fluid atoms with } z>0} \tag{5.32}$$

$$(\text{with } \delta=\mathbf{R}_s^{(0)}-\mathbf{R}).$$

We can reformulate this equation using the bulk-equation motion of the solid atom, Eq. (5.7). The dispersion relation term in the LHS of the interface-equation can be replaced by the RHS of the bulk-equation, Eq. (5.7), representing the summation over all the atoms. The first term in the RHS of the interface-equation represents the summation over the neighboring atoms in the solid, only on the left side of the interface ($z<0$). After subtracting, we get

$$\sum_{\delta_s}\underbrace{K(\delta_s)\hat{\delta}_s\hat{\delta}_s\cdot(\mathbf{Q}_{sj}-\mathbf{Q}_{s,j+\delta_s})}_{\text{solid atoms with } z>0}$$
$$=\underbrace{n\int d^3R g_{sf}(\mathbf{R}_s^{(0)},\mathbf{R})(e^{-\beta U_{sf}(|\mathbf{R}_s^{(0)}-\mathbf{R}|)}-1)[A_{sf}(\delta)\mathcal{I}+B_{sf}(\delta)\hat{\delta}\hat{\delta}]\cdot(\mathbf{Q}_{sj}-\mathbf{q}(\mathbf{R}))}_{\text{fluid atoms with } z>0} \tag{5.33}$$

Here the summation δ_s is over all the solid atoms, for which $z>0$. This summation is over the missing neighbors of the solid atom at the interface. It is useful to write this way because we only need to consider the atoms with positive z-coordinates. We set the origin of our coordinate system at the j^{th} atom at the interface, $\mathbf{R}_s^{(0)}=0\Rightarrow\mathbf{R}_s^{(0)}-\mathbf{R}\approx\mathbf{R}$ and $\delta\approx\mathbf{R}$. With this assumption, Eq. (5.33) can be modified to

$$\sum_{\delta_s}\underbrace{K(\delta_s)\hat{\delta}_s\hat{\delta}_s\cdot(\mathbf{Q}_{sj}-\mathbf{Q}_{s,j+\delta_s})}_{\text{solid atoms with } z>0}$$
$$=n\int_{z>0}d^3R g_{sf}(R)(e^{-\beta U_{sf}(R)}-1)[A_{sf}(R)\mathcal{I}+B_{sf}(R)\hat{R}\hat{R}]\cdot(\mathbf{Q}_{sj}-\mathbf{q}(\mathbf{R})). \tag{5.34}$$

Rearranging the above equation, and using the expression for the displacement of

fluid atoms Eq. (5.29), we get

$$\sum_{\delta_s} \underbrace{K(\delta_s)\hat{\delta}_s\hat{\delta}_s \cdot (\mathbf{Q}_{sj} - \mathbf{Q}_{s,j+\delta_s})}_{\text{solid atoms with } z>0} = \mathcal{M}(0,0)\cdot\mathbf{Q}_{sj} - \mathcal{M}(\mathbf{k},k_z)\cdot\mathbf{q}(0), \tag{5.35}$$

$$\text{with } \mathcal{M}(0,0) = n\int_{z>0} d^3R g_{sf}(R)(e^{-\beta U_{sf}(R)}-1)[A_{sf}(R)\mathcal{I} + B_{sf}(R)\hat{R}\hat{R}] \tag{5.36}$$

$$\text{and } \mathcal{M}(\mathbf{k},k_z)\cdot\mathbf{q}(0) = \sum_{n=1}^{3}\mathcal{M}(\mathbf{k},k_{fn})\cdot\hat{e}_{fn}T_n$$

$$\text{with } \mathcal{M}(\mathbf{k},k_{fn}) = n\int_{z>0} d^3R g_{sf}(R)(e^{-\beta U_{sf}(R)}-1)$$
$$\times[A_{sf}(R)\mathcal{I} + B_{sf}(R)\hat{R}\hat{R}]e^{i\mathbf{k}\cdot\rho + ik_{fn}z} \tag{5.37}$$

where $\mathcal{I}$ is the unit tensor and k_{fn} are the wave vectors of the three transmitted waves in fluid. We introduce the solid-fluid coupling matrix $\mathcal{M}$; both $\mathcal{M}(0,0)$ and $\mathcal{M}(\mathbf{k},k_z)$ are second rank tensors, we can write them in component form as follows:

$$\mathcal{M}(0,0) = A\mathcal{I} + B_\perp(\hat{x}\hat{x}+\hat{y}\hat{y}) + B_z\hat{z}\hat{z}, \tag{5.38}$$

$$\begin{aligned}\mathcal{M}(\mathbf{k},k_{fn}) &= M_A(\mathbf{k},k_{fn})\mathcal{I} + \hat{x}\hat{x}M_{xx}(\mathbf{k},k_{fn}) + \hat{y}\hat{y}M_{yy}(\mathbf{k},k_{fn})\\ &+ \hat{z}\hat{z}M_{zz}(\mathbf{k},k_{fn}) + (\hat{x}\hat{y}+\hat{y}\hat{x})M_{xy}(\mathbf{k},k_{fn})\\ &+ (\hat{x}\hat{z}+\hat{z}\hat{x})M_{xz}M_{yz}(\mathbf{k},k_{fn}) + (\hat{z}\hat{y}+\hat{y}\hat{z})M_{yz}(\mathbf{k},k_{fn}),\end{aligned} \tag{5.39}$$

where the different components of the $\mathcal{M}(0,0)$ are given by:

$$\begin{aligned}A &= 2\pi n\int_0^\infty dz\int_0^\infty \rho d\rho g_U sf(R)A_{sf}(R),\\ B_\perp &= \pi n\int_0^\infty dz\int_0^\infty \rho d\rho g_{Usf}(R)B_{sf}(R)\frac{\rho^2}{\rho^2+z^2},\\ B_z &= 2\pi n\int_0^\infty dz\int_0^\infty \rho d\rho g_{Usf}(R)B_{sf}(R)\frac{z^2}{\rho^2+z^2},\end{aligned} \tag{5.40}$$

$$\text{with}\quad g_{Usf}(R) = g_{sf}(R)(e^{-\beta U_{sf}(R)}-1). \tag{5.41}$$

The set of tensor elements (M_{xx}, M_{yy}, M_{zz}, M_{xy}, M_{yz}, M_{xz}) each has one term

with A_{sf} in the integrand and another term with B_{sf} in the integrand. Grouping together similar terms, we can write

$$\begin{aligned}\mathcal{M}(\mathbf{k},k_{fn}) &= M_A(\mathbf{k},k_{fn})\mathcal{I} + (\hat{x}\hat{x}+\hat{y}\hat{y})M_{0\perp}(\mathbf{k},k_{fn}) + \hat{z}\hat{z}M_{0z}(\mathbf{k},k_{fn}) \\ &- [(\hat{x}\hat{x}-\hat{y}\hat{y})\cos(2\phi_k) + (\hat{x}\hat{y}+\hat{y}\hat{x})\sin(2\phi_k)]M_{2\perp}(\mathbf{k},k_{fn}) \\ &+ i[(\hat{x}\hat{z}+\hat{z}\hat{x})\cos(\phi_k) + (\hat{z}\hat{y}+\hat{y}\hat{z})i\sin(\phi_k)]M_1(\mathbf{k},k_{fn})\end{aligned} \quad (5.42)$$

where ϕ_k is the angle between the component of the wavevector parallel to the interface and the x-axis, $\mathbf{k} = k[\cos(\phi_k),\sin(\phi_k)]$. The different elements of the tensor are given by

$$\begin{aligned}M_A(\mathbf{k},k_{fn}) &= 2\pi n\int_0^\infty dz\exp[ik_{fn}z]\int_0^\infty \rho d\rho g_{Usf}(R)A_{sf}(R)J_0(k\rho), \\ M_{l\perp}(\mathbf{k},k_{fn}) &= \pi n\int_0^\infty dz\exp[ik_{fn}z]\int_0^\infty \rho^3 d\rho g_{Usf}(R)\frac{B_{sf}(R)}{R^2}J_l(k\rho), \\ M_{0z}(\mathbf{k},k_{fn}) &= 2\pi n\int_0^\infty z^2 dz\exp[ik_{fn}z]\int_0^\infty \rho d\rho g_{Usf}(R)\frac{B_{sf}(R)}{R^2}J_0(k\rho), \\ M_1(\mathbf{k},k_{fn}) &= 2\pi n\int_0^\infty z dz\exp[ik_{fn}z]\int_0^\infty \rho^2 d\rho g_{Usf}(R)\frac{B_{sf}(R)}{R^2}J_1(k\rho),\end{aligned} \quad (5.43)$$

where $J(k\rho)$ are the Bessel functions of the first kind. The tensor $\mathcal{M}$ represents the coupling of the phonons in the solid to the sound modes of the fluid. It has nonzero tensor components that couple to longitudinal as well as transverse excitations in the fluid and solid. $\mathcal{M}$ has the units of a spring constant.

5.2.5.4 Coupling Matrix: $\mathcal{U}$, $\mathcal{V}$

We can reformulate the interface-equation of motion of the fluid atom in a similar way. Introducing the pair distribution functions, we obtain

$$\underbrace{M_f\omega^2\mathbf{q}_{fn}}_{\text{fluid atom with } z\approx 0} = \sum_j \underbrace{[A_{sf}(\delta)(\mathbf{q}_{fn}-\mathbf{Q}_{sj}) + B_{sf}(\delta)\hat{\delta}\hat{\delta}\cdot(\mathbf{q}_{fn}-\mathbf{Q}_{sj})]}_{\text{solid atoms with } z<0}$$
$$+\underbrace{n\int d^3R g_{ff}(\mathbf{R}^{(0)}_{fn},\mathbf{R})[A_{ff}(\delta_f)(\mathbf{q}_{fn}-\mathbf{q}(\mathbf{R})) + B_{ff}(\delta_f)\hat{\delta}_f\hat{\delta}_f\cdot(\mathbf{q}_{fn}-\mathbf{q}(\mathbf{R}))]}_{\text{fluid atoms with } z>0} \quad (5.44)$$

$$\text{with } \delta = \mathbf{R}_{sj}^{(0)} - \mathbf{R}_{fn}^{(0)} \text{ and } \delta_f = \mathbf{R} - \mathbf{R}_{fn}^{(0)}.$$

Using the bulk-equation for dispersion of sound waves in fluid Eq. (5.23), we can replace the LHS and obtain

$$\underbrace{n\int d^3R g(|\mathbf{R}_{fn}^{(0)}-\mathbf{R}|)[A_{ff}(\delta_f)\mathcal{I}+B_{ff}(\delta_f)\hat{\delta}_f\hat{\delta}_f]\cdot(\mathbf{q}_{fn}-\mathbf{q}(\mathbf{R}))}_{\text{fluid atoms with } z<0}$$
$$\underbrace{+n\int d^3R (g(|\mathbf{R}_{fn}^{(0)}-\mathbf{R}|)-g_{ff}(\mathbf{R}_{fn}^{(0)},\mathbf{R}))[A_{ff}(\delta_f)\mathcal{I}+B_{ff}(\delta_f)\hat{\delta}_f\hat{\delta}_f]\cdot(\mathbf{q}_{fn}-\mathbf{q}(\mathbf{R}))}_{\text{fluid atoms with } z>0}$$
$$=\sum_j \underbrace{[A_{sf}(\delta)+B_{sf}(\delta)\hat{\delta}\hat{\delta}]\cdot(\mathbf{q}_{fn}-\mathbf{Q}_{sj})}_{\text{solid atoms with } z<0}, \tag{5.45}$$

where $g_{ff}(\mathbf{R}_{fn}^{(0)},\mathbf{R})$ is the pair distribution function of the fluid near the interface. For simplicity, we assume that the pair distribution function of the fluid near the interface do not differ much from the bulk pair distribution function, so that $g(|\mathbf{R}_{fn}^{(0)}-\mathbf{R}|)\approx g_{ff}(\mathbf{R}_{fn}^{(0)},\mathbf{R})$ in the first approximation and the second term in the LHS vanishes in the above equation. Hence, we have

$$\underbrace{n\int d^3R g(|\mathbf{R}_{fn}^{(0)}-\mathbf{R}|)[A_{ff}(\delta_f)\mathcal{I}+B_{ff}(\delta_f)\hat{\delta}_f\hat{\delta}_f]\cdot(\mathbf{q}_{fn}-\mathbf{q}(\mathbf{R}))}_{\text{fluid atoms with } z<0}$$
$$=\sum_j \underbrace{[A_{sf}(\delta)+B_{sf}(\delta)\hat{\delta}\hat{\delta}]\cdot(\mathbf{q}_{fn}-\mathbf{Q}_{sj})}_{\text{solid atoms with } z<0}. \tag{5.46}$$

In order to incorporate the effect of the changing position of the fluid atom, we average over all the possible positions by multiplying both sides of the equation with $ng_{Usf}(R_{fn})$ and integrating with respect to $\mathbf{R}_{fn}$. The modified equation becomes

$$n^2\int_{z>0} d^3R_{fn}g_{Usf}(R_{fn})\int_{z<0} d^3R g(|\mathbf{R}_{fn}-\mathbf{R}|)$$
$$\times[A_{ff}(|\mathbf{R}_{fn}-\mathbf{R}|)\mathcal{I}+B_{ff}(|\mathbf{R}_{fn}-\mathbf{R}|)\frac{(\mathbf{R}-\mathbf{R}_{fn})^2}{|\mathbf{R}-\mathbf{R}_{fn}|^2}]\cdot(\mathbf{q}_{fn}-\mathbf{q}(\mathbf{R}))$$

$$= \sum_{j,z<0} n \int_{z>0} d^3 R_{fn} g_{Usf}(R_{fn}) \tag{5.47}$$
$$\times [A_{sf}(|\mathbf{R}_{fn} - \mathbf{R}_{sj}|) + B_{sf}(|\mathbf{R}_{fn} - \mathbf{R}_{sj}|) \frac{(\mathbf{R}_{fn} - \mathbf{R}_{sj})^2}{|\mathbf{R}_{fn} - \mathbf{R}_{sj}|^2}] \cdot (\mathbf{q}_{fn} - \mathbf{Q}_{sj}).$$

Renaming $R_{fn} = R'$and changing the variables from ($\mathbf{R}'$, $\mathbf{R}$) to ($\mathbf{R}'$, $\mathbf{R}' - \mathbf{R} = \mathbf{r}$) in the LHS of the above equation and from $\mathbf{R}'$ to ($\mathbf{R}' - \mathbf{R}_{sj} = \mathbf{r}$) in the RHS, we obtain

$$\sum T_n \hat{e}_{fn} \cdot \left(n^2 \int_{z>0} d^3 R' g_{Usf}(R') \int_{\text{all space}} d^3 r g(r) \right.$$
$$\left. [A_{ff}(r)\mathcal{I} + B_{ff}(r)\hat{r}\hat{r}] \cdot (e^{i\mathbf{k}_T \cdot \mathbf{R}'} - e^{i\mathbf{k}_T \cdot (\mathbf{R}' - \mathbf{r})}) \right) (\text{with } \mathbf{k}_T = (\mathbf{k}, k_{fn}))$$
$$= \sum_{j,z<0} n \int_{z>0} d^3 r g_{Usf}(|\mathbf{r} + \mathbf{R}_{sj}|)[A_{sf}(r)\mathcal{I} + B_{sf}(r)\hat{r}\hat{r}] \cdot$$
$$\left(\sum T_n \hat{e}_{fn} e^{i\mathbf{k}_T \cdot (\mathbf{r} + \mathbf{R}_{sj})} - e^{i\mathbf{k} \cdot \rho_{sj}} \left[\hat{e}_i e^{ik_i z_{sj}} I_i + \sum_{i=1}^{n} R_n \hat{e}_{sn} e^{-ik_{sn} z_{sj}} \right] \right). \tag{5.48}$$

We assume that $\mathbf{R}_{sj} \approx (0, 0, 0)$, the fluid atoms considered is closest to the solid atom at the origin and obtain

$$\sum T_n \hat{e}_{fn} \cdot \left(n^2 \int_{z>0} d^3 R' g_{Usf}(R') \int_{\text{all space}} d^3 r g(r) \right.$$
$$\left. [A_{ff}(r)\mathcal{I} + B_{ff}(r)\hat{r}\hat{r}] \cdot (e^{i\mathbf{k}_T \cdot \mathbf{R}'} - e^{i\mathbf{k}_T \cdot (\mathbf{R}' - \mathbf{r})}) \right)$$
$$= n \int_{z>0} d^3 r g_{Usf}(r)[A_{sf}(r)\mathcal{I} + B_{sf}(r)\hat{r}\hat{r}] \cdot$$
$$\left(\sum T_n \hat{e}_{fn} e^{i\mathbf{k}_T \cdot \mathbf{r}} - \left[\hat{e}_i I_i + \sum_{i=1}^{n} R_n \hat{e}_{sn} \right] \right). \tag{5.49}$$

We can write the interface equation as

$$[\mathcal{U}(\mathbf{k}, k_z) - \mathcal{V}(\mathbf{k}, k_z)] \cdot \mathbf{q}(0) = \mathcal{M}(\mathbf{k}, k_z) \cdot \mathbf{q}(0) - \mathcal{M}(0, 0) \cdot \mathbf{Q}_{sj} \tag{5.50}$$

where, $\mathcal{U}$ and $\mathcal{V}$ are the fluid-solid coupling matrices

$$\mathcal{U}(\mathbf{k}, k_{fn}) = n^2 \int_{z>0} d^3 R' g_{sf}(R')(e^{-\beta U_{sf}(R')} - 1) e^{i\mathbf{k}_T \cdot \mathbf{R}'} \int_{\text{all space}} d^3 r g(r)$$

$$\times[A_{ff}(r) + B_{ff}(r)\hat{r}\hat{r}], \tag{5.51}$$

$$\mathcal{V}(\mathbf{k}, k_{fn}) = n^2 \int_{z>0} d^3R' g_{sf}(R')(e^{-\beta U_{sf}(R')} - 1)e^{i\mathbf{k}_T\cdot\mathbf{R}'} \int_{\text{all space}} d^3r g(r) \times e^{-i\mathbf{k}_T\cdot\mathbf{r}}[A_{ff}(r) + B_{ff}(r)\hat{r}\hat{r}], \tag{5.52}$$

and $\mathcal{M}$'s are as defined before in Eq. (5.37). Both $\mathcal{U}$ and $\mathcal{V}$ are second-rank tensors and as before, we can write them in component form as follows:

$$\mathcal{U}(\mathbf{k}, k_z) = U_A(\mathbf{k}, k_{fn})\mathcal{I} + U_\perp(\mathbf{k}, k_{fn})(\hat{x}\hat{x} + \hat{y}\hat{y}) + \hat{z}\hat{z}U_z(\mathbf{k}, k_{fn}), \tag{5.53}$$

$$\begin{aligned}\mathcal{V}(\mathbf{k}, k_z) &= V_A(\mathbf{k}, k_{fn})\mathcal{I} + \hat{x}\hat{x}V_{xx}(\mathbf{k}, k_{fn}) + \hat{y}\hat{y}V_{yy}(\mathbf{k}, k_{fn}) \\ &+ \hat{z}\hat{z}V_{zz}(\mathbf{k}, k_{fn}) + (\hat{x}\hat{y} + \hat{y}\hat{x})V_{xy}(\mathbf{k}, k_{fn}) \\ &+ (\hat{x}\hat{z} + \hat{z}\hat{x})V_{xz}(\mathbf{k}, k_{fn}) + (\hat{z}\hat{y} + \hat{y}\hat{z})V_{zy}(\mathbf{k}, k_{fn}),\end{aligned} \tag{5.54}$$

where the different components of the $\mathcal{U}(\mathbf{k}, k_{fn})$ are given by:

$$\begin{aligned}U_A &= I_{surface} \times \left(2\pi n \int_{-\infty}^{\infty} dz \int_0^{\infty} \rho d\rho g(R) A_{ff}(R)\right), \\ U_\perp &= I_{surface} \times \left(\pi n \int_{-\infty}^{\infty} dz \int_0^{\infty} \rho d\rho g(R) B_{ff}(R) \frac{\rho^2}{\rho^2 + z^2}\right), \\ U_z &= I_{surface} \times \left(2\pi n \int_{-\infty}^{\infty} dz \int_0^{\infty} \rho d\rho g(R) B_{ff}(R) \frac{z^2}{\rho^2 + z^2}\right),\end{aligned} \tag{5.55}$$

$$\text{with } I_{surface} = 2\pi n \int_0^{\infty} dz' \exp[ik_{fn}z'] \int_0^{\infty} \rho' d\rho' g_{sf}(R')(e^{-\beta U_{sf}(R')} - 1)J_0(k\rho'), \tag{5.56}$$

where $J_0(k\rho)$ is the Bessel functions of the first kind. The set of tensor elements (V_{xx}, V_{yy}, V_{zz}, V_{xy}, V_{yz}, V_{xz}) each has one term with A_{ff} in the integrand and another term with B_{sff} in the integrand. Grouping together similar terms, we can write

$$\begin{aligned}\mathcal{V}(\mathbf{k}, k_{fn}) &= V_A(\mathbf{k}, k_{fn})\mathcal{I} + (\hat{x}\hat{x} + \hat{y}\hat{y})V_{0\perp}(\mathbf{k}, k_{fn}) + \hat{z}\hat{z}V_{0z}(\mathbf{k}, k_{fn}) \\ &- [(\hat{x}\hat{x} - \hat{y}\hat{y})\cos(2\phi_k) + (\hat{x}\hat{y} + \hat{y}\hat{x})\sin(2\phi_k)]V_{2\perp}(\mathbf{k}, k_{fn}) \\ &+ i[(\hat{x}\hat{z} + \hat{z}\hat{x})\cos(\phi_k) + (\hat{z}\hat{y} + \hat{y}\hat{z})i\sin(\phi_k)]V_1(\mathbf{k}, k_{fn}).\end{aligned} \tag{5.57}$$

where ϕ_k is the angle between the component of the wavevector parallel to the interface and the x-axis, $\mathbf{k} = k[\cos(\phi_k), \sin(\phi_k)]$. The different elements of the tensor are given by

$$\begin{aligned}
V_A(\mathbf{k}, k_{fn}) &= I_{surface} \times \left(2\pi n \int_{-\infty}^{\infty} dz \exp[-ik_{fn}z] \int_0^{\infty} \rho d\rho g(R) A_{ff}(R) J_0(k\rho) \right), \\
V_{l\perp}(\mathbf{k}, k_{fn}) &= I_{surface} \times \left(\pi n \int_{-\infty}^{\infty} dz \exp[-ik_{fn}z] \int_0^{\infty} \rho^3 d\rho g(R) \frac{B_{ff}(R)}{R^2} J_l(k\rho) \right), \\
V_{0z}(\mathbf{k}, k_{fn}) &= I_{surface} \times \left(2\pi n \int_{-\infty}^{\infty} z^2 dz \exp[-ik_{fn}z] \int_0^{\infty} \rho d\rho g(R) \frac{B_{ff}(R)}{R^2} J_0(k\rho) \right), \\
V_1(\mathbf{k}, k_{fn}) &= I_{surface} \times \left(-2\pi n \int_{-\infty}^{\infty} z dz \exp[-ik_{fn}z] \int_0^{\infty} \rho^2 d\rho g(R) \frac{B_{ff}(R)}{R^2} J_1(k\rho) \right).
\end{aligned} \tag{5.58}$$

The tensor $\mathcal{U}$ and $\mathcal{V}$ determine the coupling of the sound modes in the fluid. Both of them have the units of a spring constant.

Eq. (5.35) and Eq. (5.50) are the two key equations of this chapter. Each of these two equations is a vector equation with three components, and the six equations form a 6×6 set of linear equations. The six equations can be expressed in matrix form as

$$\sum_{n=1}^{3} C_{pn} R_n + \sum_{n=4}^{6} C_{pn} T_n = C_{p0} I_i, \ p = 1, \ldots 6. \tag{5.59}$$

The coefficients C_{pn} are given in Appendix B. There are six unknown amplitudes (R_n, T_n) as introduced in Eq. (5.28) and Eq. (5.29), respectively. These are the two key equations that help us determine the solution for these unknown amplitudes. The values for the transmission amplitudes yield the transmission coefficient $\mathcal{T}$, given by

$$\mathcal{T} = \left| \frac{T_n}{I_i} \right|^2, \tag{5.60}$$

where n is the index of polarization. We insert the values of the transmission coefficients into the equation for Kapitza conductance Eq. (5.4), to calculate the thermal boundary conductance at the solid-fluid interface.

5.3 Method and Results

5.3.1 Solid Phonon Modes

We consider a FCC lattice of solid Argon, the interface is marked by the (001) plane of atoms. The lattice constants for Argon is given by 5.31Å. The lattice has one atom in the unit cell. The atoms of mass M_s in the lattice, are connected to their 12 nearest neighbors by springs of stiffness K_1 and to their 6 next-nearest neighbors by springs of stiffness K_2. The spacing between nearest neighbors is $a/\sqrt{2}$. The directional vectors connecting these neighbors are given by $\delta_1 = \{\frac{a}{2}(\pm 1, \pm 1, 0)$, $\frac{a}{2}(\pm 1, 0, \pm 1)$,$\frac{a}{2}(0, \pm 1, \pm 1)\}$ and $\delta_2 = \{a(\pm 1, 0, 0)$,$a(0, \pm 1, 0)$,$a(0, 0, \pm 1)\}$, respectively. The solution for the equation of motion for the solid atom in the bulk Eq. (5.7) is assumed of the form

$$\mathbf{Q}_{sj} = \hat{e} \exp i \left(\mathbf{k}.\mathbf{r} - \omega t\right), \tag{5.61}$$

where $\hat{e}$ is the polarization vector, $\mathbf{k}$ is the wave vector and ω is the frequency of the phonon. Substitution of the solution Eq. (5.61) into the equation of motion Eq. (5.7) yields,

$$\underline{\mathrm{D}}\hat{e} = \omega^2 \hat{e} \tag{5.62}$$

where the dynamical matrix $\underline{\mathrm{D}}$ is given by

$$\underline{\mathrm{D}} = \frac{K_1}{M_s} \begin{pmatrix} 2X + 4 - 2X\cos(2\theta_x) & & \\ -2\cos(\theta_x)\cos(\theta_y) & 2\sin(\theta_x)\sin(\theta_y) & 2\sin(\theta_x)\sin(\theta_z) \\ -2\cos(\theta_x)\cos(\theta_z) & & \\ & 2X + 4 - 2X\cos(2\theta_y) & \\ 2\sin(\theta_x)\sin(\theta_y) & -2\cos(\theta_x)\cos(\theta_y) & 2\sin(\theta_y)\sin(\theta_z) \\ & -2\cos(\theta_y)\cos(\theta_z) & \\ & & 2X + 4 - 2X\cos(2\theta_z) \\ 2\sin(\theta_x)\sin(\theta_z) & 2\sin(\theta_y)\sin(\theta_z) & -2\cos(\theta_x)\cos(\theta_z) \\ & & -2\cos(\theta_y)\cos(\theta_z) \end{pmatrix}. \tag{5.63}$$

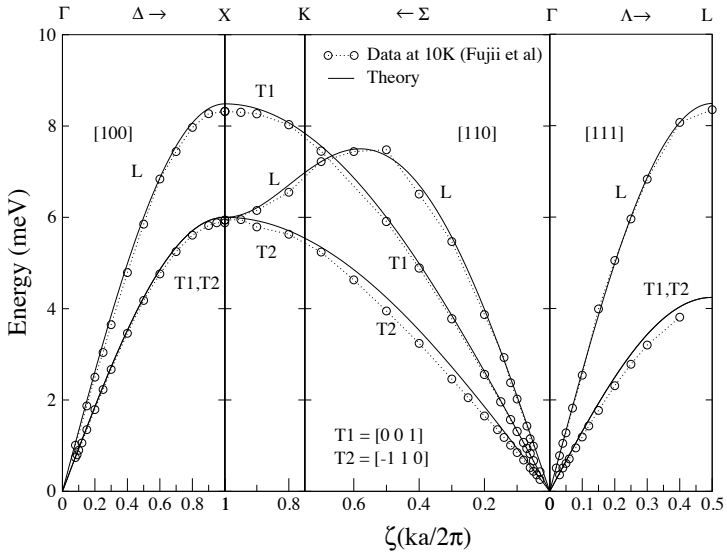

Figure 5.3. Phonon modes in solid Argon along the different symmetry lines of the FCC lattice. Experimental data taken from Fujii et al [8].

Here $\theta_i \equiv k_i a$, $X \equiv \frac{K_2}{K_1}$. The eigenvalue equation Eq. (5.62) has a solution if the secular determinant of the dynamical matrix vanishes,

$$\left|\underline{\mathrm{D}} - \omega^2 \underline{\mathrm{I}}\right| = 0. \tag{5.64}$$

For given values of the wave vector **k**, the above equation Eq. (5.64) is solved for the roots of ω^2. We equate the calculated values of ω at the different symmetry points to the experimentally measured values, to solve for the spring constants K_1 and K_2. The value of K_2 is found to be almost negligible. Hence, it is sufficient to consider the nearest neighbor interactions only for this lattice. The value for $\hbar\sqrt{K_1/M_s}$ is found to be 3.00 meV. The details of the evaluation are given in Appendix-A. In Fig. 5.3, the theoretically obtained values are shown with experimentally measured values for the phonon frequencies along the symmetry lines. The agreement between the two sets of values show that, it is sufficient to consider the nearest-neighbor interaction to obtain the phonon dispersion in inert gas solids
.

	σ(Å)	ϵ(K)
Ne-Ne [103]	2.740	36.23
Ne-Ar [104]	3.083	64.50

Table 5.1. Lennard-Jones parameters for Ne-Ne and Ne-Ar interaction potential energies.

5.3.2 Fluid Distribution Functions

We consider the interaction potential between the fluid atoms and also between a solid and a fluid atom to have the Lennard-Jones form (Eq. (3.36)),

$$V(r) = 4\epsilon \left(\frac{\sigma^{12}}{r^{12}} - \frac{\sigma^{6}}{r^{6}} \right).$$

We chose liquid Neon as the fluid sharing boundary with solid Argon. The parameters for Lennard-Jones potential of these systems are shown in Tab. 5.1. The dimensionless variables the solid-fluid systems are scaled with respect to the these parameters in the following way:

$$\begin{aligned} r^* = \frac{r}{\sigma_{sf}}, \quad k^* = k\sigma_{sf}; \quad \sigma_{sf} \Rightarrow \sigma_{\text{Ne-Ar}} \\ n^* = n\sigma_{sf}^3, \quad T^* = \tfrac{k_B T}{\epsilon_{sf}}. \end{aligned} \tag{5.65}$$

Under normal pressure, Neon remains liquid only for a very narrow temperature range, 24.56K - 27.07K. This puts some constraint over the choice of the temperature for the solid-fluid system. It turns out that the choice of the density and temperature for the liquid Neon, which would enable us to evaluate the pair distribution function described in Chapter 3, is given by $n = 0.0239$ Å^{-3} and $T = 54.345$ K. Argon remains solid at this temperature. For this choice of parameters, the pair distribution function obtained using the method described in Chapter 3 is shown in Fig. 5.4.

5.3.3 Interface

When a phonon is incident on the interface, it generates three reflected and three transmitted waves, in general. The values of the wavevectors for the incident phonons are generated at random. If the randomly generated point is close to one

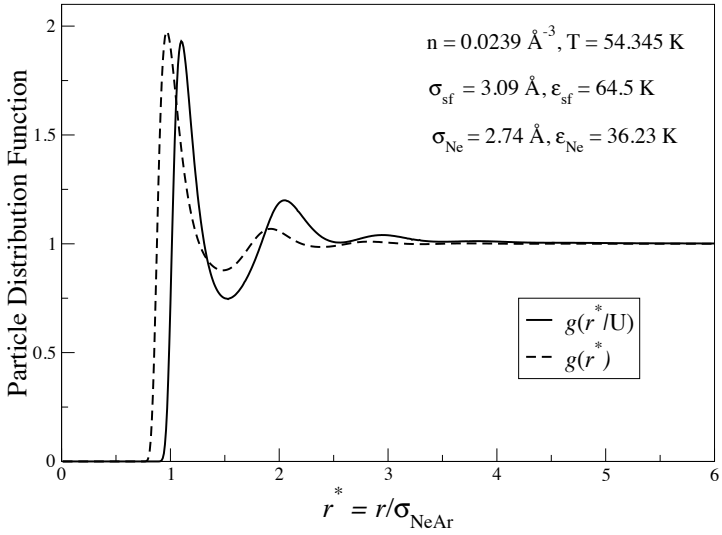

Figure 5.4. Particle distribution functions for the solid Argon- fluid Neon system. The dashed curve represents the pair distribution function for fluid Ne atoms in the bulk, evaluated using the method described in Chapter 3. The solid curve represents the one particle distribution function for Ne atoms near the solid Argon interface, evaluated using Eq. (5.9). The length variable is scaled with respect to $\sigma_{\text{Ne-Ar}}$.

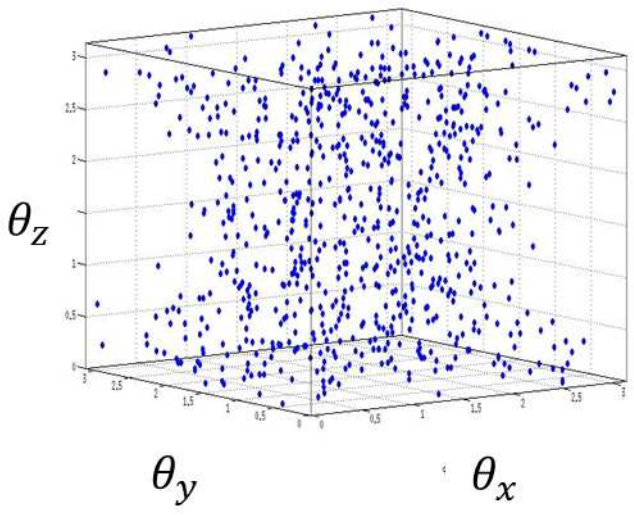

Figure 5.5. The distribution of incident wavevectors in the first Brillouin zone. Here $\theta_i = k_i a$.

of the symmetry points of FCC lattice, we disregard that point. Figure 5.5 shows the distribution of the selected 1000 points in the first Brillouin zone.

The incident phonon, the reflected phonons and the transmitted sound waves share the same frequency and the same values for the parallel component of the wave vector. This fact is used to obtain the wave vector for the reflected waves using the values of the phonon frequencies shown in Fig. 5.3.

In order to obtain the perpendicular component of the wave vectors k_{sn} for the reflected phonons, we solve Eq. (5.64) for given values of the frequency ω and the parallel components of the wavevectors, k_x and k_y. Numerical solution of Eq. (5.64) is difficult in a significant fraction of cases and usually requires large amount of computation time. We transform Eq. (5.64) into an algebraic equation that can be solved easily. To carry out the transformation we define

$$X = 2\cos(\theta_x),\ Y = 2\cos(\theta_y),\ Z = \exp(i\theta_z), \tag{5.66}$$

$$\text{and } \Omega = \frac{2M_s\omega^2}{K} - 8. \tag{5.67}$$

After some algebra, Eq. (5.64) can be written in the form

$$C_3Z^6 + C_2Z^5 + C_1Z^4 + C_0Z^3 + C_1Z^2 + C_2Z + C_3 = 0, \tag{5.68}$$

where,

$$\begin{aligned}
C_3 &= 4(X+Y),\\
C_2 &= (8+3XY)\Omega + 8XY + 32 - 8(X^2+Y^2) + 4X^2Y^2,\\
C_1 &= 2(X+Y)\Omega^2 + 3XY(X+Y)\Omega + 8XY(X+Y)\\
&\quad - 20(X+Y) + 4(X^3+Y^3),\\
C_0 &= \Omega^3 + 2XY\Omega^2 + 8(X^2+Y^2-4)\Omega + 6XY\Omega\\
&\quad + 4(X^2+Y^2)XY - 16XY + 16(X^2+Y^2) - 64.
\end{aligned}$$

For each root $Z_l\,(l = 1,\ldots 6)$, there is a corresponding root $1/Z_l$. We found that most of the roots are real, but some of them have a non-zero imaginary part. We choose the roots with positive imaginary part. The waves with real k_{sn} reflects of the interface and can carry the heat away from the interface. The waves with complex k_{sn} do not carry heat away from the interface, but we still include

them to satisfy the boundary conditions. Using the roots for k_{sn}, we solve for the eigenvectors in Eq. (5.62), which are the polarization vectors for these reflected waves.

The wave vectors for the transmitted sound waves in the fluid are found out using the dispersion relations for sound waves in fluid, Eq.s (5.14) and (5.15) in the following way. The dispersion relations are given by integral equations and it is very computationally expensive to solve these integral equations for wave vectors for given values of ω. We take the following approach to work around the problem. For small values of k, we used the approximation $(1-\exp(ikz)) \approx \frac{k^2z^2}{2}$ and solved the integrals

$$\begin{aligned} \omega_l^2(k) &= 3\omega_0^2 + \frac{nk^2}{2M_f}\int d^3r g(r) z^2 \frac{\partial^2}{\partial z^2} V_{ff}(r) && (5.69) \\ \omega_t^2(k) &= \omega_0^2 + \frac{nk^2}{2M_f}\int d^3r g(r) z^2 \frac{\partial^2}{\partial x^2} V_{ff}(r) && (5.70) \\ \omega_0^2 &= k^2 \frac{k_B T}{M_f}. \end{aligned}$$

For intermediate values of k, the frequency values for the sound modes are obtained for a range of k values using the dispersion relations (Eq.s (5.14) and (5.15)), as shown in Fig. 5.6. The functions $\omega_l(k)$ and $\omega_t(k)$ are then approximated as polynomials in k:

$$\omega(k) = \sum_{p=1}^{m} \alpha_p k^p,$$

and α_p's are obtained by fitting the curves shown in Fig. 5.6. We kept the terms till $p = 6$, to obtain a satisfactory fit, and the two functions are joined smoothly to obtain functional forms for ω for all ranges of k. These functional forms are used to evaluate the wavevectors for given values of ω. Note that k here represents the norm of the full wavevector, $k = \sqrt{k_x^2 + k_y^2 + k_z^2}$. The z-component of the wavevector for the transmitted waves are then calculated using given values of k_x and k_y, $k_{z(l \text{ or } t)} = \sqrt{k_{(l \text{ or } t)}^2 - k_x^2 - k_y^2}$. The polarization vectors for the sound modes are constructed in the following way:

$$\hat{e}_l = \frac{(k_x, k_y, k_{zl})}{\sqrt{k_x^2 + k_y^2 + k_{zl}^2}}, \ , \hat{e}_{t1} = \frac{(-k_y, k_x, 0)}{\sqrt{k_x^2 + k_y^2}}, \ \hat{e}_{t2} = \frac{(-k_x k_{zt}, -k_y k_{zt}, k_x^2 + k_y^2)}{\sqrt{k_x^2 + k_y^2 + k_{zt}^2}\sqrt{k_x^2 + k_y^2}}. \quad (5.71)$$

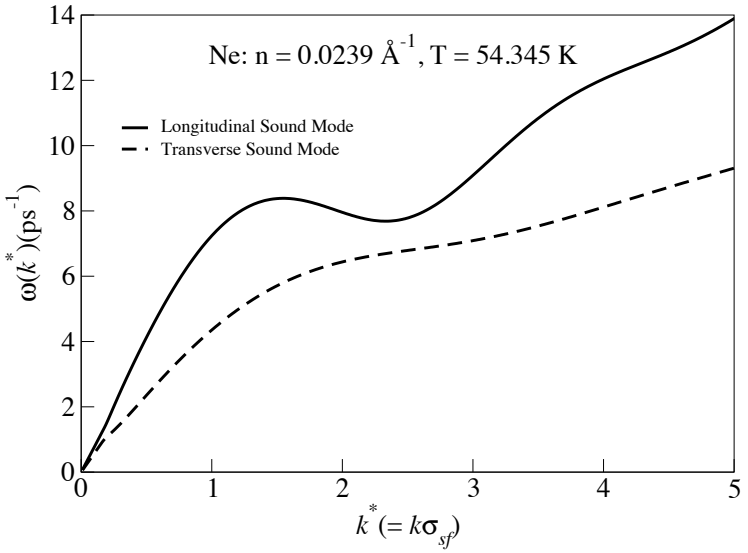

Figure 5.6. Longitudinal and transverse sound modes in liquid Neon at $n = 0.0239\text{Å}^{-3}$ and $T = 54.345$K.

Using the form of the Lennard-Jones potential Eq. (3.36), parts of the integrals in the different elements of the tensors $\mathcal{M}$, $\mathcal{U}$ and $\mathcal{V}$ can be evaluated analytically. The rest of the integration is performed numerically using `MATLAB`. The matrix equations Eq. (5.35) and Eq. (5.50) are solved to obtain the phonon reflection and transmission coefficients at the solid-fluid interface. The phonon transmission coefficients for different polarizations are shown in Fig. 5.7. The distribution for the group velocities are shown in Fig. 5.8. Using these values in Eq. (5.4), we obtain the value for Kapitza conductance for solid Argon-fluid Neon interface to be $\sigma = 0.0374\text{GW/K m}^2$.

5.4 Summary

We develop a method to estimate the thermal boundary resistance at a neutral solid-fluid interface. The resistance is obtained by calculating the phonon transmission coefficients at the solid-fluid interface. We consider the coupling between the phonons in the solid and sound wave excitations in the fluid to obtain the transmission coefficients. We consider both longitudinal and transverse sound modes in fluid. The sound wave dispersion in classical fluids can be evaluated from the knowledge of the pair distribution function in the bulk. We used the approximate

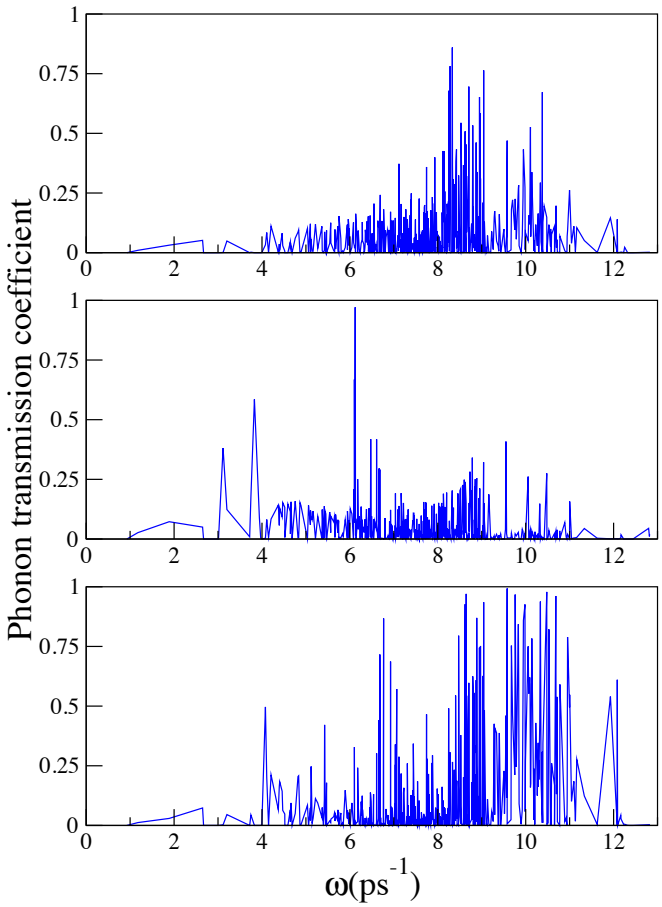

Figure 5.7. Phonon transmission coefficient $\mathcal{T}$ at the interface between solid Argon and fluid Neon. The density and the temperature of the fluid are given by $n = 0.0239\mathring{A}^{-3}$ and $T = 54.345$K, respectively.

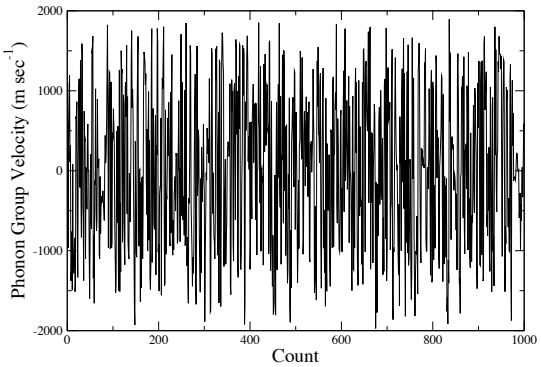

Figure 5.8. Phonon group velocities for the chosen incident wave vectors. The values are consistent with the experimentally measured values of sound velocities in solid Argon [9].

integral theories to obtain the bulk pair distribution function of the fluid. As we discussed in Chapter 3, these methods can yield accurate results only when the thermodynamic parameters of the system is within a specific region. We have chosen the density and temperature of the fluid such that these method can give stable results. We have chosen the fluid-fluid and solid-fluid interactions to be of the form of the Lennard-Jones interaction potential.

When a phonon of arbitrary polarization is incident on the interface from the solid side, it generates three reflected and three transmitted waves. The boundary condition imposes the constraint that the frequency (ω) and the component of the wavevector parallel to the interface ($k_{\parallel}$), is conserved for all the waves. The only parameter that changes is the component of the wavevector perpendicular the interface, $k_{\perp}$. The $k_{\perp}$values for the reflected waves are obtained by solving the dynamical matrix for given values of ω and $k_{\parallel}$. Some of the roots were imaginary, which means that the waves are damped. We chose the roots with positive imaginary part. The polarization vectors for these damped waves are also imaginary. The $k_{\perp}$ values for the transmitted waves are calculated from the dispersion relations for sound waves in fluids.

The $k_{\perp}$roots and the polarization vectors are used to obtain the equations of motion for the solid and the fluid atoms near the interface. The two coupled equations of motion for the interface atoms, Eq. (5.35) and Eq. (5.50), can be solved to evaluate the reflection and transmission amplitudes for the different modes at the interface. The values for these amplitudes give the transmission coefficients $\mathcal{T}$. When we insert the values of these transmission coefficients into the equation for Kapitza conductance, Eq. (5.4), we obtain an estimate for the thermal boundary conductance. The Kapitza conductance for solid Argon-fluid Neon interface is found to be $\sigma = 0.0374$GW/K m^2 using the method we described here.

Appendix A

Determination of the Spring Constants for FCC Argon

The dynamical matrix $\underline{\mathrm{D}}$, for an FCC lattice with lattice constant a and nearest neighbor distance $a/\sqrt{2}$ is given by (Eq.(5.63))

$$\underline{\mathrm{D}} = \frac{K_1}{M_s} \begin{pmatrix} 2X+4-2X\cos(2\theta_x) & -2\cos(\theta_x)\cos(\theta_y) & -2\cos(\theta_x)\cos(\theta_z) \\ -2\cos(\theta_x)\cos(\theta_y) & 2X+4-2X\cos(2\theta_y) & -2\cos(\theta_y)\cos(\theta_z) \\ -2\cos(\theta_x)\cos(\theta_z) & -2\cos(\theta_y)\cos(\theta_z) & 2X+4-2X\cos(2\theta_z) \end{pmatrix} \begin{matrix} 2\sin(\theta_x)\sin(\theta_y) & 2\sin(\theta_x)\sin(\theta_z) \\ 2\sin(\theta_y)\sin(\theta_z) & \\ & \end{matrix} \begin{matrix} 2\sin(\theta_x)\sin(\theta_z) \\ 2\sin(\theta_y)\sin(\theta_z) \\ \end{matrix} . \tag{A.1}$$

Here $\theta_i \equiv k_i a$. Below are the dynamical matrices and the roots for the phonon frequencies at some of the symmetry points of the FCC lattice:

$$\text{symmetry point X} = \frac{\pi}{a}(1,0,0) \rightarrow \theta = (\pi,0,0),$$

$$\underline{D} = \begin{bmatrix} 8 & 0 & 0 \\ 0 & 4 & 0 \\ 0 & 0 & 4 \end{bmatrix}$$
$$\Rightarrow \omega = \sqrt{\frac{8K_1}{M}}, \sqrt{\frac{4K_1}{M}}, \sqrt{\frac{4K_1}{M}} \tag{A.2}$$

symmetry point $\mathrm{K} = \frac{\pi}{a}(\frac{3}{4}, \frac{3}{4}, 0) \rightarrow \theta = (\frac{3\pi}{4}, \frac{3\pi}{4}, 0)$,

$$\underline{D} = \begin{bmatrix} \frac{2K_2}{K_1} + (3+\sqrt{2}) & 1 & 0 \\ 1 & \frac{2K_2}{K_1} + (3+\sqrt{2}) & 0 \\ 0 & 0 & 4+2\sqrt{2} \end{bmatrix}$$
$$\Rightarrow \omega = \sqrt{\frac{(4+\sqrt{2})K_1 + 2K_2}{M}}, \sqrt{\frac{(2+\sqrt{2})K_1 + 2K_2}{M}}, \sqrt{\frac{2(2+\sqrt{2})K_1}{M}} \tag{A.3}$$

symmetry point $\mathrm{L} = \frac{\pi}{a}(\frac{1}{2}, \frac{1}{2}, \frac{1}{2}) \rightarrow \theta = (\frac{\pi}{2}, \frac{\pi}{2}, \frac{\pi}{2})$,

$$\underline{D} = \begin{bmatrix} \frac{4K_2}{K_1} + 4 & 2 & 2 \\ 2 & \frac{4K_2}{K_1} + 4 & 2 \\ 2 & 2 & \frac{4K_2}{K_1} + 4 \end{bmatrix}$$
$$\Rightarrow \omega = \sqrt{\frac{4(2K_1 + K_2)}{M}}, \sqrt{\frac{2(K_1 + 2K_2)}{M}}, \sqrt{\frac{2(K_1 + 2K_2)}{M}} \tag{A.4}$$

Comparison with experimentally measured values yield:

$$\mathrm{X}{:}\hbar\sqrt{\tfrac{8K_1}{M}} = 8.320 \Rightarrow \hbar\sqrt{\tfrac{K_1}{M}} = 2.942 \; ; \; \hbar\sqrt{\tfrac{4K_1}{M}} = 5.880 \Rightarrow \hbar\sqrt{\tfrac{K_1}{M}} = 2.940$$
$$\mathrm{L}{:}\hbar\sqrt{\tfrac{4(2K_1+K_2)}{M}} = 8.350, \; \sqrt{\tfrac{2(K_1+2K_2)}{M}} = 3.970, \Rightarrow \hbar\sqrt{\tfrac{K_1}{M}} = 3.090, \; \tfrac{K_2}{K_1} = -0.0583$$

The average value of $\hbar\sqrt{\frac{K_1}{M}} = 3.00$ meV and the value of the next-nearest neighbor spring constant is taken to be zero.

Appendix B

Coefficient List for Solid-Fluid Coupling Matrix Equations

The coefficients $C_{pn}$for the three reflected waves ($n = 1, 2, 3$) are

$$
\begin{aligned}
C_{1n} &= K\left[\left(1-(\cos(k_x a)\exp(-ik_z^{(n)}a))\right)e_x^{(n)} - i\sin(k_x a)\exp(-ik_z^{(n)}a)e_z^{(n)}\right] \\
&\quad - \mathcal{M}(0,0)\,[1,1]\,e_x^{(n)}, \\
C_{2n} &= K\left[\left(1-(\cos(k_y a)\exp(-ik_z^{(n)}a))\right)e_y^{(n)} - i\sin(k_y a)\exp(-ik_z^{(n)}a)e_z^{(n)}\right] \\
&\quad - \mathcal{M}(0,0)\,[2,2]\,e_y^{(n)}, \\
C_{3n} &= K\left[-i\sin(k_x a)\exp(-ik_z^{(n)}a)e_x^{(n)} - i\sin(k_y a)\exp(-ik_z^{(n)}a)e_y^{(n)}\right. \\
&\quad \left. + \left(2-((\cos(k_x a)+\cos(k_y a))\exp(-ik_z^{(n)}a))\right)e_z^{(n)}\right] - \mathcal{M}(0,0)\,[3,3]\,e_z^{(n)}, \\
C_{4n} &= \mathcal{M}(0,0)\,[1,1]\,e_x^{(n)}, \\
C_{5n} &= \mathcal{M}(0,0)\,[2,2]\,e_y^{(n)}, \\
C_{6n} &= \mathcal{M}(0,0)\,[3,3]\,e_z^{(n)}.
\end{aligned}
\tag{B.1}
$$

The coefficients for the incident wave are ($n = 0$)

$$
\begin{aligned}
C_{10} &= -K\left[\left(1-(\cos(k_x a)\exp(ik_z^{(0)}a))\right)e_x^{(0)} - i\sin(k_x a)\exp(ik_z^{(0)}a)e_z^{(0)}\right] \\
&\quad + \mathcal{M}(0,0)\,[1,1]\,e_x^{(0)}, \\
C_{20} &= -K\left[\left(1-(\cos(k_y a)\exp(ik_z^{(0)}a))\right)e_y^{(0)} - i\sin(k_y a)\exp(ik_z^{(0)}a)e_z^{(0)}\right] \\
&\quad + \mathcal{M}(0,0)\,[2,2]\,e_y^{(0)},
\end{aligned}
$$

$$
\begin{aligned}
C_{30} &= -K\left[-i\sin(k_x a)\exp(ik_z^{(0)}a)e_x^{(0)} - i\sin(k_y a)\exp(ik_z^{(0)}a)e_y^{(0)}\right. \\
&\quad \left. + \left(2 - \left(\left(\cos(k_x a) + \cos(k_y a)\right)\exp(ik_z^{(0)}a)\right)\right)e_z^{(0)}\right] + \mathcal{M}(0,0)\,[3,3]\,e_z^{(0)}, \\
C_{40} &= \mathcal{M}(0,0)\,[1,1]\,e_x^{(0)}, \\
C_{50} &= \mathcal{M}(0,0)\,[2,2]\,e_y^{(0)}, \\
C_{60} &= \mathcal{M}(0,0)\,[3,3]\,e_z^{(0)}.
\end{aligned} \tag{B.2}
$$

The coefficients $C_{pn}$for the three transmitted waves $(n = 4, 5, 6)$ are

$$
\begin{aligned}
C_{1n} &= \mathcal{M}(\mathbf{k}, k_{fn})\,[1,1]\,e_x^{(n)} + \mathcal{M}(\mathbf{k}, k_{fn})\,[1,2]\,e_y^{(n)} + \mathcal{M}(\mathbf{k}, k_{fn})\,[1,3]\,e_z^{(n)}, \\
C_{2n} &= \mathcal{M}(\mathbf{k}, k_{fn})\,[2,1]\,e_x^{(n)} + \mathcal{M}(\mathbf{k}, k_{fn})\,[2,2]\,e_y^{(n)} + \mathcal{M}(\mathbf{k}, k_{fn})\,[2,3]\,e_z^{(n)}, \\
C_{3n} &= \mathcal{M}(\mathbf{k}, k_{fn})\,[3,1]\,e_x^{(n)} + \mathcal{M}(\mathbf{k}, k_{fn})\,[3,2]\,e_y^{(n)} + \mathcal{M}(\mathbf{k}, k_{fn})\,[3,3]\,e_z^{(n)},
\end{aligned}
$$

$$
\begin{aligned}
C_{4n} &= \left(\mathcal{U}(\mathbf{k}, k_{fn})\,[1,1] - \mathcal{V}(\mathbf{k}, k_{fn})\,[1,1] - \mathcal{M}(\mathbf{k}, k_{fn})\,[1,1]\right)e_x^{(n)} \\
&\quad + \left(-\mathcal{V}(\mathbf{k}, k_{fn})\,[1,2] - \mathcal{M}(\mathbf{k}, k_{fn})\,[1,2]\right)e_y^{(n)} \\
&\quad + \left(-\mathcal{V}(\mathbf{k}, k_{fn})\,[1,3] - \mathcal{M}(\mathbf{k}, k_{fn})\,[1,3]\right)e_z^{(n)}, \\
C_{5n} &= \left(-\mathcal{V}(\mathbf{k}, k_{fn})\,[2,1] - \mathcal{M}(\mathbf{k}, k_{fn})\,[2,1]\right)e_x^{(n)} \\
&\quad + \left(\mathcal{U}(\mathbf{k}, k_{fn})\,[2,2] - \mathcal{V}(\mathbf{k}, k_{fn})\,[2,2] - \mathcal{M}(\mathbf{k}, k_{fn})\,[2,2]\right)e_y^{(n)} \\
&\quad + \left(-\mathcal{V}(\mathbf{k}, k_{fn})\,[2,3] - \mathcal{M}(\mathbf{k}, k_{fn})\,[2,3]\right)e_z^{(n)}, \\
C_{6n} &= \left(-\mathcal{V}(\mathbf{k}, k_{fn})\,[3,1] - \mathcal{M}(\mathbf{k}, k_{fn})\,[3,1]\right)e_x^{(n)} \\
&\quad + \left(-\mathcal{V}(\mathbf{k}, k_{fn})\,[3,2] - \mathcal{M}(\mathbf{k}, k_{fn})\,[3,2]\right)e_y^{(n)} \\
&\quad + \left(\mathcal{U}(\mathbf{k}, k_{fn})\,[3,3] - \mathcal{V}(\mathbf{k}, k_{fn})\,[3,3] - \mathcal{M}(\mathbf{k}, k_{fn})\,[3,3]\right)e_z^{(n)}.
\end{aligned} \tag{B.3}
$$

Bibliography

[1] Gordon, W. L., C. H. Shaw, and J. G. Daunt (1958) "Radial Atomic Distribution in Liquid Helium–4 by X-Ray Scattering," *J. Phys. Chem. Solids*, **5**, pp. 117–128.

[2] Henshaw, D. G. (1960) "Effect of the λ Transition on the Atomic Distribution in Liquid Helium by Neutron Diffraction," *Physical Review*, **119**, pp. 9–13.

[3] Svensson, E. C., V. F. Sears, A. D. B. Woods, and P. Martel (1980) "Neutron-Diffraction Study of the Static Structure Factor and Pair Correlations in Liquid 4He," *Physical Review B*, **21**, pp. 3638–3651.

[4] McMillan, W. L. (1965) "Ground State of Liquid He4," *Physical Review*, **138**, pp. A442–A451.

[5] Murphy, R. D. and R. O. Watts (1970) "Ground State of Liquid 4He," *Journal of Low Temperature Physics*, **2**, pp. 507–519.

[6] Francis, W. P., G. V. Chester, and L. Reatto (1970) "Ground State of Liquid He4," *Physical Review A*, **1**, p. 86.

[7] Feynman, R. P. (1954) "Atomic Theory of the Two-Fluid Model of Liquid Helium," *Physical Review*, **94**, pp. 262–277.

[8] Fujii, Y., N. A. Lurie, R. Pynn, and G. Shirane (1974) "Inelastic Neutron Scattering From Solid 36Ar," *Physical Review B*, **10**, pp. 3647–3659.

[9] Moeller, H. R. and C. F. Squire (1966) "Ultrasonic Velocities in Solid Argon," *Physical Review*, **151**, pp. 689–693.

[10] Cahill, D. G., W. K. Ford, K. E. Goodson, G. D. Mahan, A. Majumdar, H. J. Maris, R. Merlin, and S. R. Phillpot (2003) "Nanoscale Thermal Transport," *Journal of Applied Physics*, **93**, p. 793.

[11] Prosen, T. and D. K. Campbell (2005) "Normal and Anomalous Heat Transport in One-Dimensional Classical Lattices," *Chaos*, **15**, p. 015117.

[12] Dhar, A. (2008) "Heat Transport in Low-Dimensional Systems," *Advances in Physics*, **57**, pp. 457–537.

[13] Bonetto, F., J. L. Lebowitz, and L. Rey-Bellet (2000) "Fourier's Law: A Challenge To Theorists," in *Mathematical Physics 2000* (A. Fokas, A. Grigoryan, T. Kibble, and B. Zegarlinski, eds.), Imperial College, London, p. 128150.

[14] Lepri, S., R. Livi, and A. Politi (2003) "Thermal Conduction in Classical Low-Dimensional Lattices," *Physics Reports*, **377**, pp. 1–80.

[15] Toda, M. (1979) "Solitons and Heat Conduction," *Physica Scripta*, **20**, pp. 424–430.

[16] Fermi, E., J. Pasta, S. Ulam, and M. Tsingou (1955) "Studies of Nonlinear Problems. I." *Los Alamos report LA-1940*.

[17] in *Collected Papers of Enrico Fermi* (E. Segre, ed.) (1965) University of Chicago Press, Chicago.

[18] Ford, J. P. (1992) "The Fermi-Pasta-Ulam Problem: Paradox Turns Discovery," *Physics Reports*, **213**, pp. 271–310.

[19] Zabusky, J. (2005) "FPU, Solitons, and the Fabric of Nonlinear and Computational Science: History, Synergetics, and Visiometrics," *Chaos*, **15**, p. 015102.

[20] Berman, P. and F. M. Izrailev (2005) "The Fermi-Pasta-Ulam Problem: 50 Years of Progress," *Chaos*, **15**, p. 015104.

[21] Weissert, T. P. (1997) *The Genesis of Simulation in Dynamics: Pursuing the Fermi-Pasta-Ulam Problem*, Springer, New York.

[22] Iijima, S. (1991) "Helical Microtubules of Graphitic Carbon," *Nature(London)*, **354**, p. 56.

[23] Zhao, X., Y. Ando, Y. Liu, M. Jinno, and T. Suzuki (2003) "Carbon Nanowire Made of a Long Linear Carbon Chain Inserted Inside a Multiwalled Carbon Nanotube," *Physical Review Letters*, **90**, p. 187401.

[24] Berber, S., Y. K. Kwon, and D. Tom'anek (2000) "Unusually High Thermal Conductivity of Carbon Nanotubes," *Physical Review Letters*, **84**, pp. 4613–4616.

[25] Choi, S. U. S. (2009) "Nanofluids: From Vision to Reality Through Research," *Journal of Heat Transfer*, **131**, p. 033106.

[26] Keblinskia, P., J. A. Eastmanb, and D. G. Cahill (2005) "Nanofluids for Thermal Transport," *Materials Today*, **8**, pp. 36–44.

[27] Kapitza, P. L. (1941) "The Study of Heat Transfer in Helium II," *Journal of Physics (USSR)*, **4**, pp. 181–200.

[28] Little, W. A. (1959) "The transport of Heat Between Dissimilar Solids at Low Temperatures," *Canadian Journal of Physics*, **37**, pp. 334–349.

[29] Pollack, G. L. (1969) "Kapitza Resistance," *Reviews of Modern Physics*, **41**, pp. 48–81.

[30] Maris, H. J. (1979) "Phonon Transmission Across Interfaces and the Kapitza Resistance," *Physical Review B*, **19**, pp. 1443–1457.

[31] Schwartz, E. T. and R. O. Pohl (1987) "Thermal Resistance at Interfaces," *Applied Physics Letters*, **51**, pp. 2200–2202.

[32] Schwartz, E. T. and R. O. Pohl (1989) "Thermal Boundary Resistance," *Reviews of Modern Physics*, **61**, pp. 605–668.

[33] Ge, Z., D. G. Cahill, and P. V. Braun (2006) "Thermal Conductance of Hydrophilic and Hydrophobic interfaces," *Physical Review Letters*, **96**, p. 186101.

[34] Khalatnikov, I. M. (1952) *Zhurnal Eksperimental'noi i Teoreticheskoi Fiziki*, **22**, p. 687.

[35] Olson, J. R. and R. O. Pohl (1994) "Kapitza Resistance Between Silicon and Helium-4," *Journal of Low Temperature Physics*, **94**, p. 539.

[36] Kinder, H. and K. Weiss (1993) "Kapitza Conduction by Thin Lossy Surface Layers," *Journal of Physics: Condensed Matter*, **5**, p. 2063.

[37] Nakayama, T. (1989) in *Progress in Low Temperature Physics* (D. F. Brewer, ed.), North-Holland, Amsterdam, p. 115.

[38] Young, D. A. and H. J. Maris (1989) "Lattice-Dynamical Calculation of the Kapitza Resistance Between FCC Lattices," *Physical Review B*, **40**, pp. 3685–3693.

[39] Pettersson, S. and G. D. Mahan (1990) "Theory of the Thermal Boundary Resistance Between Dissimilar Lattices," *Physical Review B*, **42**, pp. 7386–7390.

[40] Ikeshoji, T. and B. Hafskjold (1994) "Non-Equilibrium Molecular Dynamics Calculation of Heat Conduction in Liquid and Through Liquid-Gas Interface," *Molecular Physics*, **81**, pp. 251–261.

[41] Twu, C. J. and J. R. Ho (2003) "MD Study of Energy Flow and the Kapitza Conductance Across an Interface with Imperfection Formed by Two Dielectric Thin Films," *Physical Review B*, **67**, p. 205422.

[42] Xue, L., P. Klebinski, S. R. Phillpot, S. U. S. Choi, and J. A. Eastman (2003) "Two Regimes of Thermal Resistance at a Liquid-Solid Interface," *Journal of Chemical Physics*, **118**, pp. 337–339.

[43] Xue, L., P. Klebinski, S. R. Phillpot, S. U. Choi, and J. A. Eastman (2004) "Effect of Liquid Layering at the Liquid-Solid Interface on Thermal Transport," *International Journal of Heat and Mass Transfer*, **47**, pp. 4277–4284.

[44] Murad, S. and I. K. Puri (2008) "Thermal Transport Across Nanoscale Solid-Fluid Interfaces," *Applied Physics Letters*, **92**, p. 133105.

[45] Lepri, S., R. Livi, and A. Politi (1997) "Heat Conduction in Chains of Nonlinear Oscillators," *Physical Review Letters*, **78**, p. 1896.

[46] Russell, J. S. (1844) "Report on Waves," in *Report of the Fourteenth Meeting of the British Association for the Advancement of Science* (J. Murray, ed.), pp. 311–90.

[47] Korteweg, D. J. and G. de Vries (1895) "On the Change of Form of Long Waves Advancing in a Rectangular Canal and on a New Type of Long Stationary Waves," *Philosophical Magazine 5th Series*, **36**, pp. 422–443.

[48] Zabusky, N. J. and M. D. Kruskal (1965) "Interaction of Solitons in a Collisionless Plasma and the Recurrence of Initial States," *Physical Review Letters*, **15**, pp. 240–243.

[49] Kosevich, Y. A., R. Khomeriki, and S. Ruffo (2004) "Supersonic Discrete Kink-Solitons and Sinusoidal Patterns with Magic Wave Number in Anharmonic Lattices," *Europhysics Letters*, **66**, pp. 21–27.

[50] Hu, B., B. Li, and H. Zhao (1998) "Heat Conduction in One-Dimensional Chains," *Physical Review E*, **57**, pp. 2992–2995.

[51] Wei, N., G. Wu, and J. Dong (2004) "Heat Conduction in a Carbon Chain," *Physics Letters A*, **325**, pp. 403–406.

[52] Mahan, G. D. (2006) "Traveling Solitons in One-Dimensional Quartic Lattices," *Physical Review B*, **74**, p. 094304.

[53] Mahan, G. D. (2005) "Classical Waves on Nonlinear Lattices," *Physical Review B*, **72**, p. 144302.

[54] Budinsky, N. and T. Bountis (1983) "Stability of Nonlinear Modes and Chaotic Properties of 1D Fermi-Pasta-Ulam Lattices," *Physica D*, **8**, p. 445.

[55] Sievers, A. J. and S. Takeno (1988) "Intrinsic Localized Modes in Anharmonic Crystals," *Physical Review Letters*, **61**, pp. 970–973.

[56] Page, J. B. (1990) "Asymptotic Solutions for Localized Vibrational Modes in Strongly Anharmonic Periodic Systems," *Physical Review B*, **41**, pp. 7835–7838.

[57] Bickham, S. R. and A. J. Sievers (1991) "Intrinsic Localized Modes in a Monatomic Lattice with Weakly Anharmonic Nearest-Neighbor Force Constants," *Physical Review B*, **43**, pp. 2339–2346.

[58] Huang, G. X., Z. P. Shi, and Z. Xu (1993) "Asymmetric Intrinsic Localized Modes in a Homogeneous Lattice with Cubic and Quartic Anharmonicity," *Physical Review B*, **47**, pp. 14561–14564.

[59] Kosevich, Y. A. (1993) "Nonlinear Sinusoidal Waves and Their Superposition in Anharmonic Lattices," *Physical Review Letters*, **71**, pp. 2058–2061.

[60] Kivshar, Y. S. (1993) "Creation of Nonlinear Localized Modes in Discrete Lattices," *Physica Review E*, **48**, pp. 4132–4135.

[61] Wang, S. (1993) "Localized Vibrational Modes in an Anharmonic Chain," *Physics Letters A*, **182**, pp. 105–108.

[62] Poggi, P. and S. Ruffo (1997) "Exact Solutions in the FPU Oscillator Chain," *Physica D*, **103**, pp. 251–272.

[63] Rosenau, P. (2003) "Hamiltonian Dynamics of Dense Chains and Lattices: Or How to Correct the Continuum," *Physics Letters A*, **311**, pp. 39–52.

[64] Bourbonnais, R. and R. Maynard (1990) "Energy Transport in One- and Two-Dimensional Anharmonic Lattices with Isotopic Disorder," *Physical Review Letters*, **64**, pp. 1397–1400.

[65] Burlakov, V. M., S. A. Kiselev, and V. N. Pyrkov (1990) "Computer Simulation of Intrinsic Localized Modes in One-Dimensional and Two-Dimensional Anharmonic Lattices," *Physical Review B*, **42**, pp. 4921–4927.

[66] Bickham, S. R., A. J. Sievers, and S. Takeno (1992) "Numerical Measurements of the Shape and Dispersion Relation for Moving One-Dimensional Anharmonic Localized Modes," *Physical Review B*, **45**, pp. 10344–10347.

[67] Bickham, S. R., S. A. Kiselev, and A. J. Sievers (1993) "Stationary and Moving Intrinsic Localized Modes in One-Dimensional Monatomic Lattices with Cubic and Quartic Anharmonicity," *Physical Review B*, **47**, pp. 14206–14211.

[68] Wallis, R. F., A. Franchini, and V. Bortolani (1994) "Localized Modes in Inhomogeneous One-Dimensional Anharmonic Lattices," *Physical Review B*, **50**, pp. 9851–9859.

[69] Dusi, R. and M. Wagner (1995) "Gauss Procedure For the Construction of Self-Localized Solitons in Discrete Systems," *Physical Review B*, **51**, pp. 15847–15855.

[70] Dusi, R., G. Viliani, and M. Wagner (1996) "Breathing Self-Localized Solitons in the Quartic Fermi-Pasta-Ulam Chain," *Physical Review B*, **54**, pp. 9809–9818.

[71] Kiselev, S. A. (1990) "Stationary Vibrational Modes of a Chain of Particles Interacting via an Even Order Potential," *Physics Letters A*, **148**, pp. 95–97.

[72] Kiselev, S. A. and V. I. Rupasov (1990) "Stationary Vibrational Modes of a Polyatomic Chain of Particles Interacting via an Even Order Potential," *Physics Letters A*, **148**, pp. 355–358.

[73] Tsuboi, T. and F. M. Toyama (1991) "Computer Experiments on Solitons in a Nonlinear Transmission Line. I. Formation of Stable Solitons," *Physical Review A*, **44**, pp. 2686–2690.

[74] Percus, J. K. (1964) "The Pair Distribution Function in Classical Statistical Mechanics," in *The Equilibrium Theory of Classical Fluids* (H. L. Frisch and J. L. Lebowitz, eds.), W. A. Benjamin, Inc., New York, pp. II–33.

[75] Percus, J. K. (1962) "Approximation Methods in Classical Statistical Mechanics," *Physical Review Letters*, **8**, pp. 462–463.

[76] Stell, G. (1963) "Percus-Yevick Equation for Radial Distribution Function of a Fluid," *Physica*, **29**, p. 517.

[77] Boer, J. D., J. M. J. V. Leeuwen, and J. Groeneveld (1964) "Calculation of the Pair Correlation Function: II. Results for the 12-6 Lennard-Jones Interaction," *Physica*, **30**, pp. 2265–2289.

[78] Verlet, L. (1964) "On the Theory of Classical Fluids-III," *Physica*, **30**, pp. 95–104.

[79] Levesque, D. (1966) "Etude des equations de percus et yevick, d'hyperchaine et de born et green dans le cas des fluides classiques," *Physica*, **32**, p. 1985.

[80] Throop, G. J. and R. J. Bearman (1966) "The Pair Correlation Function and Thermodynamic Properties for the Lennard-Jones 612 Potential and the Percus-Yevick Equation," *Physica*, **32**, pp. 1298–1318.

[81] Verlet, L. and D. Levesque (1967) "On the Theory of Classical Fluids VI," *Physica*, **36**, pp. 254–268.

[82] Hansen, J. P. and I. R. McDonald (1976) *Theory of Simple Liquids*, Academic Press, New York.

[83] Thiele, E. (1963) "Equation of State for Hard Spheres," *Journal of Chemical Physics*, **39**, p. 474.

[84] Lebowitz, J. L. (1964) "Exact Solution of Generalized Percus-Yevick Equation for a Mixture of Hard Spheres," *Physical Review*, **133**, pp. A895–A899.

[85] Ceperley, D. M. and E. L. Pollock (1987) "The Momentum Distribution of Normal and Superfluid Liquid 4He," *Canadian Journal of Physics*, **65**, p. 1416.

[86] Ceperley, D. M. and E. L. Pollock (1989) "Path-Integral Simulation of the Superfluid Transition in 2-dimensional He," *Physical Review B*, **39**, p. 2084.

[87] Lebowitz, J. L. and J. K. Percus (1966) "Mean Spherical Model for Lattice Gases with Extended Hard Cores and Continuum Fluids," *Physical Review*, **144**, pp. 251–258.

[88] Smith, W. R., D. Henderson, and Y. Tago (1977) "Mean Spherical Approximation and Optimized Cluster Theory for the SquareWell Fluid," *Journal of Chemical Physics*, **67**, p. 5308.

[89] Dubinin, N. E., V. V. Filippov, and N. A. Vatolin (2007) "Structure and Thermodynamics of the One- and Two-Component Square-Well Fluid," *Journal of Non-Crystalline Solids*, **353**, pp. 1798–1801.

[90] Dubinin, N. E., V. V. Filippov, O. G. Malkhanova, and N. A. Vatolin (2009) "Structure Factors of Binary Liquid Metal Alloys Within the Square-Well Model," *Central European Journal of Physics*, **7**, pp. 584–590.

[91] Jastrow, R. (1955) "Many-Body Problem with Strong Forces," *Physical Review*, **98**, pp. 1479–1484.

[92] Aziz, R. A., V. P. S. Nain, J. C. Carley, W. L. Taylor, and G. T. McConville (1979) "An Accurate Intermolecular Potential for Helium," *Journal of Chemical Physics*, **70**, p. 4330.

[93] Kinsler, E. and A. R. Frey (1950) *Fundamentals of Acoustics*, Wiley, New York.

[94] Steinbruchel, C. (1976) "The Scattering of Phonons of Arbitrary Wavelength at a Solid-Solid Interface: Model Calculation and Applications," *Zeitschrift fur Physik B*, **24**, pp. 293–299.

[95] Montroll, E. W. (1947) "Dynamics of a Square Lattice I. Frequency Spectrum," *Journal of Chemical Physics*, **15**, p. 575.

[96] Mahan, G. D. (2008) "Kapitza Resistance at a Solid-Fluid Interface," *Nanoscale and Microscale Thermophysical Engineering*, **12**, pp. 294–310.

[97] March, H. and M. Tosi (2002) *Introduction to Liquid State Physics*, World Scientific, Singapore.

[98] Chung, C. H. and S. Yip (1969) "Generalized Hydrodynamics and Time Correlation Functions," *Physical Review*, **182**, pp. 323–339.

[99] Schaich, W. L. (1978) "Phonon Emission into a Diffusive Medium," *Journal of Physics C*, **11**, pp. 4341–4346.

[100] Bron, W. E., J. L. Patel, and W. L.Schaich (1979) "Transport of Phonons into Diffusive Media," *Physical Review B*, **20**, pp. 5394–5397.

[101] Zwanzig, R. (1967) "Elementary Excitations in Classical Liquids," *Physical Review*, **156**, p. 190.

[102] Zwanzig, R. and R. D. Mountain (1965) "High-Frequency Elastic Moduli of Simple Fluids," *Journal of Chemical Physics*, **43**, pp. 4464–4471.

[103] Kittel (2005) *Introduction to Solid State Physics*, John Wiley and Sons, Inc., chapter 3, Table 4.

[104] Klein, L. and J. A. Venables (1976) *Rare Gas Solids*, vol. 1, Academic, London, table XII.

Vita

Sanghamitra Neogi

Contact Information

104 Davey Laboratory
Department of Physics
The Pennsylvania State University
University Park, PA 16802 USA

Office: (814) 865-2414
Cell: (814) 574-9207
E-mail: sun114@psu.edu
Webpage: www.personal.psu.edu/sun114/

Research Interests

Transport properties, correlated systems, solitons, nonlinear systems, phase transition and critical phenomena.

Education

The Pennsylvania State University, University Park, Pennsylvania USA
Ph.D. Physics December 2011
Dissertation Topic: "Transport in Nonlinear Chains And across Several Condensed Matter Interfaces"
Advisor: Dr. Gerald D. Mahan

Indian Institute of Technology, Kanpur, India
M.Sc. Physics, May 2002

Jadavpur University, Kolkata, India
B.Sc. Physics, December 2000 Minors: Chemistry, Mathematics

Publications

Neogi, S., and Mahan, G.D. (2011), Study of Kapitza resistance at the ideal gas solid and ideal fluid interfaces. (in preparation).

Neogi, S., and Mahan, G.D. (2009), "Pair distribution function of a square-well liquid," submitted to Physical Review B. (arXiv:cond-mat/0909.3078v1).

Kumar N., Neogi S., Kent P., Bandura A., Kubicki J., Cole D., Wesolowski D. and Sofo J. (2009), "Hydrogen Bonds and Vibrations of Water on (110) Rutile," J. Phys. Chem. C 113, 13732 - 13740 (2009).

Neogi, S., and Mahan, G.D. (2008), "Generation of traveling solitons in one-dimensional monatomic quartic lattices," Physical Review B, Vol. 78(6), 064306 (2008)